The Journal of Gemmology

Volume 37 / No. 7 / 2021

History of London's Lapidaries (Part 1)

Dominican Blue Amber with Patchy Green Colouration

Electric-Pulse Processing of Emerald Ore

Cobalt Spinel from Pakistan

SSEF SCHWEIZERISCHES GEMMOLOGISCHES INSTITUT SWISS GEMMOLOGICAL INSTITUTE INSTITUT SUISSE DE GEMMOLOGIE

Gem-A THE GEMMOLOGICAL ASSOCIATION OF GREAT BRITAIN

# SSEF

SCHWEIZERISCHES GEMMOLOGISCHES INSTITUT
SWISS GEMMOLOGICAL INSTITUTE
INSTITUT SUISSE DE GEMMOLOGIE

ORIGIN DETERMINATION · TREATMENT DETECTION

DIAMOND GRADING · PEARL TESTING

EDUCATION · RESEARCH

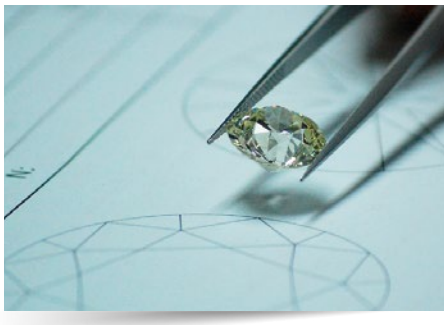

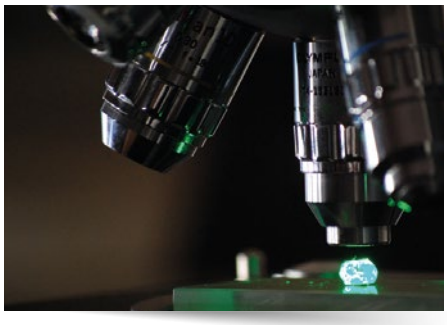

THE SCIENCE OF GEMSTONE TESTING™

Aeschengraben 26, 4051 Basel, Switzerland Tel. +41 61 262 06 40 Fax + 41 61 262 06 41 admin@ssef.ch www.ssef.ch

The Journal of Gemmology

Volume 37 / No. 7 / 2021

***Cover photo:*** *Jewels of the Cheapside Hoard show the evolution of cut styles for coloured stones, particularly during the Renaissance, and this is explored further in the article on the history of London's lapidaries on pp. 688–701 of this issue. Shown here from left to right are three enamelled gold jewels from the hoard, consisting of an earring or pendant that is set with step-cut sapphires, a spinel briolette and emeralds (34 × 10 × 3 mm); an elongate piece (possibly a fan handle) set with rose-cut amethysts and pale blue sapphires (64 × 21 × 9 mm); and a pendant containing amethyst briolettes (67 × 21 mm). The photos in this composite image are © Museum of London; inventory nos. A14109, A14165 and A14163.*

## COLUMNS






## ARTICLES



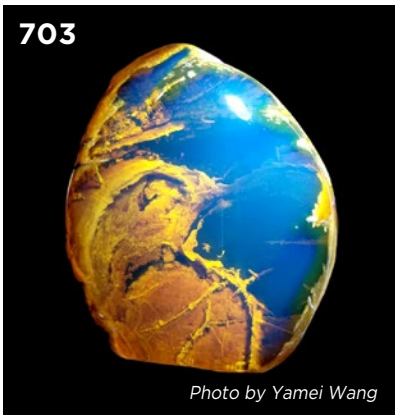


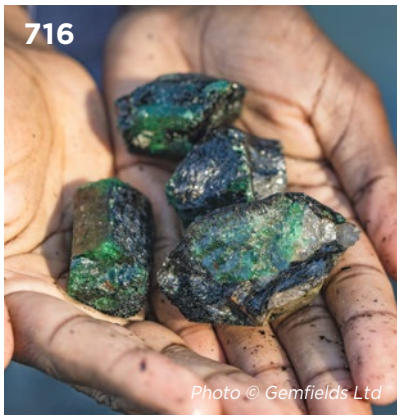




*The Journal* is published by Gem-A in collaboration with SSEF and with the support of AGL.

Gem-A THE GEMMOLOGICAL ASSOCIATION OF GREAT BRITAIN

SSEF SCHWEIZERISCHES GEMMOLOGISCHES INSTITUT SWISS GEMMOLOGICAL INSTITUTE INSTITUT SUISSE DE GEMMOLOGIE

AGL AMERICAN GEMOLOGICAL LABORATORIES

The Journal of Gemmology




## COVERED BY THE FOLLOWING ABSTRACTING AND INDEXING SERVICES:

Clarivate Analytics' (formerly Thomson Reuters/ISI) Science Citation Index Expanded (in the Web of Science), *Journal Citation Reports (Science Edition)* and *Current Contents (Physical, Chemical and Earth Sciences)*; Elsevier's Scopus; Australian Research Council's Excellence in Research for Australia (ERA) Journal List; China National Knowledge Infrastructure (CNKI Scholar); EBSCO's Academic Search Ultimate; ProQuest (Cambridge Scientific Abstracts); GeoRef; CrossRef; Chemical Abstracts (CA Plus); Mineralogical Abstracts; Index Copernicus ICI Journals Master List; Gale Academic OneFile; British Library Document Supply Service; and Copyright Clearance Center's RightFind application.

Science Citation Index Expanded
Web of Science Clarivate Analytics

## CONTENT SUBMISSION

The Editor-in-Chief is glad to consider original articles, news items, conference reports, announcements and calendar entries on subjects of gemmological interest for publication in *The Journal of Gemmology*. A guide to the various sections and the preparation of manuscripts is given at https://gem-a.com/membership/journal-of-gemmology/submissions, or contact the Editor-in-Chief.

## SUBSCRIPTIONS

Gem-A members receive *The Journal* as part of their membership package, full details of which are given at https://gem-a.com/membership. Laboratories, libraries, museums and similar institutions may become direct subscribers to *The Journal*; download the form from *The Journal*'s home page.

## ADVERTISING

Enquiries about advertising in *The Journal* should be directed to advertising@gem-a.com. For more information, see https://gem-a.com/news-publications/media-pack-2021.





## DESIGN & PRODUCTION

Zest Design, London. www.zest-uk.com

## PRINTER

DG3 Group (Holdings) Ltd, London. www.dg3.com

FSC Mixed Sources
Product group from well-managed forests and other controlled sources
www.fsc.org Cert no. TT-COC-002454
© 1996 Forest Stewardship Council



ISSN 1355-4565 (Print), ISSN 2632-1718 (Online)


Gem-A
THE GEMMOLOGICAL ASSOCIATION OF GREAT BRITAIN

21 Ely Place
London EC1N 6TD
UK
t: +44 (0)20 7404 3334
f: +44 (0)20 7404 8843
e: information@gem-a.com
w: https://gem-a.com

Registered Charity No. 1109555
A company limited by guarantee and registered in England No. 1945780
Registered office: Palladium House, 1–4 Argyll Street, London W1F 7LD

# What's New

## NEWS AND PUBLICATIONS

### CIBJO's *Laboratory-Grown Diamond Guidelines*

In June 2021, CIBJO released *The Laboratory-Grown Diamond Guidelines* to strengthen consumer confidence in synthetic diamonds and the jewellery industry in general. The 18-page report outlines principles for describing lab-grown diamonds, along with due diligence for companies that handle them, including how to make disclosures on sales and other documents. Download the guidelines at www.cibjo.org/wp-content/uploads/2021/06/CIBJO-LGD-Guidelines-2021.pdf.

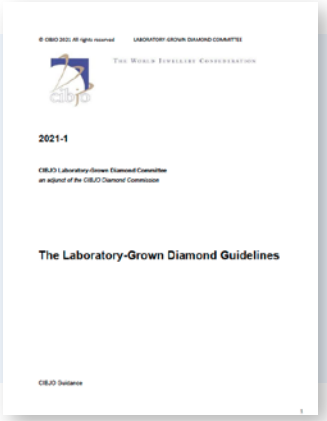


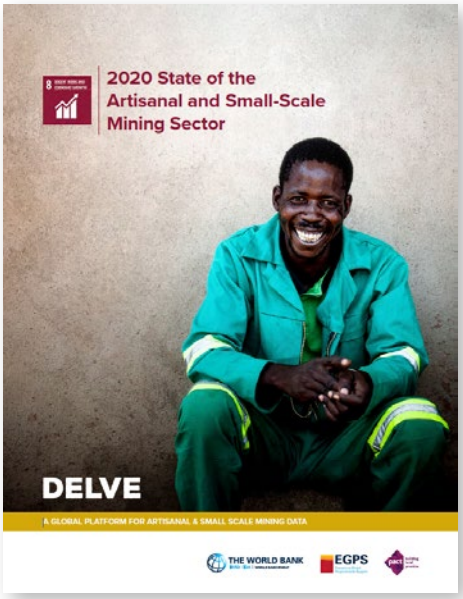


### Delve 2020 State-of-the-Sector and Country Profiles

Delve is a global online platform for artisanal and small-scale mining (ASM) data pertaining to gold, gems and other commodities. Its state-of-the-ASM-sector report for 2020 was released in May 2021 and covers Delve's contribution to United Nations' Sustainable Development Goal 8 (SDG8), which focuses on improving occupational health and safety, stimulating economic growth, making production sustainable (and eliminating mercury from ASM gold-mining operations), ensuring gender equality, and eradicating child labour while promoting youth employment. Download the 170-page report at https://delvedatabase.org/resources/2020-state-of-the-artisanal-and-small-scale-mining-sector. Delve also provides information on gem mining in its Country Profiles, with recent reports covering Afghanistan, Liberia, Madagascar and Nigeria, which are available at https://tinyurl.com/h3tvu7tt.

### Indexes Available for DGemG's Journal

Deutsche Gemmologische Gesellschaft eV
German Gemmological Association

At the end of each year, the German Gemmological Association (DGemG) updates the subject and author indexes for its journal, *Zeitschrift der Deutschen Gemmologischen Gesellschaft* (currently covering Vols. 18–69, 1969–2020). The journal was previously titled *Zeitschrift der Deutschen Gesellschaft für Edelsteinkunde* (Nos. 1–88, 1952–1968), and those issues are also included in the indexes. Visit https://dgemg.com/mitgliedschaft/zeitschrift.html to download the indexes in PDF format (in German).

## *Platinum Jewellery Business Review* 2021

Platinum Guild International (PGI) issued its latest *Platinum Jewellery Business Review* in May 2021, accompanied by a 25-minute video (including a transcript). The report covers production and sales developments in 2020 in China, India, Japan and the USA, followed by a forecast for 2021. Platinum jewellery fabrication in China declined only slightly, but in India it fell 48% compared to 2019. Not surprisingly, sales in China, India and Japan declined, but they increased slightly in the USA. For 2021, PGI forecasts continued jewellery sales growth as the retail jewellery market recovers from the pandemic. Visit https://platinumguild.com/platinum-jewellery-business-review-2021 to access the report and video.


## RJC Progress Report 2021


The Responsible Jewellery Council (RJC) released its annual progress report in May 2021. Titled *A Year of Collective Action*, it covers RJC's accomplishments in 2020, including the organisation's 15th anniversary. Key milestones included launching the Generation Equality campaign and the 'Roadmap to 2030 and Beyond' (focusing on six key sustainable development goals applicable to the jewellery and watch industry), as well as signing the UN Women's Empowerment Principles and establishing the Sustainable Development Goals Taskforce. Now with 1,424 members in 68 countries, RJC also looks back at 15 years of accomplishments. Download the report at https://responsiblejewellery.com/wp-content/uploads/RJC-Progress-Report-2021.pdf.

## SSEF *Facette* Magazine


Issue no. 27 of the Swiss Gemmological Institute SSEF's annual *Facette* magazine was released in June 2021. The 76-page issue provides an extensive array of articles on topics that include Afghan emeralds; a machine learning algorithm for visualising trace-element data; DNA fingerprinting and age dating of pearls and coral; new Cu-bearing tourmalines from Nigeria; a visit to the Mong Hsu ruby deposit in Myanmar; age dating of cobalt spinel and sapphire; heated ruby and spinel; asteriated diamonds; green-dyed natural pearls; and much more. Download the PDF at www.ssef.ch/wp-content/uploads/2021/06/facette-2021-web.pdf.

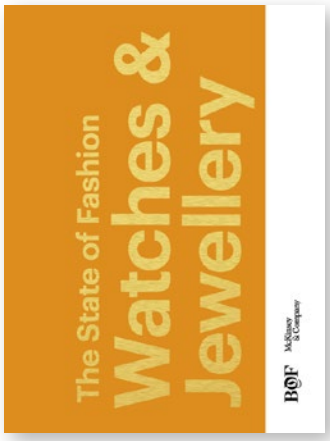


## *The State of Fashion: Watches & Jewellery*

This June 2021 report is the first in a special-edition series from *The Business of Fashion* and McKinsey & Co. It focuses on the 'global fine jewellery market for pieces priced over $360' and 'watches priced over $180' (prices given in USD), with each of these markets taking roughly half of the document. The report predicts that the fine-jewellery market will grow significantly, with Asia leading the way. Branded fine jewellery is poised to take a larger share of the market, and online jewellery sales are expected to grow to 18–21% of sales by 2025. In addition, sustainability considerations are likely to influence 20–30% of fine jewellery purchases by 2025. The report includes interviews with executives from Cartier, Christie's, Mejuri, De Beers and Shaun Leane. Download the PDF file at https://tinyurl.com/bnthcf4d.

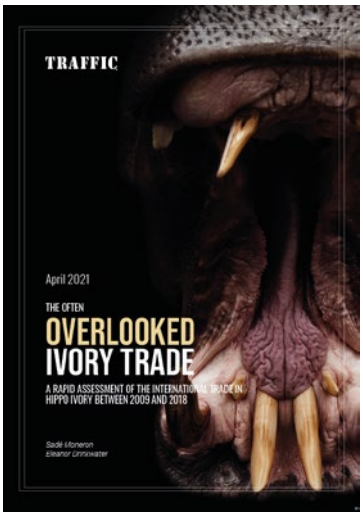


## TRAFFIC Reports on Hippo Ivory and the Tortoiseshell Trade


Two reports recently released by TRAFFIC include *The Often Overlooked Ivory Trade: A Rapid Assessment of the International Trade in Hippo Ivory Between 2009 and 2018* (April 2021) and *Shell Shocked: Japan's Role in the Illegal Tortoiseshell Trade* (May 2021). The former focuses on hippopotamus ivory from eastern and southern Africa, with 48 countries and territories implicated in its illegal trade. The second report, produced in conjunction with WWF Japan and the Japan Tiger and Elephant Fund, highlights Japan's continued trade in tortoise shell from the hawksbill turtle, a species listed as 'critically endangered' on the IUCN Red List. For these and other TRAFFIC reports, go to https://www.traffic.org/publications.

# OTHER RESOURCES

## Webinars and Other Videos for Online Gemmological Education

A number of gem industry organisations and hobbyist groups provide webinars and other archived video and audio content on their websites or YouTube channels that are of interest to gemmologists, with many items added recently due to the COVID-19 pandemic (see also those listed in several previous What's New sections).

- The **Fallbrook Gem and Mineral Society** (California, USA) offers video recordings of recent online presentations on its YouTube channel at www.youtube.com/channel/UCe4VPy2m6AP95We3o1y-VBA. Topics include ametrine (with Dr George Rossman), mineral photography (with Jeff Scovil), gem cutting (with Meg Berry) and unusual gemstones from California (with Walter Lombardo).

FALLBROOK GEM AND MINERAL SOCIETY Est. 1957

- **GemQuest** webinars have taken place since November 2020 and are available on Jolyon Ralph's YouTube channel at www.youtube.com/user/jolyonralph. Each presentation is approximately 1–2 hours long and focuses on a single gem material, covering diamond, opal and garnet to date.


GemQuest Episode 3 - GARNET

The Goldsmiths' Centre
CREATIVITY | CRAFTSMANSHIP | COMMUNITY

- **The Goldsmiths' Centre** provides educational videos and jeweller interviews on its YouTube channel (https://www.youtube.com/channel/UCzVNoArKNqRHVXKvlYdOPlQ/playlists), in both its 'Meet the Makers Series' and 'Talks Series'. In addition, videos from its 'Materials in Focus' series cover pearls (https://goldsmiths-centre.org/resources/knowledge-materials-focus-pearls) and Whitby jet (https://goldsmiths-centre.org/resources/knowledge-materials-focus-whitby-jet).

- The **Maine Mineral and Gem Museum** (Bethel, Maine, USA) recently posted several videos on its website, including three from their 'Tourmaline Turns 200' lecture series celebrating the 200th anniversary of the discovery of tourmaline at Mount Mica. Other videos of interest to gemmologists include the 'Artist Talks' series featuring jewellers and lapidary artists who created pieces on display at the museum, as well as 'Lucky Finds', consisting of short films describing important gem and mineral discoveries in Maine. Visit https://mainemineralmuseum.org/videos.


- The **San Francisco Gem and Mineral Society** (California, USA) offers video recordings of some recent presentations on its Facebook page at www.facebook.com/SFgem.mineral/videos. Of particular interest to gemmologists are those on sapphires from Sri Lanka (with Sheahan Stephen) and historic paintings of jewels with implications for the evolution of gem-cutting styles (with Justin K Prim).

- **The MVEye**, a USA-based marketing company specialising in the gem and jewellery industry, now provides links to recordings of its past interviews, webinars and podcasts on its website at www.themveye.com/events.php. The 2021 events to date focus on marketing and sales of synthetic diamonds and coloured stones.

- The **Swiss Gemmological Institute SSEF** has posted several videos on its Vimeo channel, with the most recent ones covering natural- and cultured-pearl formation (in English, French and Chinese). Also available is an animation showing the 3D view of an asteriated diamond that appears to have only three lobes after it was cut, and a rotational video clip demonstrating the 3D clustering of trace-element data for emeralds from various localities. Visit https://vimeo.com/ssef.

# MISCELLANEOUS

## DGemG's Gemstone Library

DGemG now provides an online Gemstone Library (in English and German) that is accessible only to DGemG members and contains information on numerous gem materials. A summary of crystallographic, chemical and physical characteristics is provided for each gem, along with tabulations of varieties, localities, treatments and synthetics. Photo galleries are also available with images of inclusions and in some cases also crystals, cut stones, localities and treatments. Further gem materials and information continue to be added to this resource. Visit https://library.dgemg.com/en.

## Natural Diamond Price Guidance

The Natural Diamond Prices website and database (www.naturaldiamondprices.com) were initiated in September 2020 by UNI Diamonds and IDEX (International Diamond Exchange) to provide transparent, unbiased wholesale pricing for polished natural diamonds. The secure data collaboration platform was developed by QEDIT using privacy-enhancing technology, and includes pricing information from more than 120 companies globally. Additional qualified diamond industry members are invited to join and contribute to the database. The latest price guides for round- and fancy-cut diamonds are accessible after signing up for an account.

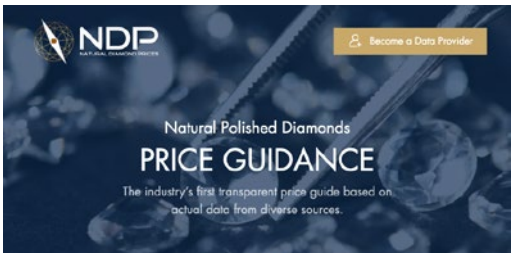


## SSEF's 'Understanding Gemstones' Courses

The Swiss Gemmological Institute SSEF now offers free online courses covering major gem materials—diamond, ruby, sapphire, emerald and pearls—that are available in English, French and simplified Chinese. They are designed for anyone who is curious to learn about gems, as well as trade members looking for expert insight on synthetics, treatments, origins and colour terminology. The courses are self-paced, and each offers a quiz at the end. Visit www.ssef.ch/masterclass.

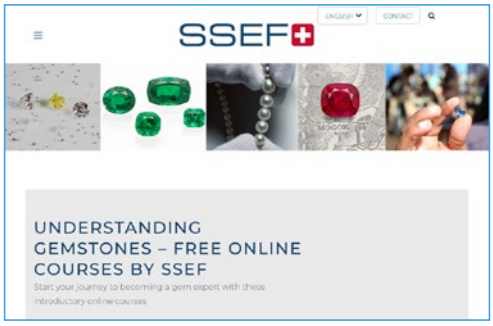


**What's New** provides announcements of new instruments/technology, publications, online resources and more. Inclusion in What's New does not imply recommendation or endorsement by Gem-A. Entries were prepared by Carol M. Stockton unless otherwise noted.

# Gem Notes

## COLOURED STONES

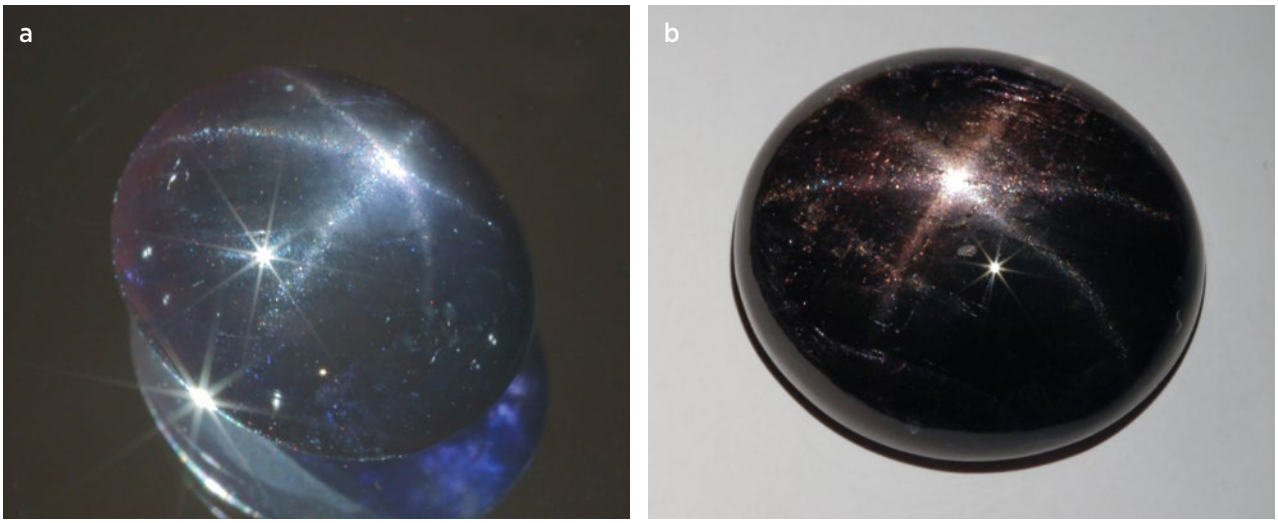


**Figure 1:** The two cabochons shown here weigh 7.02 ct (**a**) and 199 ct (**b**), and display a bluish white six-rayed star, a phenomenon that rarely occurs in iolite. Photos by M. P. Steinbach.

### Origin of Asterism and Chatoyancy in Rare Six-Rayed Star Iolite

*Iolite* is the common gem name for cordierite, a mineral species in the orthorhombic crystal system, which is also sometimes called *water sapphire* or *dichroite*. It is most well known for its strong eye-visible pleochroism, typically in blue, violet and pale yellow, which is due to $Fe^{2+}$–$Fe^{3+}$ intervalence charge transfer (IVCT; Faye *et al.* 1968; Fritsch & Rossman 1988).

We report here on two iolite cabochons weighing 7.02 and 199 ct that each shows a six-rayed star (Figure 1). The occurrence of chatoyancy and asterism in iolite has been reported in the literature but only occasionally illustrated (Da Cunha 1994; Steinbach 2011 [7.02 ct stone described here]; Steinbach 2016, pp. 342–343 [both stones described here]).

The stones were translucent to nearly opaque when viewed from above, and the larger one in particular was partially fractured. They both were very dark in colour but strong lighting revealed a violet body colour. The six-rayed stars appeared bluish white and were of moderate intensity with rather broad rays. The centre of each star was also accompanied by a sheen that reduced its sharpness. Detailed examination revealed a sharp, intense white chatoyant band around the entire circumference of each cabochon (e.g. Figure 2). The narrow illuminated area adjacent to the chatoyant band displayed a reddish colour reminiscent of so-called bloodshot cat's-eye iolite reported by Da Cunha (1994).

Optical microscopy through the dome of each cabochon showed two types of inclusions (Figure 3a). Short acicular inclusions that were responsible for the asterism were oriented along three directions at 60° to one another. The quality of the star was directly related

**Figure 2:** When examined from the side, the star iolite exhibits chatoyancy around the entire circumference, as illustrated here for the 199 ct cabochon. Photo by J.-P. Gauthier.

to the low aspect ratio and low density of these acicular inclusions. Larger platelets contributing to the sheen that appeared superimposed on the asterism had edges that were mostly parallel to the acicular inclusions. Both types of inclusions displayed various colours due to thin-film interference from their nanometre-scale thickness.

Observation through the rim of each sample revealed parallel acicular inclusions oriented along the cabochon axis (i.e. perpendicular to the dome; see Figure 3b). Their high aspect ratio and abundance were consistent with the sharp, intense chatoyant streak as compared to the weaker arms of the six-rayed star. In addition to thin-film interference, many of these inclusions showed a brownish red body colour.

The inclusions producing the asterism, as well as the sheen, were identified by Raman spectroscopy as hematite. The acicular inclusions causing the chatoyant band around the stones are likely also hematite. Hematite inclusions are well known in iolite, particularly the bloodshot variety (Gübelin & Koivula 1986, p. 269).

The crystallographic orientation of the cabochons could be determined from their strong pleochroism since $Fe^{2+}$–$Fe^{3+}$ IVCT takes place in a plane perpendicular to the *c*-axis (Faye *et al*. 1968; Fritsch & Rossman 1988). Although it was challenging to see inside the stones due to their diaphaneity, we were able to observe that their six-rayed star (which was perpendicular to the chatoyant streak) was oriented in the direction in which the violet hue was most visible. This observation is in agreement with Kammerling and Koivula (1991), who described a cat's-eye iolite in which the side of the cabochon (perpendicular to the chatoyant streak) appeared dark violet. As illustrated by Fritsch & Rossman (1988), a violet or intense blue hue can be observed along the *a*-axis of cordierite. This means that the acicular inclusions responsible for the six-rayed star in the present stones were oriented in three directions within the *a*-plane—that is, perpendicular to the *a*-axis—while those responsible for the cat's-eye were parallel to the *a*-axis. These crystallographic observations are identical to those reported in a comprehensive study of cat's-eye and star chrysoberyl from the same (orthorhombic) crystal system (Schmetzer *et al*. 2016). The specific orientation of the six-rayed stars within the *a*-plane remains undetermined and needs further investigation.

In agreement with Da Cunha (1994), we believe at least two types of cat's-eye iolite exist. The cat's-eyes in the two samples of this study are both similar to the chatoyant bloodshot iolite reported by Da Cunha (1994). A second type would display a narrow and fine chatoyant band, as reported by Kammerling & Koivula (1991). Nevertheless, both types seem to be oriented in the same crystallographic direction (with respect to the *a*-axis) but might contain acicular inclusions of different natures.

*Thanh Nhan Bui FGA (tnhan93@gmail.com)*
*Université catholique de Louvain*
*Louvain-la-Neuve, Belgium*

*Aurélien Delaunay and Ugo Hennebois*
*Laboratoire Français de Gemmologie*
*Paris, France*

*Martin P. Steinbach*
*Steinbach – Gems with a Star*
*Idar-Oberstein, Germany*

*Prof. Jean-Pierre Gauthier*
*Centre de Recherches Gemmologiques*
*Nantes, France*

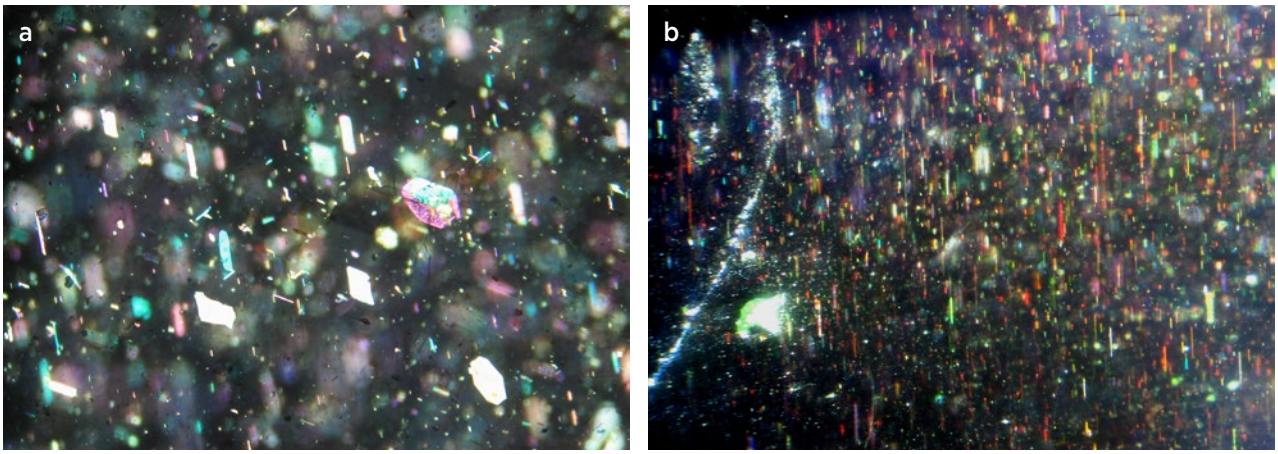


**Figure 3:** (**a**) Optical microscopy through the dome of each star iolite reveals short acicular inclusions in three orientations and larger platelets. Both types lie in the same plane, and the platelets contribute to the sheen superimposed on the asterism. (**b**) Viewed along the rim of the iolite cabochons, parallel acicular inclusions are responsible for the chatoyancy visible around the entire circumference. Photomicrographs by J.-P. Gauthier using fibre-optic illumination; image widths 1.3 mm.

## References

Da Cunha, C. 1994. Cordiérites à effets spéciaux. *Revue de Gemmologie* A.F.G., No. 19, 11–14.

Faye, G.H., Manning, P.G. & Nickel, E.H. 1968. The polarized optical absorption spectra of tourmaline, cordierite, chloritoid and vivianite: Ferrous-ferric electronic interaction as a source of pleochroism. *American Mineralogist*, **53**(7–8), 1174–1201.

Fritsch, E. & Rossman, G.R. 1988. An update on color in gems. Part 2: Colors involving multiple atoms and color centers. *Gems & Gemology*, **24**(1), 3–15, https://doi.org/10.5741/gems.24.1.3.

Gübelin, E.J. & Koivula, J.I. 1986. *Photoatlas of Inclusions in Gemstones*. ABC Edition, Zurich, Switzerland, 532 pp.

Kammerling, R.C. & Koivula, J.I. 1991. Two strongly pleochroic chatoyant gems. *Journal of Gemmology*, **22**(7), 395–398, https://doi.org/10.15506/JoG.1991.22.7.395.

Schmetzer, K., Bernhardt, H.-J. & Gilg, H.A. 2016. Characterization of oriented inclusions in cat's-eye, star and other chrysoberyls. *Journal of Gemmology*, **35**(1), 28–54, https://doi.org/10.15506/JoG.2016.35.1.28.

Steinbach, M.P. 2011. Neue künstlich geritzte Sternsteine und ihre natürlichen Gegenstücke. *Gemmologie: Zeitschrift der Deutschen Gemmologischen Gesellschaft*, **60**(1/2), 25–36.

Steinbach, M.P. 2016. *Asterism – Gems with a Star*. MPS Publishing and Media, Idar-Oberstein, Germany, 896 pp.


## Chatoyant Anorthoclase Feldspar from Dong Nai Province, Vietnam

The feldspar group includes several varieties used as gem materials, and some show interesting optical phenomena such as labradorescence (in labradorite), adularescence (in moonstone) and four-rayed asterism and chatoyancy (in moonstone and sunstone; Ward & Ward 2008). These phenomena have been well described for these feldspars. However, anorthoclase—a type of sodic plagioclase that mainly occurs in high-temperature volcanic rocks—is much less well known to gemmologists (e.g. Laurs *et al.* 2019), and to date the authors are not aware of chatoyancy being reported in this type of feldspar.

During a survey of gems related to basaltic origin in south-eastern Vietnam, we found transparent gem-quality feldspar crystals hosted in basalt and laterite. Among these specimens, we discovered two that showed eye-visible chatoyancy when polished (Figures 4 and 5): sample 1 was yellowish grey and originally weighed 83.0 g, while sample 2 was near-colourless and

**Figure 4:** The two samples of chatoyant anorthoclase from Vietnam described here weigh 325.12 ct (left, sample 1) and 22.66 ct (right, sample 2). Photo by Pham Minh Tien.


**Figure 5:** (**a**) A wide band of yellowish white chatoyancy appears along the length of anorthoclase sample 1. (**b**) A white cat's-eye is displayed by anorthoclase sample 2. Photos by Le Ngoc Nang.

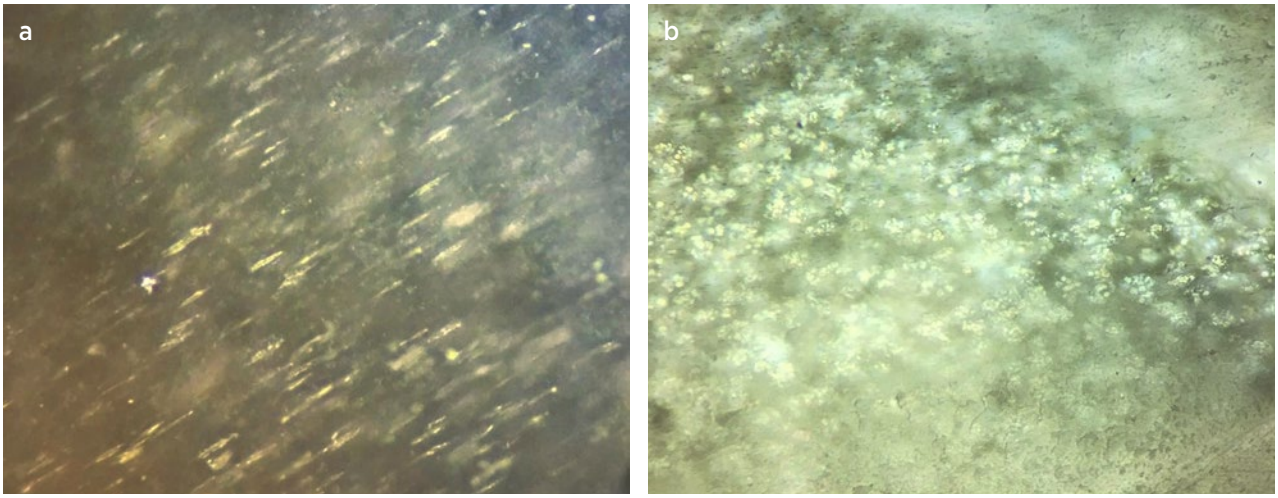


**Figure 6:** The chatoyant effect in the anorthoclase is caused by plate-like fluid inclusions, shown here (**a**) in the direction parallel to the edge of the inclusions and (**b**) in a view nearly 90° to the plane of the inclusions. Photomicrographs by Le Ngoc Nang; magnified 45×.

originlly weighed 8.2 g. We polished sample 1 into a somewhat cylindrical shape (325.12 ct and 55.01 × 26.94 mm; see Figure 4, left) and cut sample 2 into a cabochon (22.66 ct and 21.90–13.89 × 10.03 mm; see Figure 4, right). Sample 1 showed a yellowish white cat's-eye running parallel to the length of the specimen, while the chatoyancy of sample 2 displayed a white colour and was developed horizontally across the cabochon.

Both were tested by standard gemmological methods, as well as Raman and Fourier-transform infrared (FTIR) spectroscopy, at Liu Gemmological Research and Application Center. The RIs were measured as approximately 1.53 for sample 1 (by the spot method) and 1.520–1.532 for sample 2. The hydrostatic SG value of both samples was 2.59. Both were inert to long- and short-wave UV radiation, and they displayed two perfect cleavages at right angles. Sample 2's optical properties indicated an anisotropic, biaxial mineral. Thus, the gemmological characteristics confirmed these specimens to be feldspar (cf. Liddicoat 1993). Microscopic observation showed that their chatoyancy was caused by a dense array of parallel, flattened, roundish fluid inclusions (Figure 6). The chatoyancy was best seen approximately parallel to the edges of the inclusions, while a broad sheen was visible perpendicular to that direction.

FTIR spectroscopy of both specimens displayed prominent absorption bands at 1112, 998, 775 and 712 $cm^{-1}$, indicative of K-feldspar (Bosch-Reig *et al.* 2017). The Raman spectra displayed peaks at 510, 472, 287, 192 and 165 $cm^{-1}$, consistent with anorthoclase (Mernagh 1991).

The recent find of chatoyant anorthoclase in Dong Nai, Vietnam, has enriched the variety of gem species related to basaltic origin from this region. Others include sapphire, garnet and zircon.

*LE Ngoc Nang[1,2] (nang@liulab.edu.vn) and PHAM Minh Tien[2]*

*[1]University of Science, Vietnam National University, Ho Chi Minh City, Vietnam*

*[2]Liu Gemmological Research and Application Center, Ho Chi Minh City, Vietnam*

## References

Bosch-Reig, F., Gimeno-Adelantado, J.V., Bosch-Mossi, F. & Doménech-Carbó, A. 2017. Quantification of minerals from ATR-FTIR spectra with spectral interferences using the MRC method. *Spectrochimica Acta Part A: Molecular and Biomolecular Spectroscopy*, **181**, 7–12, https://doi.org/10.1016/j.saa.2017.02.012.

Laurs, B.M., Evans, C., Daly, P. & Renfro, N.D. 2019. Gem Notes: 'Black anorthoclase' from Antarctica. *Journal of Gemmology*, **36**(5), 402–403.

Liddicoat, R.T. 1993. *Handbook of Gem Identification*, 12th edn. Gemmological Institute of America, Santa Monica, California, USA, 364 pp.

Mernagh, T.P. 1991. Use of the laser Raman microprobe for discrimination amongst feldspar minerals. *Journal of Raman Spectroscopy*, **22**(8), 453–457, https://doi.org/10.1002/jrs.1250220806.

Ward, F. & Ward, C. 2008. *Phenomenal Gems*. Gem Book Publishers, Malibu, California, USA, 64 pp.

## Bicoloured Grossular from Tanzania

Tsavorite is a variety of grossular with a characteristic green colour caused by $V^{3+}$, sometimes in combination with $Cr^{3+}$ (Feneyrol *et al*. 2014). In 2019, some unusual rough bicoloured green and nearly colourless grossular samples were purchased by author RH at the gem market in Arusha, northern Tanzania. The dealer stated that the material came from near the Lelatema Hills in north-eastern Tanzania (the same area mentioned by Kane *et al*. 1990), but the specific location of the deposit was unknown. The eight samples consisted of broken pieces with no crystal faces and weighed approximately 0.5–2 g (e.g. Figure 7). They were subsequently faceted into step cuts (0.81–1.11 ct) to emphasise their colour zoning. Each of the stones contained a nearly colourless portion with a pale yellowish tinge, bordered by a narrow intense green band and then a yellowish green zone (e.g. Figure 8).

Standard gemmological properties were measured for all eight of the faceted stones. Their RI ranged from 1.732 to 1.738 and their hydrostatic SG value was 3.60–3.61; these are typical of lower values for grossular. In general they fluoresced deep red to long-wave UV and brownish yellow to short-wave UV radiation. However, the narrow intense green band in the stones was inert to both long- and short-wave UV radiation. Viewed with the Chelsea filter, the yellowish green and intense green sections of the stones appeared distinct red, while the nearly colourless zone looked very light green. All of the samples contained numerous fluid inclusions, which were only visible with a 10× loupe. In addition, tiny mineral inclusions could be seen with the microscope (minimum 100×).

**Figure 7:** This gemmy fragment of grossular from Tanzania (1.8 g) shows distinct colour zoning. Photo by Ľubomír Kyrc.

**Figure 8:** This 0.85 ct bicoloured grossular has a narrow intense green band that separates the larger yellowish green and nearly colourless zones. Photo by R. Hanus.

Raman spectroscopy with 532 nm laser excitation was performed on both the nearly colourless and yellowish green portions of the stones. No significant difference was found between these two colour zones (Figure 9), but during the measurement there was a slightly increased background in the lower-wavenumber portion of the spectrum, mainly in the yellowish green parts of the samples. The spectra otherwise correlated well with features seen in tsavorite, with characteristic peaks at around 373, 542, 822 and 878 $cm^{-1}$ relating to different types of $SiO_4$ tetrahedra vibrations (Kolesov & Geiger 1998).

The sharp colour zoning shown by these garnets is quite different from the gradual shift in colouration (from very light to strong green) shown by grossulars from Kenya that were documented by Zwaan (2014). In the future, the authors plan to undertake a more detailed mineralogical and gemmological study of these interesting Tanzanian samples.

*Terézia Babirádová*[1], *Dr Radek Hanus (hanusrdk@gmail.com)*[2], *Kamil Sobek*[1] *and Dr Jan Cempírek*[1]

[1]*Department of Geological Sciences, Masaryk University, Faculty of Science, Brno, Czech Republic*

[2]*Gemological Laboratory of* e-gems.cz, *Prague, Czech Republic*

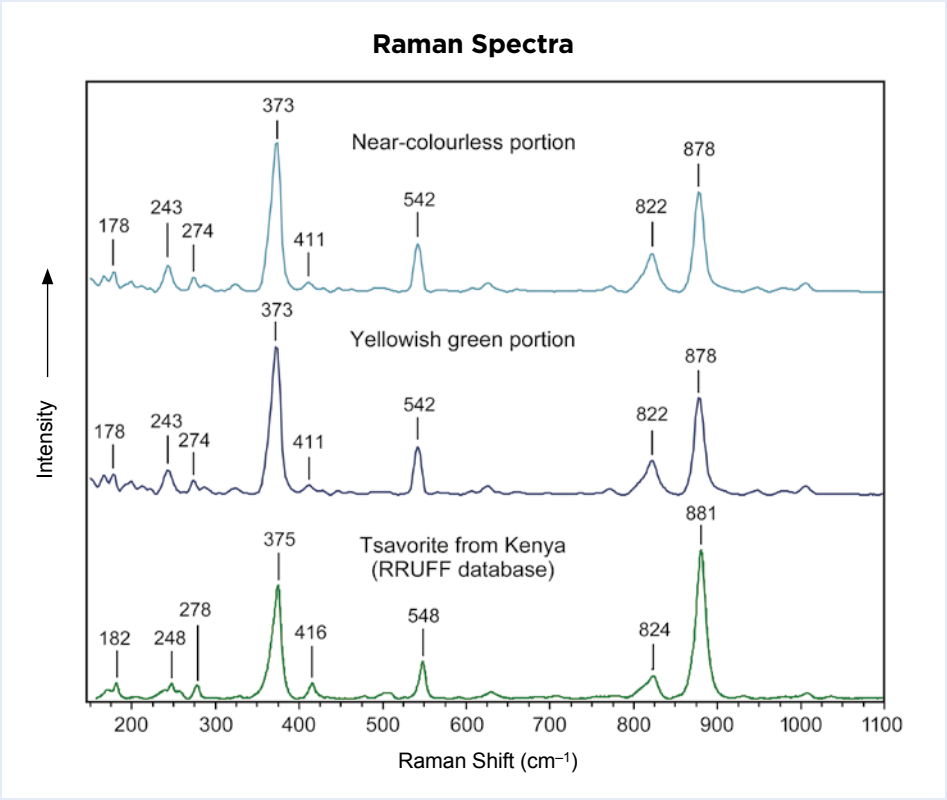


**Figure 9:** Representative background-corrected Raman spectra of the nearly colourless and yellowish green zones of the bicoloured grossular from Tanzania are compared to typical tsavorite from Kenya.

## References


Feneyrol, J., Giuliani, G., Ohnenstetter, D., Rondeau, B., Fritsch, E., Fallick, A.E., Ichang'i, D., Omito, E. *et al.* 2014. New typology and origin of tsavorite based on trace-element chemistry. *European Journal of Mineralogy*, **26**, 293–308, https://doi.org/10.1127/0935-1221/2014/0026-2367.

Kane, R.E., Kampf, A.R. & Krupp, H. 1990. Well-formed tsavorite gem crystals from Tanzania. *Gems & Gemology*, **26**(2), 142–148, https://doi.org/10.5741/gems.26.2.142.

Kolesov, B.A. & Geiger, C.A. 1998. Raman spectra of silicate garnets. *Physics and Chemistry of Minerals*, **25**(2), 142–151, https://doi.org/10.1007/s002690050097.

Zwaan, J.C. 2014. Gem Notes: Bicoloured grossular from Kambanga, Kenya. *Journal of Gemmology*, **34**(3), 195–197.


## Pargasite from Lajuar Madan, Badakhshan, Afghanistan

During the February 2018 gem shows in Tucson, Arizona, USA, gem dealer Dudley Blauwet (Dudley Blauwet Gems, Louisville, Colorado, USA) loaned the authors two faceted samples of pargasite from Afghanistan for gemmological examination. The specimens were cut from rough material that was obtained by Blauwet in June 2014, and was reportedly mined from the famous skarn-hosted lapis lazuli deposits near Lajuar Madan in the Kuran wa Munjan District of Badakhshan Province.

The two stones consisted of transparent faceted oval cuts weighing 0.27 ct (5.22 × 3.54 × 2.33 mm) and 0.65 ct (6.68 × 4.98 × 3.22 mm), and were light yellowish brown (Figure 10). The RIs of both stones were 1.620–1.642,

**Figure 10:** These yellowish brown gems (left, 0.65 ct; right, 0.27 ct) from Badakhshan, Afghanistan, proved to be pargasite. Photo by J. C. Zwaan.

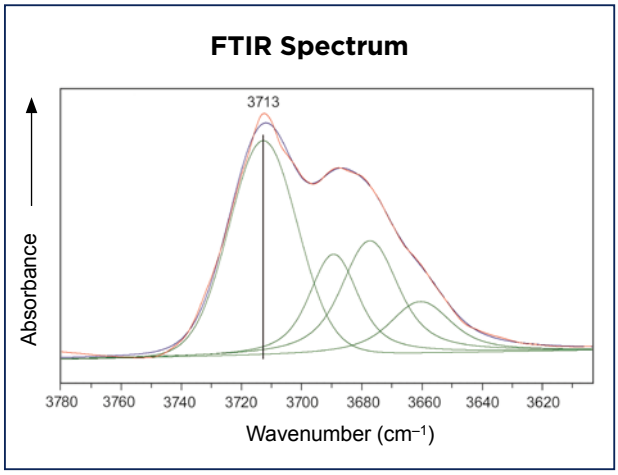


**Figure 11:** A representative FTIR spectrum in the OH-stretching region corresponds to the spectrum of pargasite (cf. Day *et al.* 2018). The red curve is the spectrum of the 0.27 ct sample and the dark blue curve is the resultant fitted line from the deconvolution of the spectrum (as shown by the green traces).

yielding a birefringence (DR) of 0.022. The optic character was biaxial positive. Average hydrostatic SG values were 3.10 and 3.07, respectively. Using a calcite dichroscope, weak pleochroism in pale yellow and slightly brownish yellow colours was discerned. The gems fluoresced very weak red under long-wave UV radiation, and moderate yellow (0.27 ct) or weak yellow (0.65 ct) under short-wave UV.

The 0.27 ct oval contained parallel growth tubes and a cluster of small mineral inclusions near the pavilion. Raman analysis identified diopside, zircon and sodalite in the cluster. The 0.65 ct oval contained partially healed fissures consisting of rectangular multiphase inclusions. Due to their small sizes and positions, these inclusions could not be analysed in further detail.

Using standard gemmological testing alone, it was difficult to identify these stones with confidence. From the optical data, the samples were established as amphiboles, and their optic character prevents confusion with tourmaline. However, the RI, birefringence and SG values closely match those of various amphiboles, including richterite (RI 1.605–1.641, DR 0.017–0.022, SG 2.97–3.45), pargasite (RI 1.613–1.650, DR 0.020–0.022, SG 3.07–3.81) and edenite (RI 1.606–1.672, DR 0.023–0.025, SG 3.00–3.06; Dedeyne & Quintens 2007). The SG values are at the highest and lowest limits for edenite and pargasite, respectively.

Day *et al.* (2018) characterised colourless gem-quality richterite and pargasite, also from Afghanistan. Fitted FTIR spectra in the OH-stretching region of the present samples accordingly corresponded to the spectrum of pargasite, with the strongest band at 3713 $cm^{-1}$ (Figure 11). This excluded richterite (strongest band at 3730 $cm^{-1}$) as a possibility. However, Raman spectra seemed to more closely match the spectra of edenite in the RRUFF database, which show a principal band at 674 $cm^{-1}$, slightly shifted from the typical position for pargasite at 668 $cm^{-1}$ (Figure 12).

Therefore, to confirm the identification of these samples, they were analysed by electron microprobe by authors MD and FCH. Based on three spot analyses on each stone, the analyses gave the following average compositions for the 0.27 ct (1) and 0.65 ct (2) specimens:

(1) $(Na_{0.87}K_{0.13})_{1.00}(Ca_{1.60}Na_{0.40})_2(Mg_{4.03}Al_{0.70}Ti_{0.09}Fe^{2+}_{0.02}Mn_{0.01})_{4.85}(Si_{6.82}Al_{1.18})_8O_{22}(OH_{1.67}F_{0.33})_2$

(2) $(Na_{0.85}K_{0.12})_{0.97}(Ca_{1.60}Na_{0.40})_2(Mg_{4.20}Al_{0.61}Ti_{0.09}Fe^{2+}_{0.02}Mn_{0.01})_{4.93}(Si_{6.79}Al_{1.21})_8O_{22}(OH_{1.69}F_{0.31})_2$

Considering the general formula $AB_2C_5T_8O_{22}W_2$ for amphibole supergroup minerals and their current classification (Hawthorne *et al.* 2012), the specimens clearly are calcium amphiboles, based on $^{B}Ca/^{B}(Ca+Na) = 0.8$. According to the compositional boundaries of calcium amphiboles, they plot nicely in the pargasite field, with $^{A}(Na+K+2Ca) = 1.00$ and 0.88, and $^{C}(Al+Fe^{3+}+2Ti) = 0.97$ and 0.79, respectively (Figure 13).

The current classification of amphiboles is based on the A, B and C cations, rather than on the A, B and T cations as proposed earlier by Leake *et al.* (1997). The 6.8 Si atoms at the T site would have classified these samples as edenite in this previous classification (5.5–6.5 Si for pargasite, >6.5 Si for edenite). This could explain the discrepancy of the Raman spectra indicating edenite, showing a main band at 674 $cm^{-1}$, which is assigned to vibration of bridging oxygen atoms ($O_b$) that link adjacent $SiO_4$ tetrahedra (Si–$O_b$–Si symmetrical stretching; Apopei & Buzgar 2010).

These examples show that there are limitations in the use of standard gemmological equipment and Raman spectroscopy to correctly identify an amphibole, and that reference Raman spectra of amphiboles need re-evaluation, updating (including the OH-stretching region in the higher spectral range) and further study.

*Dr J. C. (Hanco) Zwaan FGA*
*(hanco.zwaan@naturalis.nl)*
*Netherlands Gemmological Laboratory*
*Naturalis Biodiversity Center*
*Leiden, The Netherlands*

*Maxwell C. Day and Dr Frank C. Hawthorne*
*University of Manitoba*
*Winnipeg, Manitoba, Canada*

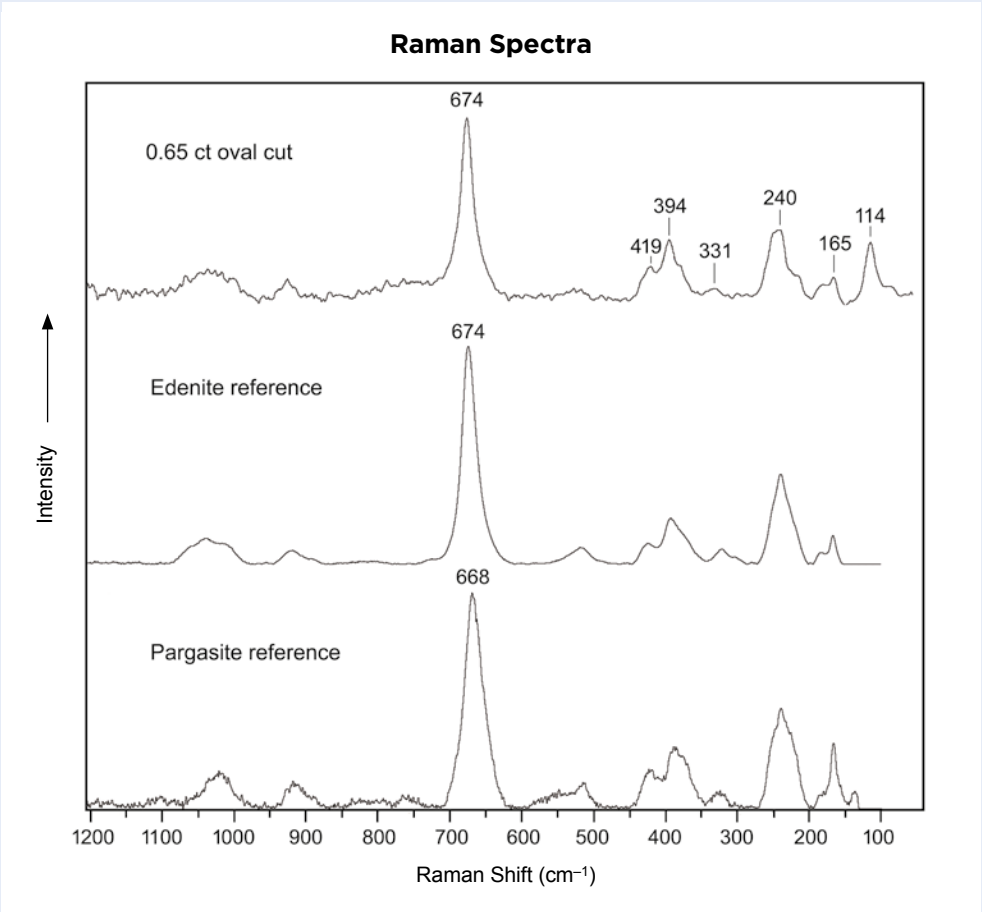


**Figure 12:** Raman spectra of both stones gave a best match with edenite spectra in the RRUFF database. The spectrum shown here is for the 0.65 ct sample.

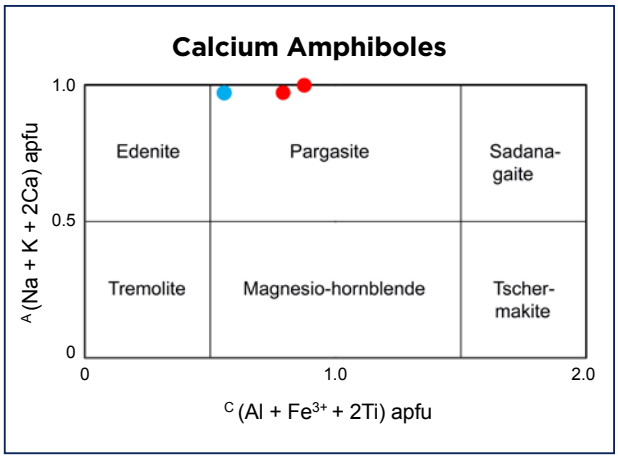


**Figure 13:** Compositional boundaries of calcium amphiboles show that the two faceted samples examined here (red dots) fall within the pargasite field. For comparison, the blue dot indicates the composition of a pargasite from Afghanistan analysed previously by Day *et al.* (2018).

## References


Apopei, A.I. & Buzgar, N. 2010. The Raman study of amphiboles. *Analele Ştiinţifice ale Universităţii "Al. I. Cuza" Iaşi*, **56**(1), 57–83.

Day, M.C., Hawthorne, F.C., Susta, U., Della Ventura, G. & Harlow, G.E. 2018. Short-range order-disorder in gem richterite and pargasite from Afghanistan: Crystal-structure refinement and infrared spectroscopy. *Canadian Mineralogist*, **56**(6), 939–950, https://doi.org/10.3749/canmin.1800052.

Dedeyne, R. & Quintens, I. 2007. *Tables of Gemstone Identification*. Glirico, Gent, Belgium, 309 pp.

Hawthorne, F.C., Oberti, R., Harlow, G.E., Maresch, W.V., Martin, R.F., Schumacher, J.C. & Welch, M.D. 2012. Nomenclature of the amphibole supergroup. *American Mineralogist*, **97**(11–12), 2031–2048, https://doi.org/10.2138/am.2012.4276.

Leake, B.E., Woolley, A.R., Arps, C.E.S., Birch, W.D., Gilbert, M.C., Grice, J.D., Hawthorne, F.C., Kato, A. *et al.* 1997. Nomenclature of amphiboles: Report of the Subcommittee on Amphiboles of the International Mineralogical Association Commission on New Minerals and Mineral Names. *European Journal of Mineralogy*, **9**(3), 623–651, https://doi.org/10.1127/ejm/9/3/0623.

**Figure 14:** These violet-to-purple and reddish brown-to-pink spinels were mined from the Kuran wa Munjan District in Badakhshan Province, Afghanistan. The faceted stones at the bottom weigh 0.47–1.23 ct. Photo by S. Hänsel.

## Update on Purple Spinel from Afghanistan

Afghanistan is known for high-quality emerald, ruby and lapis lazuli, as well as spinel. Pink-to-red spinel has been mined from the Badakhshan region of eastern Afghanistan, close to the famous mines of Kuh-i-Lal, Tajikistan, since ancient times (Hughes 1994). Starting in early 2017, attractive purple spinels from Badakhshan entered the markets in Thailand and the USA (Boehm 2017). Recently, one of the authors (SH) purchased 450 g of small-sized rough violet-to-purple spinel from a Pakistani dealer, who reported that it came from the Zo Valley in the Kuran wa Munjan District of southern Badakhshan. Several others who buy rough gems from that area confirmed this locality. Surprisingly, 90% of the rough material showed not only lamellar growth lines but also complex twinning in several directions (e.g. Figure 14, centre), and only a few pieces had the classic octahedral shape that is typical of spinels from some other primary deposits.

After cutting some of the rough spinel, author SH selected eight faceted violet-to-purple gems (0.47–1.23 ct; Figure 14, bottom row) for standard gemmological testing. In addition, windows were polished on several of the remaining rough samples. The gemmological properties were typical for natural spinel: RI = 1.715 (± 0.001) and SG = 3.53 (± 0.05). Most stones were inert to both long- and short-wave UV radiation, although some clean ones showed a slightly greenish reaction to long-wave UV. All of them exhibited a strong pink reaction when viewed with the Chelsea Colour Filter.

Microscopic observation revealed mineral inclusions consisting of rutile (Figure 15a–c), apatite (Figure 15d) and zircon (Figure 15e). Clusters of mica (Figure 15f) were also present in some stones and resembled those documented in Afghan purple spinel by Boehm (2017). The identity of all of these inclusions was confirmed by Raman micro-spectroscopy using a Renishaw inVia instrument.

Additional testing of 11 violet-to-purple rough and faceted samples was done at The Gem and Jewelry Institute of Thailand (GIT). Ultraviolet-visible (UV-Vis) spectroscopy performed with a PerkinElmer Lambda 1050 spectrophotometer revealed absorption features at 372, 386, 458 and 555 nm (Figure 16) related to iron. The absorption at 458 nm is due to $Fe^{3+}$, while those at 372, 386 and 555 nm are due to $Fe^{2+}$ (D'Ippolito *et al.* 2015); together they create transmission windows

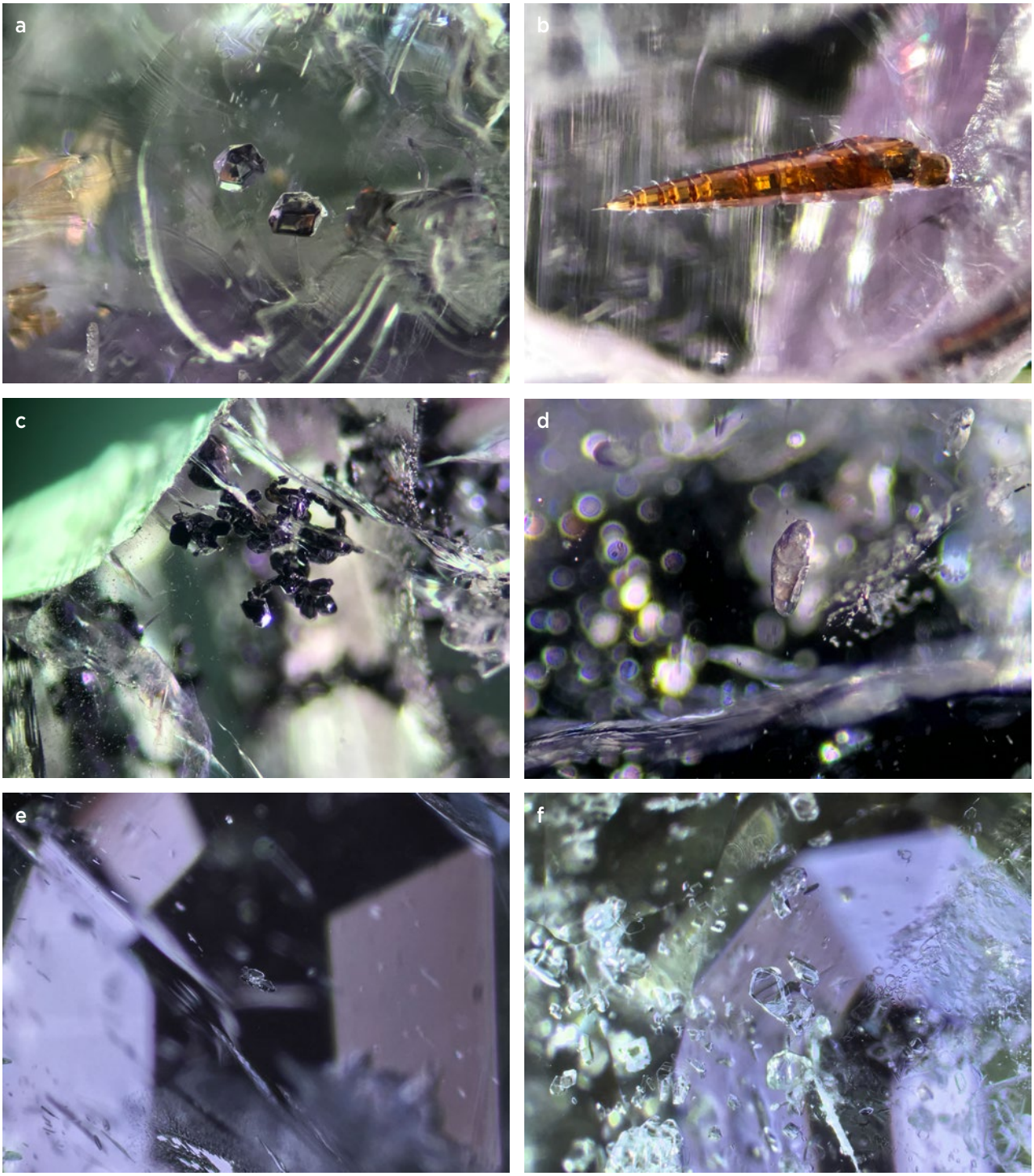


**Figure 15:** Mineral inclusions in the spinels consist of rutile (**a**–**c**), apatite (**d**), zircon (**e**) and mica (**f**). Photomicrographs by S. Hänsel in darkfield illumination; magnified approximately 90×.

in the red and blue regions that are responsible for the purple colouration.

Chemical analysis of these 11 samples was performed at GIT by laser ablation inductively coupled plasma mass spectrometry (LA-ICP-MS) using a Thermo Scientific iCAP RQ ICP-MS coupled to a New Wave Research NWR213 laser ablation unit. Iron was by far the most abundant trace element (average 10,170 ppm), consistent with the absorption features recorded in the UV-Vis spectrum. Also present were traces of Zn, Ga, Mn, Ti, Ni, V, Be, Li, Co, Cr and Cu (Table I). All of these elements have been documented previously in gem spinels from various deposits (cf. Peretti *et al.* 2015).

The seller of these purple spinels indicated that such material is more commonly appearing in the local markets of Afghanistan and Pakistan, often mixed with

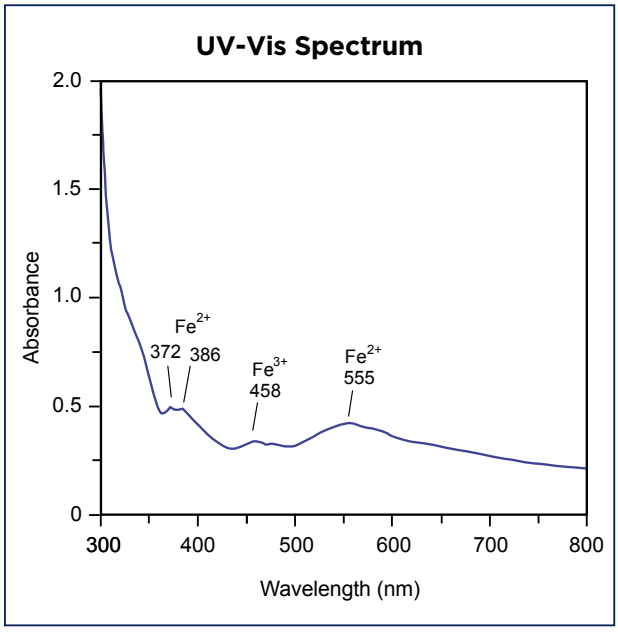


**Figure 16:** This representative UV-Vis spectrum of a purple spinel from Afghanistan (about 3.0 mm path length) shows absorption peaks related to $Fe^{2+}$ and $Fe^{3+}$.

purplish pink spinel. Both colour varieties are said to originate from mines in the Kuran wa Munjan District. The carrot-shaped crystal form of the rutile inclusions documented here is not commonly encountered in spinels from other deposits and may provide a good indicator for Badakhshan material.

*Sebastian Hänsel FGA*
*International Colored Gemstone Laboratory*
*Bangkok, Thailand*

*Thanapong Lhuaamporn (lthanapong@git.or.th),*
*Montira Seneewong-Na-Ayutthaya and*
*Cheewaporn Suphan*
*GIT Gem Testing Laboratory*
*Bangkok, Thailand*

**Table I:** Trace-element concentrations in violet-to-purple spinels from Afghanistan, as determined by LA-ICP-MS.

| Element | Average (ppm) | Range (ppm) |
|---|---|---|
| Li | 23.3 | 8.60–39.7 |
| Be | 26.2 | 12.7–53.0 |
| Ti | 83.5 | 69.4–99.9 |
| V | 28.0 | 17.3–39.5 |
| Cr | 1.04 | <0.36–3.60 |
| Mn | 243 | 196–287 |
| Fe | 10170 | 8720–12210 |
| Co | 8.91 | 5.49–15.2 |
| Ni | 39.7 | 18.9–59.3 |
| Cu | 0.23 | <0.03–4.37 |
| Zn | 1160 | 420–2510 |
| Ga | 329 | 185–526 |

## References

Boehm, E.W. 2017. Gem Notes: Purple spinel from Badakhshan, Afghanistan. *Journal of Gemmology*, **35**(8), 694–697.

D'Ippolito, V., Andreozzi, G.B., Hålenius, U., Skogby, H., Hametner, K. & Günther, D. 2015. Color mechanisms in spinel: Cobalt and iron interplay for the blue color. *Physics and Chemistry of Minerals*, **42**(6), 431–439, https://doi.org/10.1007/s00269-015-0734-0.

Hughes, R.W. 1994. The rubies and spinels of Afghanistan — A brief history. *Journal of Gemmology*, **24**(4), 256–267, https://doi.org/10.15506/JoG.1994.24.4.256.

Peretti, A., Kanpraphai-Peretti, A. & Günther, D. 2015. World of magnificent spinel: Provenance and identification. *Contributions to Gemology*, No. 11, 285–292.

# DIAMONDS

## Treated Greenish Yellow Diamond with Brown Radiation Stains

The Swiss Gemmological Institute SSEF recently analysed a treated greenish yellow diamond showing evidence of artificial irradiation and annealing (Figure 17). This 1.07 ct cushion-shaped stone exhibited very strong greenish yellow fluorescence under long-wave UV radiation (with slightly less intensity under short-wave UV). The greenish yellow fluorescence was visible even in normal daylight.

Infrared spectroscopy (Figure 18) revealed that it was type IaAB, and contained approximately 64 ppm nitrogen as A centres and 135 ppm nitrogen as B centres (based on absorption coefficients given in Boyd *et al.* 1994, 1995), as well as platelets and hydrogen-related defects. In addition, two clear absorption lines at 5163 and 4934 $cm^{-1}$ indicated the presence of H1c and H1b centres, respectively (Figure 18, inset).

**Figure 17:** The 1.07 ct greenish yellow diamond described here was identified as having been artificially irradiated and annealed. Photo by Luc Phan, © SSEF.

Low-temperature (–120°C) UV-Vis absorption spectroscopy indicated the presence of N7, N6, N4, N3, H4 and H3 centres (Figure 19). The H3 centre, causing an absorption line at 503.2 nm, also emits light at the same wavelength when excited by UV radiation, which explains the strong greenish yellow fluorescence. According to Collins (2003), when both the H3 and H4 optical centres are dominant in a diamond, they suggest that the stone was artificially irradiated and annealed. In irradiated and annealed type Ia diamonds, the ratio of H3 to H4 is proportional to the ratio of A to B aggregates as observed in the infrared region. However, traces of the H4 defect can occasionally be detected in untreated stones. In that case, the H4 is always much weaker than the H3 centre, even if most of the nitrogen is found in B centres (Collins 2003). Figure 19 shows that the strength of the H4 line in the greenish yellow stone described here is of the same order of magnitude as the H3 line, providing further evidence that the stone was subjected to artificial treatment. This is confirmed by the observation of H1c and H1b features in the infrared spectrum.

A series of naturals along the faceted girdle of the stone could be seen with the gemmological microscope. Interestingly, two brown stains were also visible (Figure 20). The larger of the two stains coincided with a small natural, perhaps resembling in shape the remnants of a stained etch channel after polishing (cf. Moses & Reinitz 1991).

Brown and green radiation stains on natural diamonds have been described by many authors (e.g. Nasdala *et al*. 2013; Eaton-Magaña & Moe 2016) and are often regarded as indicating that the colour of a diamond is of natural origin. Fake green stains introduced deliberately

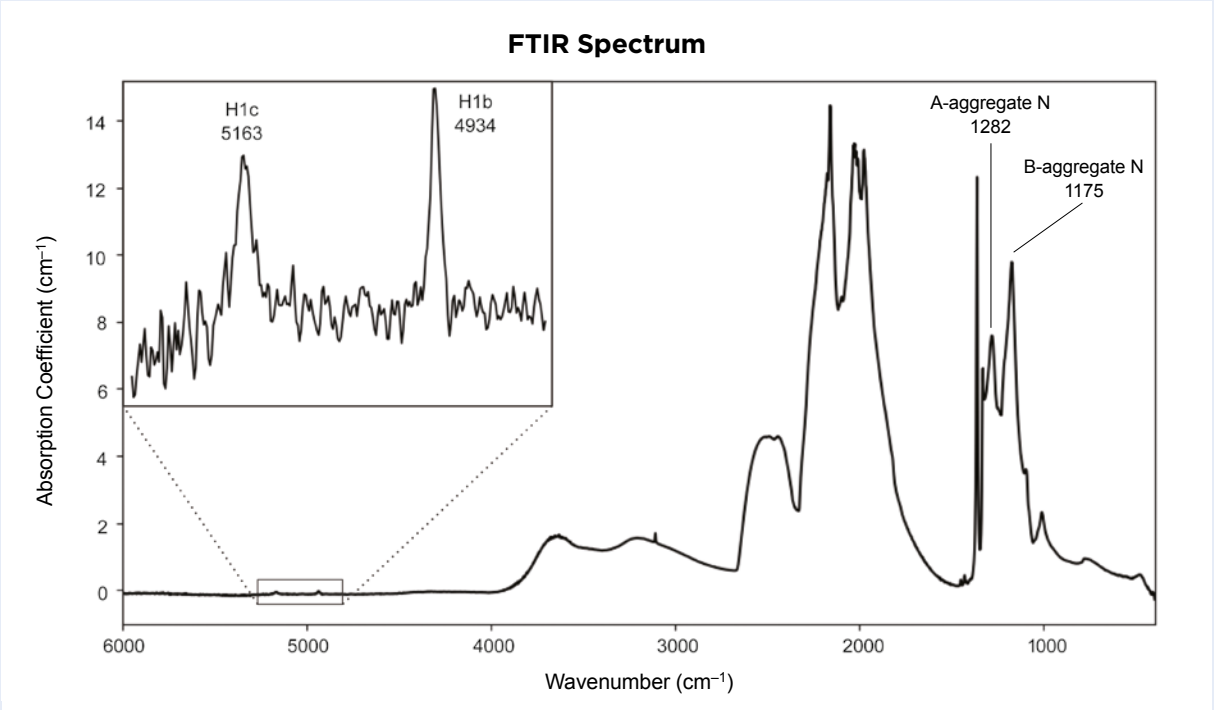


**Figure 18:** The infrared spectrum of the diamond indicates that it is type IaAB, containing nitrogen in the form of A aggregates (approximately 64 ppm) and B aggregates (about 135 ppm). The inset of the area between 5300 and 4800 $cm^{-1}$ shows that H1b and H1c lines are clearly visible, pointing towards treatment.

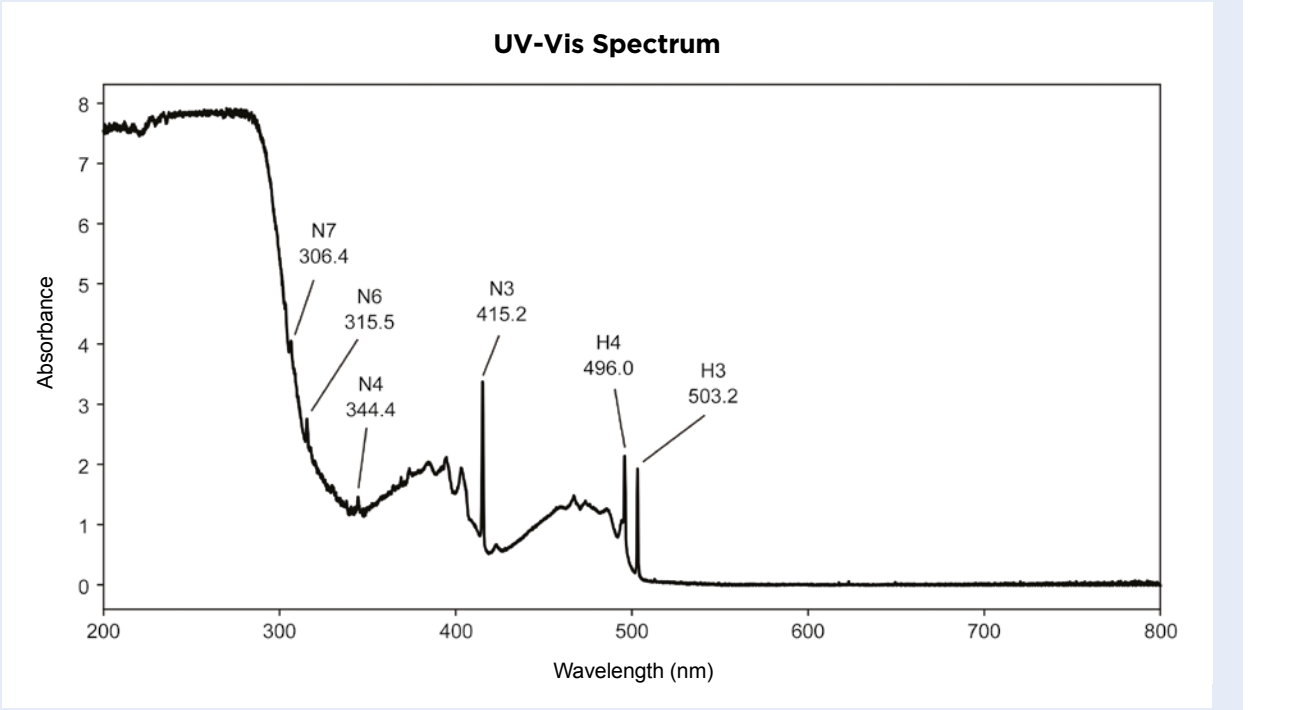


**Figure 19:** The UV-Vis spectrum of the treated greenish yellow diamond exhibits a large N3 feature, as well as related N4, N6 and N7 lines. The H3 centre in conjunction with a strong H4 line provides strong evidence of treatment.

to mimic natural radiation stains have also been reported (Schwartz & Breeding 2019). The stains seen in Figure 20, however, cannot be confused with fake stains (e.g. such as those consisting of platy green Cr-oxide crystals adhering to the surface that can easily be removed).

The absence of GR1 and 594 nm spectral features and the presence of the H4 centre in the greenish yellow diamond described here imply that is was annealed at a temperature greater than 800°C (Collins 2003). In addition, when subjected to heat treatment, irradiation stains in diamond first change from green to brown, and then become fainter and eventually disappear at temperatures greater than 1400°C (Nasdala *et al.* 2013; Eaton-Magaña & Moe 2016). Thus, the conditions of heating to which this diamond apparently was subjected are consistent with the faint brown stains we observed.

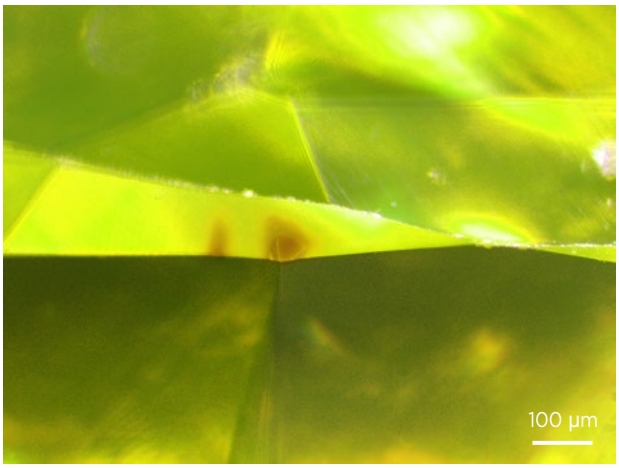


**Figure 20:** Two brown radiation stains can be seen on the girdle of the treated greenish yellow diamond in Figure 17. The stain to the right coincides with a natural. Photomicrograph by L. Speich, © SSEF.

Determining the colour authenticity of greenish yellow diamonds is challenging since they can be of natural colour (e.g. Chalain *et al.* 2004), HPHT treated (e.g. Collins *et al.* 2000), or irradiated and annealed like the stone described here. Radiation stains are often regarded as a strong indicator of natural colour and, to the best of our knowledge, brown stains occurring on the surface of a treated diamond have not been reported previously. However, our findings show that the presence of brown radiation stains does not preclude artificial modification of a diamond's colour, so further examination by spectroscopy is needed.

*Jean-Pierre Chalain and*
*Dr Laura Speich (diamonds@ssef.ch)*
*Swiss Gemmological Institute SSEF*
*Basel, Switzerland*

### References

Boyd, S.R., Kiflawi, I. & Woods, G.S. 1994. The relationship between infrared absorption and the A defect concentration in diamond. *Philosophical Magazine B*, **69**(6), 1149–1153, https://doi.org/10.1080/01418639408240185.

Boyd, S.R., Kiflawi, I. & Woods, G.S. 1995. Infrared absorption by the B nitrogen aggregate in diamond. *Philosophical Magazine B*, **72**(3), 351–361, https://doi.org/10.1080/13642819508239089.

Chalain, J.-P., Bosshart, G. & Hammer, V. 2004. Spectroscopic properties of an historical greenish yellow diamond. *55th Diamond Conference*, University of Warwick, 3 pp. (unpublished).

Collins, A.T. 2003. The detection of colour-enhanced and synthetic gem diamonds by optical spectroscopy. *Diamond and Related Materials*, **12**(10–11), 1976–1983, https://doi.org/10.1016/s0925-9635(03)00262-0.

Collins, A.T., Kanda, H. & Kitawaki, H. 2000. Colour changes produced in natural brown diamonds by high-pressure, high-temperature treatment. *Diamond and Related Materials*, **9**(2), 113–122, https://doi.org/10.1016/s0925-9635(00)00249-1.

Eaton-Magaña, S.C. & Moe, K.S. 2016. Temperature effects on radiation stains in natural diamonds. *Diamond and Related Materials*, **64**, 130–142, https://doi.org/10.1016/j.diamond.2016.02.009.

Moses, T. & Reinitz, I. 1991. Gem Trade Lab Notes: Diamond—Green, with radiation stains in etch channels. *Gems & Gemology*, **27**(2), 110.

Nasdala, L., Grambole, D., Wildner, M., Gigler, A.M., Hainschwang, T., Zaitsev, A.M., Harris, J.W., Milledge, J. *et al*. 2013. Radio-colouration of diamond: A spectroscopic study. *Contributions to Mineralogy and Petrology*, **165**(5), 843–861, https://doi.org/10.1007/s00410-012-0838-1.

Schwartz, V.A. & Breeding, C.M. 2019. Lab Notes: Rough diamond crystal with an unusual coating of fake green "radiation stains". *Gems & Gemology*, **55**(2), 247–249.


# INSTRUMENTATION

## Portable Spectroscopy Using a GoSpectro Device with a Smartphone

GoyaLab, a French start-up company, offers spectroscopy-based tools (www.goyalab.com). Among these is the GoSpectro (Stockton 2017), a handheld diffraction-type spectrometer that can be connected via an adapter to the camera of a compatible smartphone or tablet. Since the adapter does not fit every smartphone, it is important to check the list of compatible devices on GoyaLab's website. An optional optical fibre with a stand is available separately to make the device easier to handle (Figure 21). The GoSpectro device requires an app, which is freely available for use with either iOS or Android mobile devices.


**Figure 21:** The set-up used for the experiments described in this report consisted of the GoSpectro device attached to a smartphone (Sony Xperia Z2), with the optional optical fibre and stand. A KL2 fibre-optic lamp (Schneider Gemmologie, Idar-Oberstein) was used as the light source. Photo by Q. Wang, German Gemmological Association.

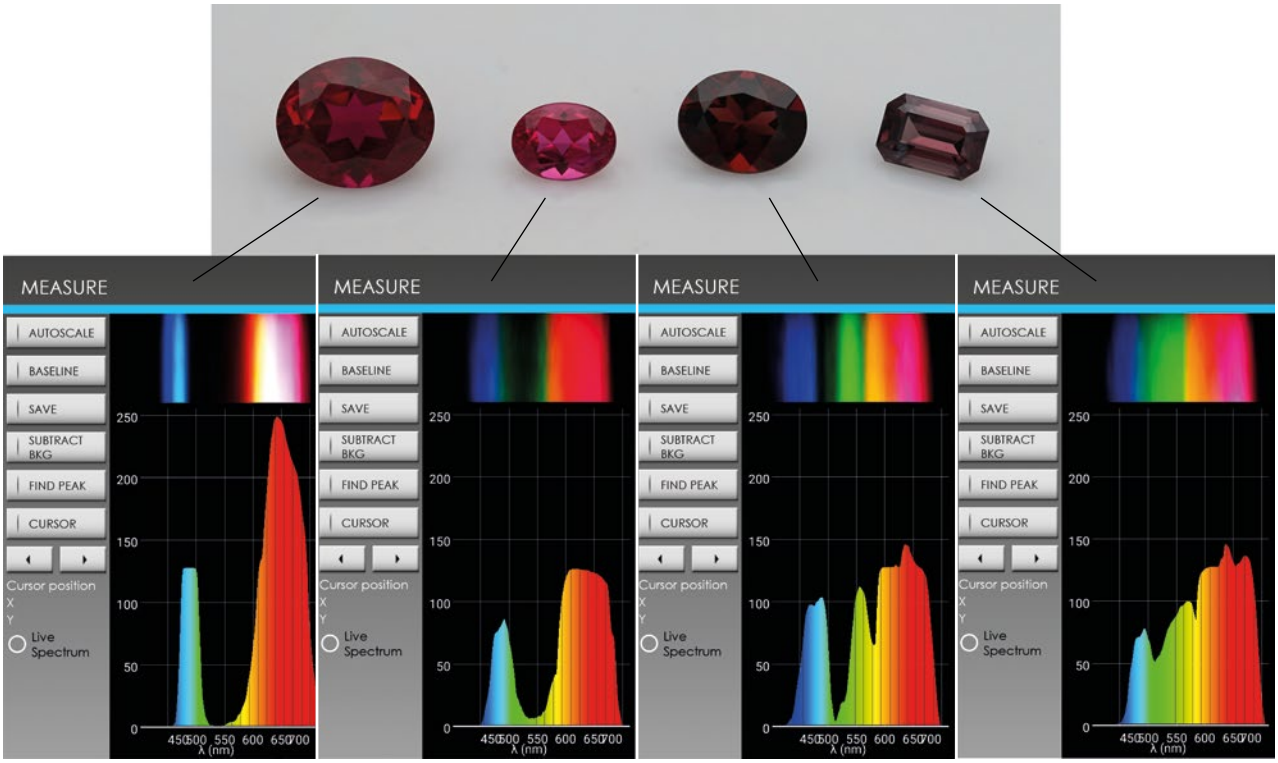


**Figure 22:** The absorption and transmission spectra of four samples (left to right: synthetic ruby, spinel, almandine and zircon) are shown here for comparison. The 'classic' visible absorption spectrum at the top of the app's display is sometimes a bit blurry and narrow absorption lines are often not visible. The transmission spectrum below it, however, is clearer.

According to GoyaLab, the spectrometer operates in the visible range (400–750 nm) with a spectral resolution of 10 nm and reproducibility of 1 nm. It allows one to characterise the spectral composition of different light sources and measure visible-range spectra in emission, transmission or reflection, and—using a UV lamp as a light source—also fluorescence spectra. A short application note is available on GoyaLab's website at https://tinyurl.com/6wz4445c. Setting up the device requires some time and practise, but once it has been properly adjusted, using the hardware and the app is more-or-less self-explanatory. With the app, not only can the 'classic' visible absorption spectrum of gem materials be observed, but the device also can display the graphical transmission spectrum (i.e. graph of wavelength vs transmittance).

The author tested the GoSpectro device on various gem samples, including natural stones, synthetics and imitations. As an example, Figure 22 shows the spectra measured for four pink-to-red stones: a Verneuil synthetic ruby, a pinkish red spinel, an almandine and a greyish pink zircon. In all of the experiments undertaken for this report, the measurement of the spectra worked very well, especially for the major absorption bands of samples with saturated colour. If not perfectly adjusted, the 'classic' visible absorption spectrum displayed at the top of the screen was often a bit blurry, but the graphical transmission spectrum below it clearly showed the positions of the absorption bands. It took a little getting used to, since the graphical spectra are shown in transmission rather than absorption, but the spectral-coloured background helps explain a sample's colouration (again, see Figure 22).

Almost every artificial light source generates some absorption features (e.g. Figure 23, left). In laboratory spectroscopy, these inhomogeneities can be removed by measuring the background and subtracting the reference spectrum of the light source. However, the GoSpectro app does not offer the option to completely remove the narrow peaks of most light sources. As a result, problems can occur with the detection of narrow absorption features of some gem materials (e.g. apatite, peridot, zircon, etc.) if they overlap these artefacts. A similar problem may occur when measuring less-saturated stones, where weaker bands are superimposed by artefacts from the light source. Therefore, before measuring a stone's spectrum with the GoSpectro device, it is important to carefully investigate the spectrum of the light source to learn the position of such artefacts (as also recommended when using a 'classic' handheld spectroscope).

The 'Analyze' function of the GoSpectro app allows the user to save spectra as TXT files, to display and compare them, and to use a zoom function as well as a cursor to mark the exact position of an absorption feature (Figure 24).

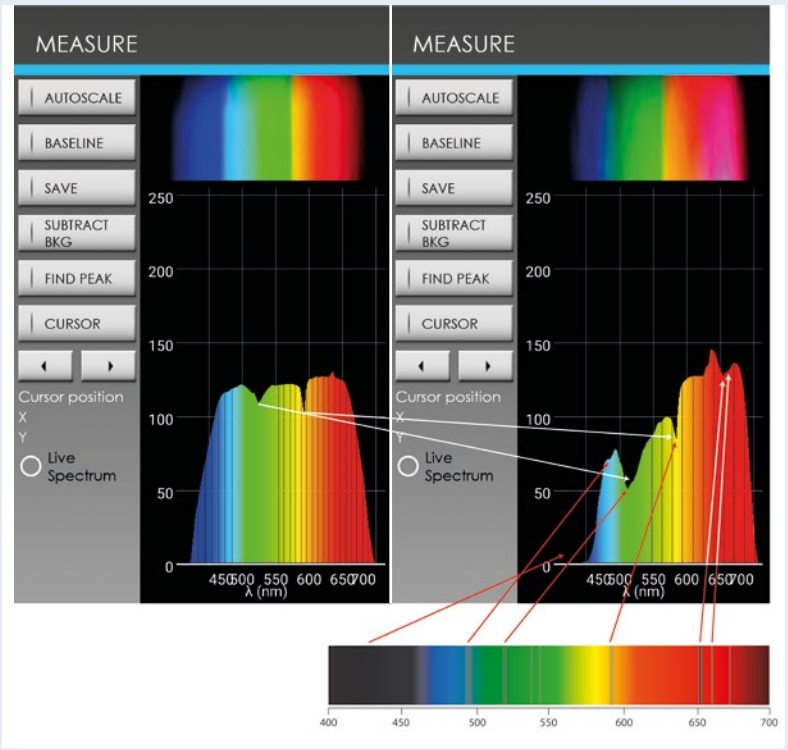


**Figure 23:** A comparison of the spectra obtained from the light source (left-hand screen) and the zircon sample from Figure 22 (right-hand screen) reveals the presence of two artefacts from the light source at approximately 525 and 590 nm in the zircon spectrum, although the latter one overlaps an absorption intrinsic to zircon. The absorption spectrum shown below was taken from the same zircon with a handheld spectroscope. The artefacts were not visible when using the spectroscope in the 'classic' handheld way, so the app seems to be more sensitive than the unaided eye.

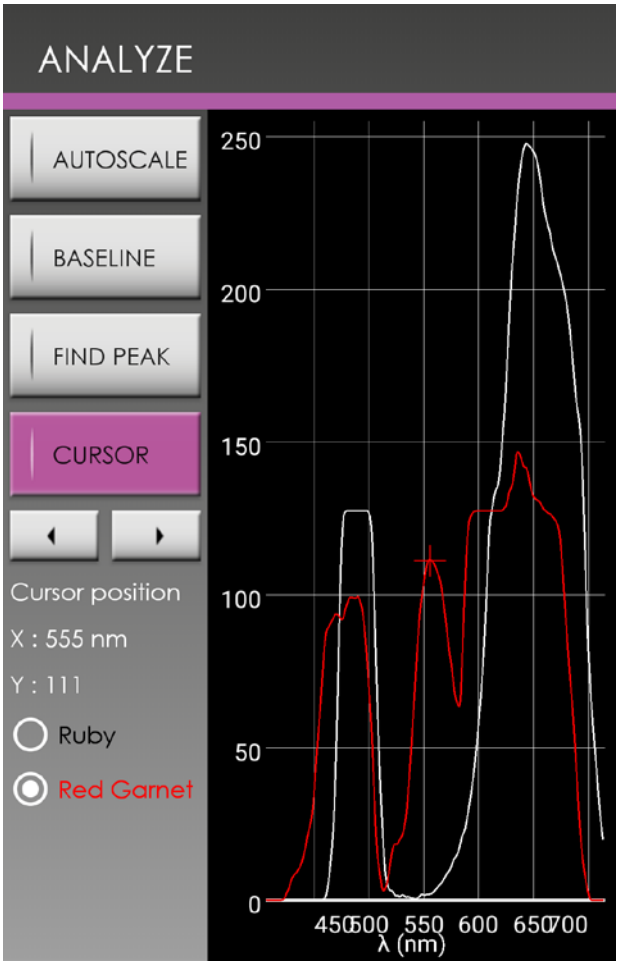


**Figure 24:** The 'Analyze' function of the GoSpectro app displays the spectral curves in transmission, as shown here for the synthetic ruby (white trace) and the almandine (red trace) spectra from Figure 22. It is possible to zoom into the spectra, and a cursor can be used to identify the position of each absorption feature.

The GoSpectro handheld spectrometer is a first step into 'advanced spectroscopy' for a reasonable price. Handling the device takes a little practise, but the optical fibre accessory is helpful. Viewing spectra in transmission instead of absorption also takes some getting used to, but the spectra are of good quality when the device is adjusted properly. In the author's opinion, this device does not completely replace the handheld spectroscope, especially for pale stones and those with narrow absorption lines; these are easier to observe in the 'classic' way. However, it is also possible to unmount the device from the adapter and use it like a normal handheld spectroscope.

*Dr Tom Stephan (t.stephan@dgemg.com)*
*German Gemmological Association*
*Idar-Oberstein, Germany*

## Reference

Stockton, C.M. 2017. What's New: GoSpectro smartphone-based spectrometer. *Journal of Gemmology*, **35**(6), 464.

# PEARLS

## An Unusual Assembled Cultured Blister

In May 2021, the Laboratoire Français de Gemmologie (LFG) received the sample shown in Figure 25 for testing. It was oval-shaped with a flat bottom, white to cream in colour and measured 34.46 × 20.56 × 12.30 mm. With the unaided eye and under magnification, a junction was observed between the curved top and flat bottom (Figure 26).

An X-ray microradiograph of the sample (Figure 27) showed lighter tones along the sample's exterior, indicating material of higher density, such as calcium carbonate (usually aragonite) in the case of natural and cultured pearls, while the darker tones in the core are indicative of lower-density material such as organic matter, resin, etc. (cf. Karampelas *et al*. 2017). According to the CIBJO Blue Book on pearls (CIBJO Pearl Commission 2020), assembled cultured blisters are made of purpose-grown cultured blisters that have been cut from their shell. The original bead upon which they grew is removed and the cavity is filled with various synthetic materials, and it is then backed by a layer of shell, with the assemblage being held together by an adhesive. Sometimes these products are referred to by the word *mabe*, the Japanese term designating an assembled cultured blister, traditionally from *Pteria penguin* but nowadays from other molluscs as well (see again CIBJO Pearl Commission 2020).

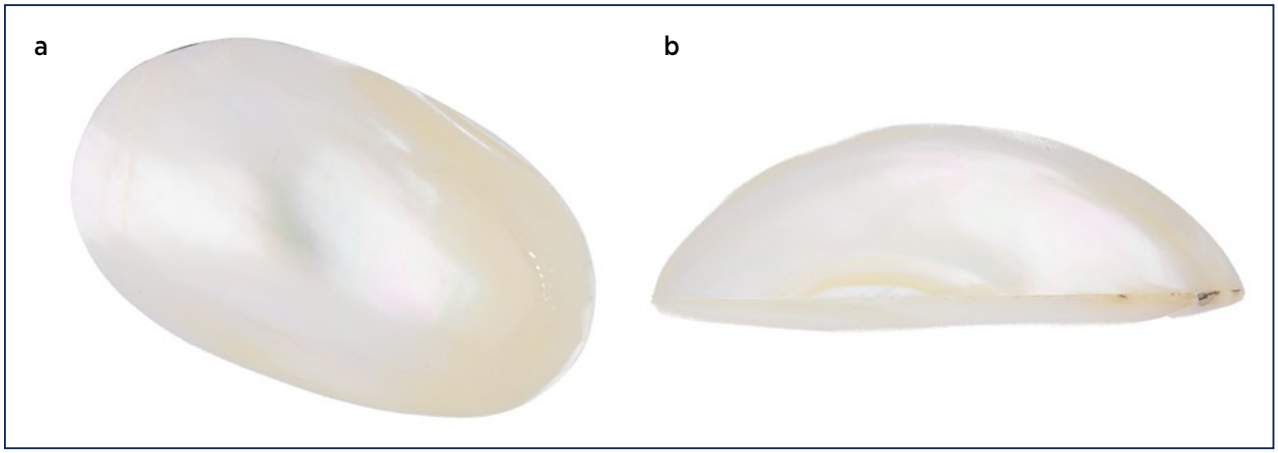


**Figure 25:** This assembled cultured blister (34.46 × 20.56 × 12.30 mm; 5.6 g) consists of (**a**) a curved top and (**b**) a flat bottom, shown from one side where the junction of the top and bottom can be seen. Photos by B. M. S. Beuve, © LFG.

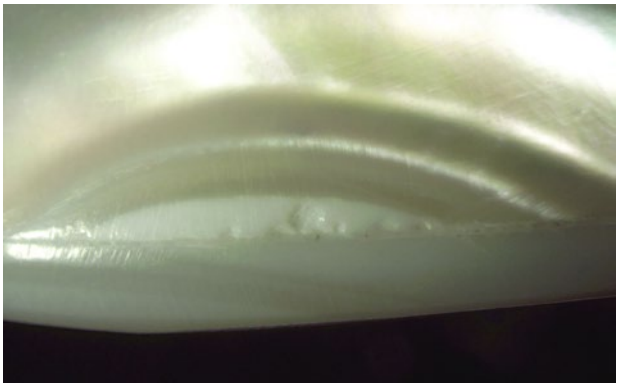

**Figure 26:** With magnification, the junction between the curved top and flat bottom of the sample in Figure 25 is easily visible. This boundary is particularly easy to see in reflected light. Photomicrograph by U. Hennebois, © LFG; image width 10 mm.

**Figure 27:** An X-ray microradiograph of the assembled cultured blister in Figure 25 (34.46 mm long) shows a lighter exterior layer due to higher-density material (aragonite), while darker tones at the core represent a lower-density material such as resin. Image by S. Leblan, © LFG.

**Figure 28:** A flame-like (crossed-lamellar) aragonite structure is seen on the flat side of the assembled cultured blister. Photomicrograph by U. Hennebois, © LFG; image width 10 mm.

Interestingly, the flat side of the present sample was non-nacreous, and when viewed with a microscope a flame-like structure was observed (Figure 28). This is also known as a crossed-lamellar structure and can be observed on the inner part of various bivalve and gastropod shells, as well as natural (and, rarely, cultured) pearls (Fritsch & Misiorowski 1987; Gauthier *et al*. 2019). The curved side of the sample had a typical nacreous appearance, but with the microscope it was not possible to observe a clear nacreous structure with overlapping layers; only pronounced polishing lines were visible. Energy-dispersive X-ray fluorescence analysis of the nacreous part showed an Mn content below the detection limit and also about 4000 ppm of Sr, indicating saltwater origin. Raman analysis of the nacreous and non-nacreous parts of the sample, using a 514 nm laser, revealed bands associated with aragonite.

Assembled cultured blisters are typically made of nacreous material on both the top and bottom. This is the first time the authors have encountered an assembled cultured blister made with nacreous and non-nacreous parts. Taking into account the size and white colour of the flat part, it might have originated from a Tridacninae bivalve shell.

*Sophie Leblan, Ugo Hennebois, Aurélien Delaunay, Bérengère Meslin Sainte Beuve, Annabelle Herreweghe and Dr Stefanos Karampelas (s.karampelas@lfg.paris)*
*LFG, Paris, France*

## References

CIBJO Pearl Commission 2020. *The Pearl Book*. CIBJO, Milano, Italy, vii + 79 pp.

Fritsch, E. & Misiorowski, E.B. 1987. The history and gemology of queen conch "pearls". *Gems & Gemology*, **23**(4), 208–221, https://doi.org/10.5741/gems.23.4.208.

Gauthier, J.-P., Fereire, J. & Bui, T.N. 2019. Evidence of rotation in flame-structure pearls from bivalves of the Tridacnidae family. *Gems & Gemology*, **55**(2), 216–228, https://doi.org/10.5741/gems.55.2.216.

Karampelas, S., Al-Alawi, A.T. & Al-Attawi, A. 2017. Real-time microradiography of pearls: A comparison between detectors. *Gems & Gemology*, **53**(4), 452–456, https://doi.org/10.5741/gems.53.4.452.

## ERRATUM

In the article by H. A. Hänni *et al*. titled 'An investigation of grinding hardness of some ornamental stones' (Vol. 37, No. 6, 2021, pp. 632–643), the authors' acknowledgements were inadvertently omitted due to an editing error, and should have been listed as follows: 'We owe our thanks to Dr Vera Hammer (Museum of Natural History Vienna, Austria) for valuable assistance with referencing older literature. We appreciate the donation of the testing material and the preparation of the sample blocks by Willi Ripp of Groh & Ripp. Without his engaged cooperation, this study could not have been performed. We thank Pascal Tschudin of the Earth Sciences department of Basel University for producing the thin sections and for lapping the samples with the Logitech device. Thanks also go to Dr H. H. Klein (Basel) for his critical and constructive review of the manuscript.'

# The History of London's Lapidaries (Part 1)

Justin K Prim

**ABSTRACT:** This two-part article weaves together the story of London as a significant European coloured-stone cutting hub, through a combination of historical materials and contemporary interviews with the current generation of lapidaries. Beginning with the industry's early history, we see the influence of foreign cutting techniques as wave after wave of immigrant craftsmen arrived in London throughout the centuries. Due to these external influences, London was able to play a prominent role in the history of European gem cutting. In addition, the evolution of cutting techniques contributed to an expansion in cut styles for coloured stones, particularly during the Renaissance, as seen in the jewels of the Cheapside Hoard. Continued influence from France, Germany and the Low Countries resulted in further developments of lapidary equipment and this, combined with the expanding availability of rough material, led to additional advances in coloured-stone cut styles. During the Victorian period, immigrants consisting of jewellers, gem cutters, clockmakers, goldsmiths and other highly skilled craftsmen settled in the Hatton Garden area, which became a hub for servicing the trade in the early- to mid-19th century.

*The Journal of Gemmology*, **37**(7), 2021, pp. 688–701, https://doi.org/10.15506/JoG.2021.37.7.688


The history of London's gem and jewellery trade has always been a story of three parallel narratives: those of the goldsmiths, the coloured-stone lapidaries and the diamond cutters. Although one would be hard-pressed to find a diamond cutter in modern London, and coloured-stone cutters have become exceedingly scarce, these three interrelated histories are quite important to understanding the role of London in European gem and jewellery craftsmanship. This two-part article pieces together the least known of these three narratives to present the largely untold history of London's coloured-stone cutters. Part 1 briefly examines the ancient beginnings of British gem cutting, followed by developments from medieval times through the Renaissance. In conjunction with the growth of the British Empire, the lapidary trade benefitted from the variety of rough gems that made their way to England and helped London to become, at one period of time, one of Europe's largest gem-cutting and trading centres. Part 2 of the article will explore how London remains one of the last European cutting centres (although quite small), and yet still preserves and transmits historic traditions for cutting coloured stones.

## ANCIENT BEGINNINGS

The art of cutting and polishing gemstones is a very old tradition in Britain. For evidence of early British gem cutting, we need to look no further than the Anglo-Saxon Staffordshire Hoard from the 6th–7th centuries. Found in 2009, the hoard contains hundreds of loose and gold-set cut-and-polished slices (Figure 1) and cabochons of garnet (Fern *et al*. 2019). To produce these gems, the garnet slices were attached to stone slabs with a mixture of brick dust and resin and then held against a rotating horizontal wheel carrying abrasive (Bimson 1985, p. 127). The polishing might have been done manually against a wooden block or possibly against a smooth piece of copper covered with abrasive powder, as has been documented in several European medieval manuscripts (Bol 2019, p. 226).

These polished garnets are more appropriately called wafers or slices rather than faceted stones (Figure 1b), but the techniques to produce them likely continued to be used and innovated upon until the present day. In London, the tradition of using copper and abrasive powder to shape and polish gemstones has continued


**Figure 1:** (**a**) This 6th–7th century gold ornament (seax fitting or knife sheath; dimensions not provided) from the Staffordshire Hoard is set with ornately shaped garnet slices that are arranged in a complex pattern. (**b**) A closer look at another piece from the Staffordshire Hoard shows the different shapes in which the garnets were cut. Photos from Fern *et al.* (2019); © Birmingham Museums Trust.

until modern times (as discussed in part 2 of this article), a technique which possibly links directly to the Anglo-Saxon tradition of cutting garnets into thin, flat shapes.

## A MEDIEVAL AND TUDOR JEWELLERY CAPITAL

Evidence of a goldsmithing quarter in London exists as far back as the 13th century. The goldsmiths and their livery company are important to this story because the history of gem cutting in London is intimately linked to the goldsmithing trade. The lapidaries of London never had a guild of their own, such as the ones in Antwerp or Paris (Bycroft & Dupré 2019, p. 10), but information about the activities of the cutters can be gleaned between the lines of The Goldsmith Company's meeting minutes. The Worshipful Company of Goldsmiths received their royal charter in 1327 (The Goldsmiths' Company n.d.), although taxation records indicate that goldsmiths were already operating in London in the 1200s (Schofield 2011, pp. 114–115). Any jeweller who wanted to do business inside the City of London needed to be a freeman of a city guild (Glanville 1979, p. 1), so the local gem cutters had to work directly with these members to do legitimate business.

A few blocks from Goldsmiths' Hall was the business hub of Cheapside, which was occupied by four-storey timber-framed buildings, and which the antiquarian John Stow described as 'the most beautiful frame of fair houses and shops in England'. Cheapside was well known throughout Europe as the centrepiece of an extraordinary market street (Stowe 1908, pp. 344–352). The shops were occupied by goldsmiths and craftsmen who specialised in working with gems, and likely also included a few gem cutters. Cheapside would prove quite significant for shedding light on the early history of Renaissance jewellery and cutting styles (see below).

There are no documented records about the techniques of London gem cutters from these early days. The jewellery styles of the time show that gem cutters and gem merchants would have been necessary in the city. Stirrup rings—simple rings usually ornamented with a central gemstone—were popular from the middle of the 12th century until at least the 15th century (Egan & Pritchard 2008). Rings from this period have been found in London (and in other cities) with sapphire, garnet or glass as the centre stone. Stones at this time were cut as round or square cabochons.

One of the earliest examples of a faceted stone in England is found in the ring of Bishop William Wytlesey, who was the Archbishop of Canterbury from 1368 to 1374. The ring (Figure 2), which is now on display at the V&A Museum in London, was made between 1362 and 1374 and includes a faceted sapphire (V&A 2002), which was considered a symbol of purity by the church (Lecouteux 2012, p. 283). The stone has a large table surrounded by eight facets, as well as a hole drilled through it, which was believed to increase its power and might also provide evidence that it came from a prior piece of jewellery.

At the start of the 16th century, most gem cutting was done outside of England (Reddaway 1975, pp. 206–207).

**Figure 2:** The sapphire in William Wytlesey's ring, which was made between 1362 and 1374, is one of the earliest examples of a faceted stone in a piece of British jewellery. The ring measures 3.1 × 2.8 × 1.4 cm. Photo © Victoria and Albert Museum, London, M.191-1975.

While England was witnessing the beginning of the Tudor period, merchants in France, Italy, the Netherlands and Germany were building the reputations of trading centres in those countries for Europe's gem and jewellery industry. In this pre-British Empire era, London was simply not yet ready to compete on a global scale.

London's goldsmiths and gem cutters were inspired by the styles and techniques of the European gem hubs at the time through the many immigrants who came to London from these cultural centres. Throughout the 1500s, there were Dutch and Flemish goldsmiths and gem cutters working in London, as well as German artisans. Craftsmen from Nuremberg and Augsburg—well-known gem-cutting centres in Bavaria—settled in London and brought their influence (Carrington & Hughes 1926, p. 4). In 1501, three Flemish gem cutters reportedly came to London to share their techniques (Reddaway 1975, p. 207). The foreign presence would have led to an exchange of skills, styles and cultural preferences, especially as the craftsmen started taking on apprentices.

The influence of foreign jewellers in London was strong throughout the Tudor period, and that influence grew as more of them emigrated there (Lever 1975, p. 18). Craftsmen of all types attempted to sell their exquisite creations to the court of Henry VIII and, later, Elizabeth I, both of whom patronised these foreign artists. Many of the craftsmen became permanent residents of London, and records from 1571 and 1593 (Scarisbrick 1994, p. 87) report 138 immigrant members of the gem and jewellery trade, 19 of whom were lapidaries, with some specified as agate, diamond or 'stone' cutters, and a few labelled specifically as *stone slippers* (Dutch for gem cutters). In addition to those of German, Dutch and Flemish ancestry, a smaller number of the immigrants hailed from France and Spain. According to Scarisbrick (1994, p. 87), 16 of the lapidaries came from the so-called Low Countries (historically, the Netherlands, Flanders or Belgica in the coastal lowland region of north-western Europe), with some specifically from Antwerp and Amsterdam.

## 16TH-CENTURY CUTTING STYLES

The Renaissance brought a reverence for the styles of classical antiquity. One of these styles was the ancient art of gem engraving of cameos and intaglios (Scarisbrick 1994, p. 82). Cameo portraits were popular throughout King Henry VIII's and Queen Elizabeth's reigns (1491–1603; Evans 1921, p. 96). Gem cutters in London such as Richard Astyll (the king's 'graver of stones'), Michael Berger and John Mayne specialised in carving these cameos (Scarisbrick 1994, p. 82). Engravings were done on all types of stones, such as ruby, chalcedony, garnet, sapphire, agate, lapis lazuli, amethyst and turquoise. These engraved gems were used as seals, crests and badges, and also set in all kinds of jewellery.

As for faceted stones, most 16th-century gems were fashioned as point cuts and table cuts (Figure 3), with an occasional multifacet cut (described further below). There is not much extant jewellery from this period (most of it was melted down and reused), but what does still exist shows the repeated use of these same two simple cuts, as well as cabochons. Since these early cuts did not have a lot of sparkle and shine, the jeweller relied on extravagant metalwork to create something eye-catching. Aside from the surviving English Renaissance jewellery, there is a wealth of pictorial evidence from which to glean details. Hans Holbein the Younger (1497–1543), who was an important court painter, recorded many images of jewellery designs in what is now known as his 'Jewellery Book,' which currently resides in the British Museum and affirms the regular use of table cuts as the main faceting style at the time (Figure 4; Evans 1921, p. 75).

The growing use of multifaceted cuts in the 16th century shows a push towards novelty in the gem-cutting world. Not only were gem cutters looking back at antiquity for inspiration, they were also starting to create innovative designs to appeal to their customers. A rare example of extant jewellery from this period containing multifaceted cuts is seen in Figure 5. For the peridot at the top, the cutter used what is now considered a standard step cut for the pavilion, but the crown was more experimental. It consists of two rectangular steps, visible along the edge of the stone, on top of which were added two triangular facets on each side to form a point instead of a table. This early use of triangular facets is uncommon,

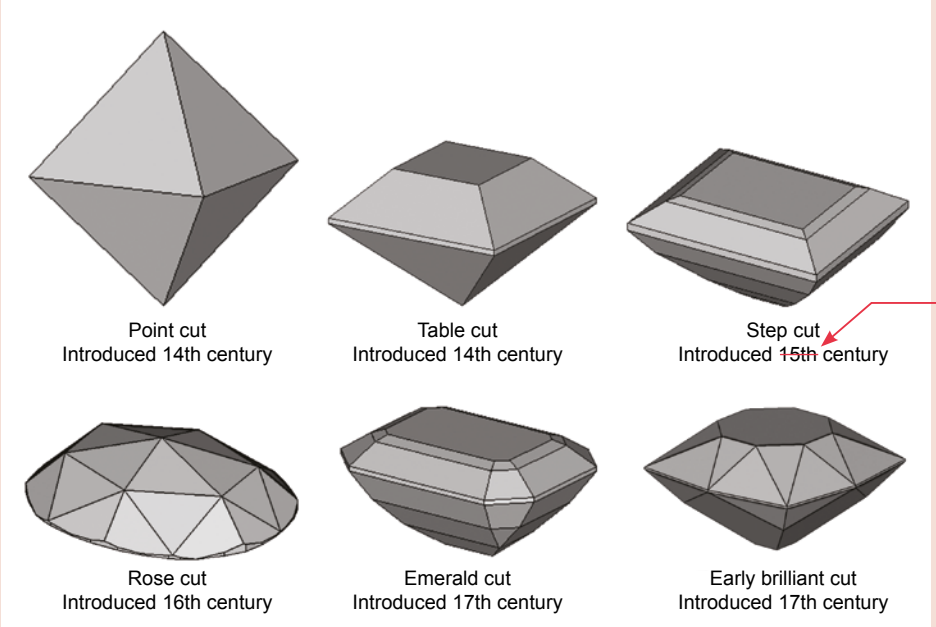


**Figure 3:** This drawing by the author illustrates the major faceting styles for coloured stones introduced during the 14th–17th centuries.

**Figure 4:** Hans Holbein's 'Jewellery Book' (1532–1543; British Museum Inventory number SL,5308.95) shows a Tudor example of table-cut stones in this pendant. It was described as being set with sapphires and pearls, and this painting depicts one of nine designs for pendant jewels. Image © The Trustees of the British Museum.

**Figure 5:** This English-made gold pendant (circa 1540–1560) is set with a faceted peridot (top) and hessonite (centre) that are accompanied by a sapphire bead. The peridot and garnet both have unusual multifacet cuts that were quite innovative at the time. The pendant measures 5.9 × 2.8 × 0.6 cm. Photo © Victoria and Albert Museum, London, M.242-1975.

probably due to the challenge of cutting them symmetrically on the crude faceting machines of the period. For the garnet mounted below it, the cutter started with a rectangle with the corners cut off. On its pavilion is a simple step cut, but the crown shows another innovation: the cutter used triangular-shaped facets, similar to those of a rose cut, to create a diagonal chequerboard pattern across the crown, which also has a keel line across the area where the table would be. This is quite a complex and unique cut for this period of Tudor jewellery. The pendant itself is also interesting because the mounting leaves the culet points of both stones exposed so that they would touch the wearer's skin in order to transmit the believed protective properties of the stones to the wearer.

## THE FLOW OF TRADE AND THE ENGLISH RENAISSANCE

Halfway through the 16th century, Britain began to shift its trading position to one of power, laying the seeds for what would become the British Empire. Until that point, the big trading companies had been Venetian and Portuguese. In 1555, a group of Londoners set up the Muscovy Company to ship goods directly from Russia to London with no continental middleman (Britannica 2013). Soon after followed the Levant Company and the East India Company, importing goods from around the Mediterranean and the Far East, respectively (Britannica 2021).

Between its new trading companies in the East, as well as the new wealth that was coming from the Americas, England found that it had suddenly become very rich. Queen Elizabeth indulged in jewellery and the country followed suit. The medieval stock of gems that had been released onto the market when Henry VIII seized the monasteries and their treasures had not yet been exhausted, and the stones coming from the trading companies were quickly added to these (Lewis 1948, p. 255). The Renaissance interest in classical gems caused an explosive obsession with gemstones and gem cutting, both engraved and faceted. Even the middle class joined in on the gemstone craze, using transparent colourless quartz rather than diamonds, and paste (glass) in place of more valuable coloured stones. Even mundane items could become ornate objects or jewellery, such as a pomander, a fan handle or even a golden toothpick.

Through Venice and Lisbon, stones came from all over the world: ruby and spinel from Burma, lapis lazuli and spinel from Afghanistan, turquoise from Persia, sapphire from Sri Lanka (formerly Ceylon), garnet from Bohemia and opal from Hungary, as well as pearls from Scotland and Venezuela (Scarisbrick 1994, p. 80). Lisbon had become a trading powerhouse when the Portuguese started bringing back gemstones, among other luxury goods, from India in 1498 (Vassalo e Silva 1993). Venice, already a powerful trading centre, continued to import stones from the Middle East and via the merchants of the Silk Road into the 1600s. English merchants stationed themselves in port cities around Europe and as far away as Turkey, with some of them becoming very wealthy as they bought and sold gems on commission.

In London itself the lapidary trade was progressing, and Figure 6 illustrates styles of cutting that were being

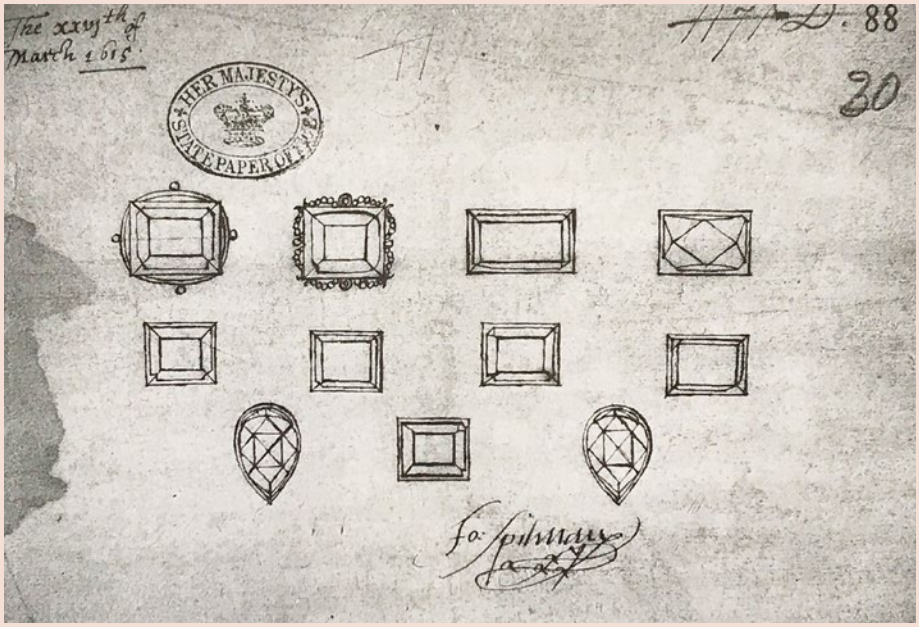


**Figure 6:** This 1615 drawing (from Pointon 2009) shows some popular cutting styles of the time. Top row: two table cuts, a baguette and a French cut; middle row: four step-cut rectangles; and bottom row: two rose-cut pears and a rectangular step cut.

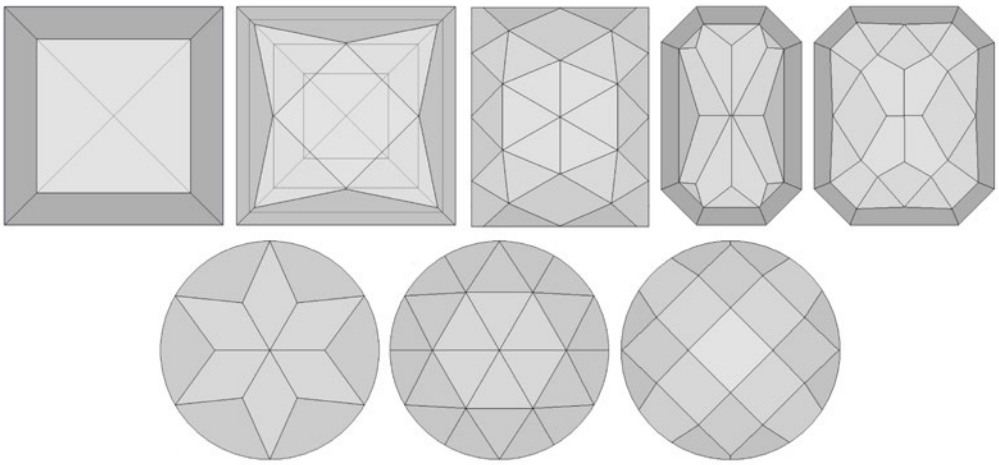

**Figure 7:** These diagrams show some of the cutting styles found in the 17th-century Cheapside Hoard. Top row, left to right: table cut, French cut, an unusual rectangular rose cut and two unusual octagonal cuts. Bottom row: Three variations on the rose-cut style. Drawings by J. Prim.

experimented with. One new addition was the rose cut, which originally developed in the mid-1500s (Ogden 2018, pp. 152–159). The drawing illustrates two pear-shaped rose cuts, as well as a 'French cut', in which the four facets of the table cut have been rotated around the stone to create four (or sometimes eight) triangles around a kite-shaped table. In 1668, the word *lapidary* appeared in a London-based list of manufacturing trades (Wilkins 1668, p. 339), and in 1677 an English-Latin dictionary defined a *lapidarius* (Latin) as a 'digger of stone, a stone cutter, a mason, a lapidary, one that cuts and sets precious stones and jewels' (Holyoake 1677, p. 792).

As in the previous century, most of London's 17th-century gem cutters were immigrants, and a few of them could be identified by name: Sophia Antine (from Dusseldorf) in Blackfriars and Cornelius Johnson (from Brussels) on Coleman Street were both professional agate cutters. Leonard Renatus (from France) of Blackfriars specialised in emeralds. A cutter from Antwerp named Harwick worked in the Tower ward and was known as a cutter of ring stones (Forsyth 2013, p. 80). Of course, some of London's gem cutters were of English origin, such as Robert Russell of Aldersgate Street, who specialised in emerald, John Blunt of Silver Street, who specialised in turquoise and ruby, and John Critchlowe of Great Wood Street, who specialised in garnet and amethyst (Forsyth 2013, p. 80).

## RENAISSANCE CUTTING STYLES —THE CHEAPSIDE HOARD

The Cheapside hoard is an incredible time capsule for the story of gem cutting, because it comes from a period with little documentation about the lapidary tools or techniques used. The hoard is a collection of more than 400 pieces of gold, gems and jewellery buried under a shop in Cheapside in the middle of the 17th century. It sat underground, untouched, for almost 300 years (Forsyth 2013, p. 6). Although the country (or countries) where the stones were cut is not known, the cutting styles show how diverse and experimental the lapidary arts were in the early 17th century (see Figure 7 and the cover of this issue). As expected, there were point cuts and table cuts, which were also common during the previous 200 years. We find several variations of the rose cut, indicating that this must have been a popular design (Wheeler 1928, p. 20). On one ring is a cluster of round rose-cut garnets (Figure 8a), and in a pendant are two sapphires with unusual rectangular variations of the rose cut (Figure 8b). This rectangular style of rose cut seems to be unique to the period and might have been a short-lived experiment for the lapidary who cut it.

Aside from the hundreds of pieces of jewellery, there are also many unset stones, which provide rare visual access to the pavilions of the gems. Included among the several types of table-cut stones is a large citrine with four facets and a table on top, and four facets and a culet on the bottom (Forsyth 2013, p. 160). The lines and symmetry are nearly perfect and the polish appears to be without blemish. The hoard also includes a variety of step-cut variations. Some have two steps, some have a keel and others have a culet. Shapes include pear, square, octagonal and oval. Round, rectangular and rough cushion shapes appear alongside numerous cabochons, briolettes, unique square rose cuts and a large collection of carvings (e.g. Weldon & Jonathan 2013).

The highlight of the hoard is an emerald watch (Figure 8c), which consists of a large Colombian emerald crystal that was hollowed out, faceted, polished and turned into a pocket watch (Forsyth 2013, p. 136). The facets on this piece are large, well polished and straight, although there are indications that they are not perfectly flat.


**Figure 8:** Examples of jewels from the Cheapside hoard include (**a**) a ring mounted with rose-cut garnets (19 × 17 mm), (**b**) an exceptional sapphire-and-spinel pendant featuring two forms of rectangular rose-cut sapphires (72 × 15 × 6 mm) and (**c**) a magnificent pocket watch with a hinged lid that was crafted from a single carved emerald crystal (32 × 24 × 21 mm). Photos © Museum of London; inventory numbers (a) A14237, (b) A14104 and (c) A14162.

## 17TH-CENTURY CUTTING TECHNIQUES

Little to no evidence exists about the techniques used by early British lapidaries. One of the first pieces of solid information is from 1652, when Thomas Nicols in his *A Lapidary, or, History of Pretious Stones* indicated that the engraving and polishing processes required the stones to be prepared by grinding them on a whetstone (or millstone) and then shaped into a more exact form. He said they must be rubbed with emery powder and then polished with tripoli, although diamonds could only be polished with diamond powder. He provided nothing specific about how facets were placed, but he did say that carving could be done with an iron or steel orb (Nicols 1652, p. 26).

The earliest documentation of definitive British lapidary technology comes from herald painter Randle Holme in his 1688 book, *The Academy of Armory*. The book is intended to be a comprehensive guide to heraldry in the 17th century, but Holme often diverged from his topic and, in one of these digressions, he produced an illustrated list of trades, which included lapidary work. He provided an image of a lapidary in his shop, as well as his tools: a lapidary mill (Figure 9a) and a 'sandbox' (Figure 9b), which were described as follows (Holme 1688, p. 382):

> There belongs to it first a strong Plank Table Cover, four square, set upon a strong Frame with four feet…. The Axis of the Left Hand Wheel comes through the Table, and is turned about with Lapidaries left hand, with a Winch fitted on the end of it.
>
> The Right Hand Wheel, hath also an Axis which comes through the top of the Table, upon which again is fixed another round Wheel, or rather a round flat piece of Lead, fitted into a round cavity upon the superficies of the Table, where it turns…
>
> About the Table Mill is fixed a square Frame, about an inch and half high, which is only to lay Stones to be ground therein, that thereby they may not be scattered abroad on the Table in time of working.
>
> In such kind of Boxes with covers, Lapidaries keep their fine Dust of Diamond, or of other kinds of Stones made into a kind of Sand, by which with the help of their Mill and Water or Oil, they cut or grind a Stone or Diamond into what form or fashion (used in Rings and Jewels) he pleaseth, afterwards he polisheth them.

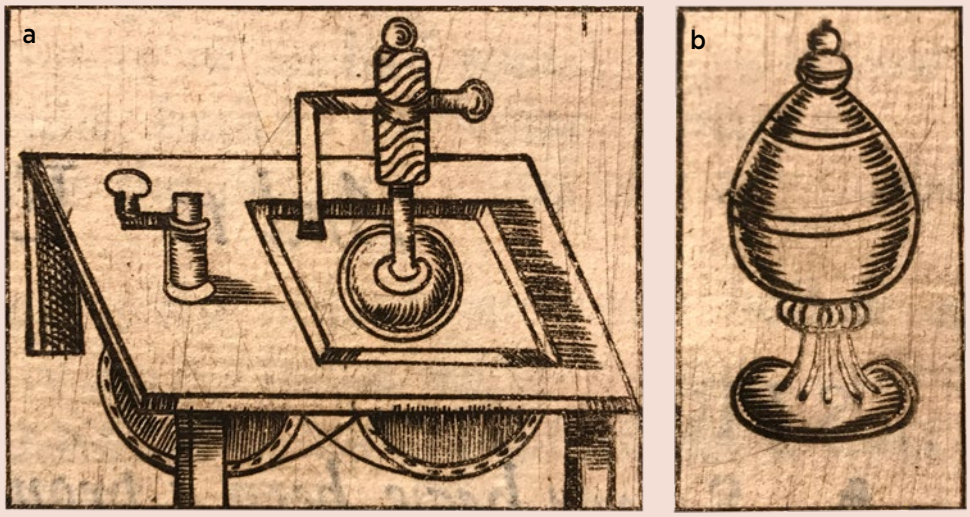


**Figure 9:** This lapidary polishing mill (**a**) and 'sandbox' (**b**) from 1688 are the earliest illustrations of British faceting tools (Holme 1688, p. 380).

book 3,

The device illustrated by Holme (again, see Figure 9a) is essentially identical to other lapidary machines seen around Europe at the time, such as in Anselmus de Boodt's *Gemmarum et Lapidum* (1609) and Andrés Félibien's *Des Principes de l'Architecture* (1676). Both of those machines featured a quadrant handpiece that held the stone and helped the cutter make the desired angles and rotations. It is curious that Holme did not mention the use of any sort of handpiece. Several later sources indicate that London lapidaries did in fact employ quadrant handpieces. The earliest mention of such a device in Britain is in John Barrow's *Dictionaries Polygraphicum* (Barrow 1735, p. 408):

> The workman turns a wheel with one hand, and with the other he forms the stone fixed to a stick, fastened in an instrument of wood, called a quadrant, because it is composed of several pieces that quadrate together, and is turned by a vice; which turning the stick, forms regularly the different angles the lapidary would make on the stone.

Before de Boodt (1609), there were few early depictions of cutting tables in Germany, where it seems this type of lapidary mill originated. The earliest known illustration appears in *Das Steinbuch* (Volmar 1498, p. 1; Figure 10), and it appears that this machine was used without the help of a quadrant-type handpiece. Writings from this period report that Nuremberg was a major cutting centre, and a Czech merchant brought one such table from Nuremberg to Prague in 1599 (Prim 2019a), so it is likely that the design for the British lapidary mill is of German origin. The predecessor to all of these machines was likely the mill recorded by Henri Arnaut, which seems to have connections to both Germany and Venice (Schmetzer 2019).

Although Holme provided a thorough description of this type of hand-cranked bench machine, he also illustrated another device that he did not give details about. This drawing shows a lapidary in his shop with stones for sale on the counter (Holme 1688, p. 95) and what appears to be a diamond-polishing mill in the background (Figure 11; see a similar machine in Schmetzer 2019, p. 548, figure 7).

This type of diamond-polishing machine is a more industrial version of the hand-cranked device used for coloured stones and is often turned by a second person, leaving the diamond cutter free to focus on faceting the stone. Although Holme did not show it, this kind of lapidary mill was always used with a wooden handpiece, called pincers (later a *tang*), which helps the cutter hold the stone at a certain angle. These types of machines

**Figure 10:** The British lapidary table likely descended from early German ones, such as this one depicted in Volmar's *Das Steinbuch* (1498).

**Figure 11:** This 17th-century illustration of a lapidary selling his goods also shows what appears to be a diamond-polishing mill in the background (Holme 1688, p. 95).

1550 *Kreuterbůch*

appeared as early as ~~1553 or 1554~~ in German manuscripts such as Eucharius Roeslin's ~~*Krueterbuch*~~ and later in 17th-century French books such as André Félibien's *Des Principes de l'Architecture* in 1676. From the presence of this mill in Holme's book, it seems possible that London's lapidaries were using this large diamond-cutting mill with a wooden tang handpiece, and that the separate traditions and trajectories of diamond cutters and coloured-stone cutters had already been established.

At the beginning of the 18th century, one more source provided concrete information on the polishing techniques of the time: *The Universal Dictionary of Arts and Sciences* (Chambers 1728). It specified that ruby, sapphire and topaz were cut on a copper wheel with olive oil and diamond powder, and polished on another copper wheel with tripoli and water. Emerald, zircon, amethyst, garnet, agate and other softer stones were cut on a lead lap with emery and water, and polished on a tin wheel with tripoli. Turquoise, lapis and opal were cut and polished on a wooden wheel with tripoli. These descriptions reflect techniques being used in other European cutting centres at the time (Félibien 1676, pp. 358–363; Prim 2019a), reinforcing the idea that many of the techniques for cutting coloured stones in London came directly from the lapidary traditions of the immigrant cutters who had relocated there.

## EUROPEAN INFLUENCES

Much of the early history of European faceting took place in France, Germany and the Low Countries, and the techniques of these cutters were handed down from master to apprentice until they finally found their way to London. Thus, religious struggles in Europe had consequences for the gem trade in London as various religious refugees relocated to England. In the 1660s, Portuguese Jewish gem merchants and cutters settled in London and helped revitalise London's local trade while also infusing it with new techniques (Claremont 1906, p. 36). Protestant Huguenots started arriving from France around 1670, and many of these jewellers and clockmakers set up in Clerkenwell, just outside the city walls, so they could sell their goods directly from their workshops without needing to be a part of London's guild system (although the Goldsmiths' Company still had the right to control the quality of their work; Lichtenstein 2013, p. 136).

In the 17th century, jewellery styles became fixated upon the gemstones themselves, and with the 18th century, that trend continued. Gem cutters became more creative and more proficient with their craft, to the point where some have called it the 'Age of the Faceted Stone' (Bradford 1967, p. 13). The biggest change that arrived with the 18th century was a new fascination with diamonds. Thanks to the discovery of the Brazilian alluvial deposits in the early 1700s, the European market was flooded with diamonds and, as a result, diamond jewellery became the dominant fashion (Ogden 2018, pp. 318–320). London was thus an important diamond-cutting centre throughout most of the 18th century.

The rose cut reached its ultimate form, along with several variations, some more elaborate than others. The brilliant cut first appeared in the mid-1600s (Figure 3) and was used in London right away (Ogden 2018, p. 171). As it evolved, the brilliant cut would continue to enchant the imagination of its viewers (Figure 12; Jeffries 1751). The quality of gem cutting in London was high, although fashion in England still generally followed the lead of France (Bradford 1967, p. 15). Foreign craftsmen continued to emigrate to London, bringing influences from Italy, France and Germany.

The 18th century saw a renewed interest in the classical period, which meant that faceted stones were no longer the only fashion trend. For example, Figure 13 shows master engraver Samuel Rogers operating his turning machine. He did public demonstrations for one shilling, and promoted the capabilities of the machine to create carved medals, gentlemen's cane handles, eggs, bezels for snuff boxes, toothpick cases and more (Anonymous 1937, p. 171).

### *An 18th Century Gem Cutter: Hyams Lapidary*

To get an idea of what the life of a gem cutter might have looked like in the 18th century, we can follow the story of jeweller, engraver and lapidary Solomon Hyam. According to his trade card (Figure 14), he set up shop at 127 Pall Mall, which was three doors down from Carlton

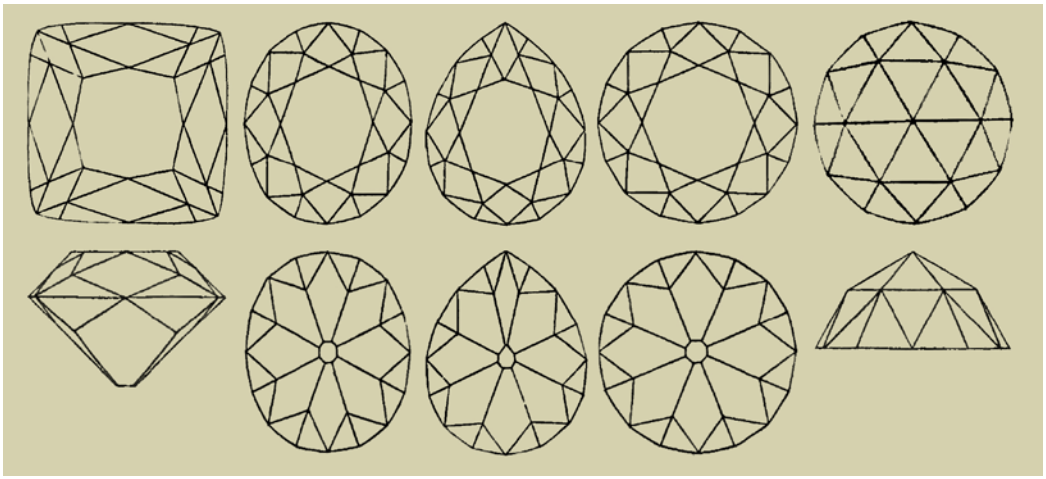

**Figure 12:** Popular 18th-century diamond-cutting styles are illustrated in David Jeffries' 1751 *Treatise on Diamonds and Pearls*, compiled here from end plates 1–10.


**Figure 13:** This 18th-century trade card depicts master engraver Samuel Rogers with his 'turning machine' (from Anonymous 1937).

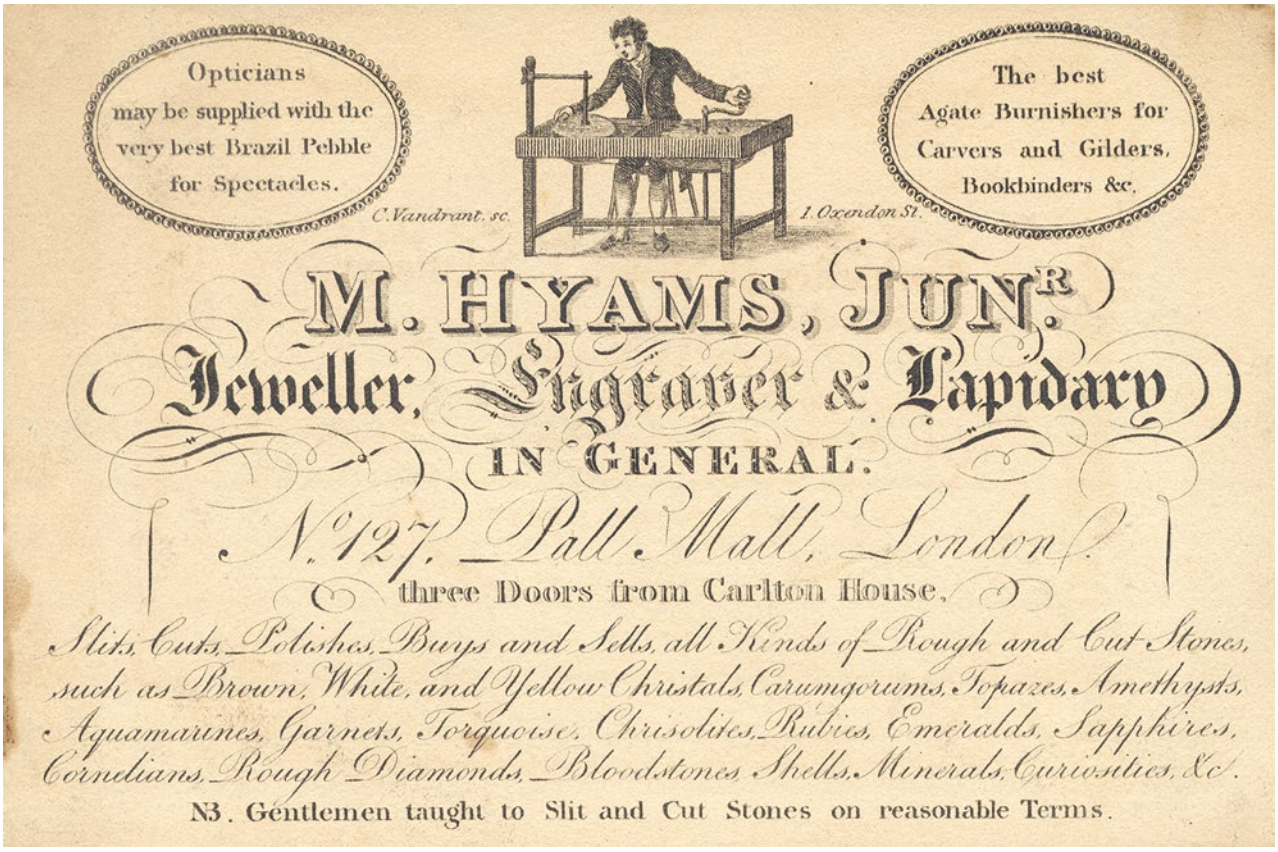


**Figure 14:** The 1780 trade card of Solomon Hyam, a lapidary of Pall Mall, illustrates him slicing stones on his British lapidary table. Courtesy of the Winterthur Library: Joseph Downs Collection of Manuscripts and Printed Ephemera.

House, the mansion where the Prince Regent lived (Hyams 1780). According to Ancestry.com[1], family legend says that Solomon's father Moses was a soldier in the Polish army who fled to Ireland after banishment for his revolutionary activity in defence of Polish freedom. In Dublin, Moses married Judith Isaacs of Germany and a year later she gave birth to their oldest son, Solomon. Around 1765, the family relocated to London. Solomon was 12 at the time and it seems likely that, after a few years in London, he would have started an apprenticeship at around age 14.

By 1780, when Solomon was 27 years old, he was advertising his services (again, see Figure 14). He was buying and selling many kinds of rough and cut gem materials, including bloodstone, carnelian, topaz, amethyst, aquamarine, garnet and turquoise, as well as rough diamond. He was slicing, cutting and polishing gem materials, as well as teaching the art of cutting for a reasonable price. In addition, he supplied opticians with 'the very best Brazil Pebble [rock crystal] for Spectacles' and also provided carvers with agate burnishers.

Solomon's trade card depicts him using the same machine that Randle Holme described in 1688. Although the image shows him slicing a stone on the side of a slitting lap, it is likely that he used a quadrant handpiece for the actual faceting and polishing of his stones. According to Ancestry.com[2], Solomon had an address in Whitechapel in 1791 before moving his shop to 254 Strand, and he moved again around 1801 to 6 Pall Mall. All four shops were generally along the route between the financial district in the City of London and the government district of Westminster—a route that London's wealthiest patrons would have travelled regularly. Sometime after closing his shop on Pall Mall, he emigrated to the United States and, later, died at age 84 in Charleston, South Carolina.

Solomon's life provides a quintessential example of British gem cutting in this period. A Jewish immigrant to London, he was trained with a skillset that likely developed during a previous generation in Lisbon, went into business as a successful gem cutter and merchant, and ran several shops in prominent locations around

[1] www.ancestry.com/family-tree/person/tree/81083503/person/412047474654?_phsrc=Jle3

[2] www.ancestry.com/family-tree/person/tree/81083503/person/412047473915/facts

London before retiring. Along the way, he passed on his skills to his apprentices, which allowed his foreign skillset to become naturalised as it was adopted by the next generation of London-based gem cutters.

## THE BIRTH OF THE HATTON GARDEN GEM DISTRICT

With the destruction of Cheapside in the 1666 Great Fire of London, its importance as a gem and jewellery trading hub declined, and a new neighbourhood slowly rose up to take its place. Less than a mile to the west was a sort of in-between neighbourhood, just outside the City of London, which was once the walled estate and garden of Sir Christopher Hatton, a favourite of Queen Elizabeth I. From this property came the name 'Hatton Garden'.

The descendants of the Huguenot jewellers and clockmakers who had originally settled in Clerkenwell started to migrate to the next neighbourhood south, and by the early 1800s a few shops had opened there. However, the neighbourhood did not start out as a gem hub. In the 1830s, there were printmakers, bookmakers, cabinetmakers and tailors, with only a few jewellers (Lichtenstein 2013, p. 138). It had a seedy reputation, with parts of it being a 'liberty'—an area free from the jurisdiction of the police and frequented by undesirable characters. Leather Lane, which runs through the centre of the neighbourhood, was described as being 'much infested by thieves, beggars, and Italian organ-grinders' (Abrahams 1955, p. 154). It did not take long for all this to change.

Aside from the descendants of French and Dutch immigrants who relocated in the early days of Hatton Garden, a wave of Italian immigration into London took place at the same time (Lichtenstein 2013, p. 193). Many of them were highly skilled craftsmen who lived in apartments above their ground-floor shops in Hatton Garden. From the 1830s onward, more jewellers, gem cutters, clockmakers and goldsmiths settled along Leather Lane, as well as on Hatton Garden Street. The success of the early Hatton Garden days was due in part to the assayers and mineralogists of Johnson Matthey & Co. Ltd (Lichtenstein 2013, pp. 160–161). The company refined and sold metal bullion to the jewellery trade that was quickly growing in the neighbourhood around them. As England passed into the Victorian period, Hatton Garden started to develop a reputation as the new gem and jewellery district of London. In the early- to mid-19th century, the neighbourhood only serviced the trade and not the public.

## THE QUADRANT HANDPIECE

Until the 19th century, the main tool used for faceting stones was the quadrant handpiece. It was employed not only in London but in the cutting centres of Prague and Paris, as well as in workshops in Germany, Russia and Sri Lanka (Prim 2019b). Although a reference was made to the London quadrant by Barrow in 1735, no images survived until the mid-1800s. Curiously, two different handpieces were depicted within a few years of each other (Reed 1833; Anonymous 1840). Figure 15a is of the earlier one, nearly identical to the one depicted by de Boodt in 1609. This early quadrant design was a major innovation in gem-cutting technology because it enabled the stone to be held at specific angles. Without the development of the quadrant handpiece, gem cutting probably would have been stuck in the 1500s, unable to progress

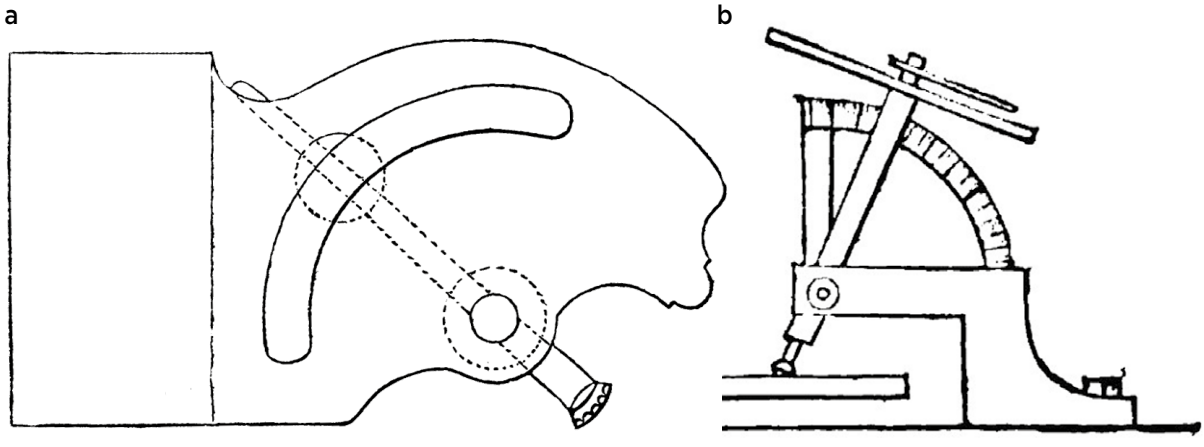


**Figure 15:** Quadrant handpieces are illustrated in two London periodicals: *Mechanics' Magazine* (**a**, Reed 1833) and *The Saturday Magazine* (**b**, Anonymous 1840). These were used by professional British coloured-stone cutters until the 1820s–1840s, when they were replaced with new lapidary technology.

much further than the simple table and point cuts so often seen before the quadrant was put to regular use.

Figure 15b seems to be a later innovation that was developed just before the quadrant went out of style. It had a more sophisticated index wheel that looks similar to a clock face with a hand that rotated around a dial to tell a cutter exactly which side of the stone was going to get cut by the lap, enabling lapidaries to be even more accurate than before. Despite its updated design, the quadrant was about to be superseded by the next development in lapidary technology.

## CONCLUSION AND PART 2 OUTLOOK

Part 1 of this article covered the advancement of gem-cutting styles from the archaic point cut to the early days of the brilliant cut. Beginning with simple styles (such as the table cut) that could be fashioned without any special tools, gemstone design evolved into more complex styles, such as rose cuts and brilliant cuts, which accompanied technological advances that enabled lapidaries to be more precise.

Part 2 of the article will progress towards the modern era, and continues with further developments in lapidary techniques and technology which enabled gem cutters in London (and abroad) to innovate new cutting styles that still dominate the jewellery market today. French innovations will be shown to improve the quality of London cutting, which in turn would help to cement Hatton Garden's role as a major European cutting centre. In addition, the founding of the first gemmology school in London in the early 20th century also assisted gem cutters there.

## REFERENCES


Abrahams, H.N. 1955. The romance of Hatton Garden. *The Gemmologist*, **24**(289), 152–156.

Anonymous 1840. On gems and precious stones. VI. *The Saturday Magazine*, No. 542, 12 December, 229–231.

Anonymous 1937. Eighteenth century lapidaries. *The Gemmologist*, **6**(67), 170–171.

Barrow, J. 1735. *Dictionarium Polygraphicum*, Vol. 1. C. Hitch and C. Davis, London, 626 pp.

Bimson, M. 1985. Dark-age garnet cutting. *Anglo-Saxon Studies in Archaeology and History*, **4**, 125–128.

Bol, M.A.H. 2019. *Polito et Claro*: The art and knowledge of polishing, 1100–1500. *In*: Dupré, S. & Bycroft, M. (eds) *Gems in the Early Modern World*. Palgrave Macmillan, Cham, Switzerland, 223–257, https://doi.org/10.1007/978-3-319-96379-2_9.

Bradford, E. 1967. *English Victorian Jewellery*. Spring Books, London, 141 pp.

Britannica, Editors of Encyclopedia. 2013. Muscovy Company. Encyclopedia Britannica, www.britannica.com/topic/Muscovy-Company, 1 August, accessed 28 July 2021.

Britannica, Editors of Encyclopedia. 2021. East India Company. Encyclopedia Britannica, www.britannica.com/topic/East-India-Company, 12 February, accessed 28 July 2021.

Bycroft, M. & Dupré, S. 2019. Introduction: Gems in the early modern world. *In*: Bycroft, M. & Dupré, S. (eds) *Gems in the Early Modern World*. Palgrave Macmillan, Cham, Switzerland, 1–32.

Carrington, J.B. & Hughes, G.R. 1926. *The Plate of the Worshipful Company of Goldsmiths*. Oxford University Press, Oxford, 158 pp.

Chambers, E. 1728. *Cyclopædia: or, an Universal Dictionary of Arts and Sciences* […], Vol. 1, 1st edn. James and John Knapton […], London, 1,048 pp.

Claremont, L. 1906. *The Gem-Cutters Craft*. George Bell and Sons, London, 296 pp.

de Boodt, A.B. 1609. *Gemmarum et Lapidum Historia*. Typis Wechelianis, apud C. Marnium et heredes J. Aubrii, Hanover, Germany, 294 pp.

Egan, G. & Pritchard, F. 2008. *Dress Accessories, 1150–1450*. Boydell Press, Suffolk, 438 pp.

Evans, J. 1921. *English Jewellery from the Fifth Century A.D. to 1800*. Methuen & Co. Ltd, London, 168 pp., https://archive.org/details/englishjewellery00evanuoft.

Félibien, A. 1676. *Des Principes de l'Architecture, de la Sculpture, de la Peinture, et des Autres Arts Qui en Dépendent: Avec un Dictionnaire des Termes Propres à Chacun de ces Arts*. Jean-Baptiste Coignard, Paris, France, 267 pp.

Fern, C., Dickinson, T. & Webster, L. (eds) 2019. *The Staffordshire Hoard: An Anglo-Saxon Treasure*. Society of Antiquaries of London, London, 640 pp., https://doi.org/10.26530/20.500.12657/39941.

Forsyth, H. 2013. *London's Lost Jewels: The Cheapside Hoard*. Philip Wilson Publishers, London, 150 pp.

Glanville, P. 1979. *Tudor London*. Museum of London, London, 33 pp.

Holme, R. 1688. *The Academy of Armory*. Printed for the Author, Chester, 501 pp.

Holyoake, F. 1677. *A Large Dictionary in Three Parts*. W. Rawlins for G. Sawbridge, W. Place, T. Basset, T. Dring, J. Leigh, and J. Place, London, 1,378 pp., https://archive.org/details/b30324476.

Jeffries, D. 1751. *A Treatise on Diamonds and Pearls*. C. and J. Ackers, London, 155 pp.

Lecouteux, C. 2012. *A Lapidary of Sacred Stones*. Inner Traditions, Rochester, Vermont, USA, 376 pp.

Lever, C. 1975. *Goldsmiths and Silversmiths of England*. Hutchinson, London, 256 pp.

Lewis, M.D.S. 1948. The historical background of English jewellery. *The Gemmologist*, **17**(206), 220–230.

Lichtenstein, R. 2013. *Diamond Street: The Hidden World of Hatton Garden*. Penguin Books, London, 368 pp.

Nicols, T. 1652. *A Lapidary, or, the History of Pretious Stones*. Thomas Buck, Cambridge, 239 pp.

Ogden, J. 2018. *Diamonds: An Early History of the King of Gems*. Yale University Press, New Haven, Connecticut, USA and London, 408 pp.

Pointon, M.R. 2009. *Brilliant Effects: A Cultural History of Gem Stones and Jewellery*. Yale University Press for the Paul Mellon Centre for Studies in British Art, New Haven, Connecticut, USA, 368 pp.

Prim, J.K 2019a. Fashioning fire from pebbles: The history of gem cutting in the Czech Republic. https://medium.com/justin-k-prim/fashioning-fire-from-pebbles-66d937273b94, 1 May, accessed 24 March 2021.

Prim, J.K 2019b. The modern history of gemstone faceting in Sri Lanka. *Journal of Gemmology*, **36**(5), 448–455, https://doi.org/10.15506/JoG.2019.36.5.448.

Reed, W. 1833. Amateur lapidary's apparatus. *Mechanics' Magazine, Museum, Register, Journal, and Gazette*, **19**(505), 19.

Roeslin, E. ~~1553 or 1554~~ 1550. *Kreuterbůch von natürlichem Nutz und gründtlichem Gebrauch der Kreuter, Bäum, Gesteud unnd Früchten*. Christian Egenolffen, Franckfurt am Meyn, Germany, 549 pp., https://doi.org/10.5962/bhl.title.7123.

Reddaway, T.F. 1975. *Early History of the Goldsmiths' Company, 1327–1509*. Edward Arnold, London, 378 pp.

Scarisbrick, D. 1994. *Jewellery in Britain, 1066–1837: A Documentary, Social, Literary and Artistic Survey*. Michael Russell Publishing, Norwich, xxiii + 431 pp.

Schmetzer, K. 2019. A 15th-century polishing machine for gemstones attributed to Henri Arnaut. *Journal of Gemmology*, **36**(6), 544–550, https://doi.org/10.15506/JoG.2019.36.6.544.

Schofield, J. 2011. *London, 1100–1600: The Archaeology of a Capital City*. Equinox Publishing, Sheffield, 324 pp.

Stowe, J. 1908. Bredstreete Warde. *In*: Kingsford, C.L. (ed) *A Survey of London. Reprinted From the Text of 1603*. Clarendon and British History Online, Oxford, 344–352.

The Goldsmiths' Company n.d. History of the Hall. www.thegoldsmiths.co.uk/company/history/history-hall, accessed 24 March 2021.

V&A 2002. William Wytlesey's ring. Victoria and Albert Museum, London, https://collections.vam.ac.uk/item/O71727/william-wytleseys-ring-ring-unknown, 9 December, accessed 24 March 2021.

Vassalo e Silva, N. 1993. The Portuguese gem trade in the sixteenth century. *Jewellery Studies*, **6**, 19–28.

Volmar 1498. *Das Steinbuch*. Hans Spörer, Erfurt, Germany, 143 pp., https://digital.staatsbibliothek-berlin.de/werkansicht/?PPN=PPN853184453.

Weldon, R. & Jonathan, C. 2013. The Museum of London's extraordinary Cheapside Hoard. *Gems & Gemology*, **49**(3), 126–137, https://doi.org/10.5741/gems.49.3.126.

Wheeler, R.E.M. 1928. *The Cheapside Hoard of Elizabethan and Jacobean Jewellery.* London Museum Catalogues, No. 2, Lancaster House, London, 35 pp.

Wilkins, J. 1668. *An Essay Towards a Real Character and a Philosophical Language.* Sa: Gellibrand, and for John Martyn Printer to the Royal Society, London, xv + 615 pp.

## The Author

**Justin K Prim**
Institute of Gem Trading, Bangkok, Thailand
E-mail: justinkprim@gmail.com

## Acknowledgements

This article would have been impossible to write without a research grant from the Society of Antiquaries of London. I would also like to thank my host in London, Kim Rix. Finally, a big thank you goes out to the following for their help with researching this article: Dr Jack Ogden, Hazel Forsyth at the Museum of London (in part for pointing me towards the Randle Holme manuscript), Rachel Church and Joanna Whalley at the Victoria and Albert Museum, and the staff of the British Library and the British Museum.

# Characterisation of Patchy Blue and Green Colouration in Dominican Blue Amber

Chenxing Xin, Yan Li, Yamei Wang and Guanghai Shi

**ABSTRACT:** Dominican amber typically shows a yellow, brownish yellow or brownish red body colour, but also may present blue to greenish blue hues under daylight illumination when viewed over a black background. In addition, it displays bright blue to green luminescence when exposed to UV radiation. Such 'blue amber' may occasionally show irregular green spots or patches when observed over a black background or with UV radiation. This appearance may cause confusion with reconstructed amber. Five Dominican amber specimens displaying the unusual patchy colouration were investigated using optical microscopy, three-dimensional fluorescence spectroscopy, scanning electron microscopy and Fourier-transform infrared spectroscopy. The green colour patches correspond to the superposition of the yellow body colour with naturally occurring areas of weaker blue fluorescence. Blue amber with a higher degree of maturity is usually accompanied by stronger blue fluorescence. Understanding this fluorescence mechanism allows us to explore the relationship between the maturity of the amber and the evolution of its geological diagenesis, and may have implications for origin determination.

*The Journal of Gemmology*, **37**(7), 2021, pp. 702–715, https://doi.org/10.15506/JoG.2021.37.7.702


Amber is a popular organic gem material that exhibits a range of colourful luminescence. It is a complex biogenic polymer originating from ancient tree resin buried during various geological periods and fossilised over tens of millions of years. It is widely distributed worldwide as individual pieces or layers in coal or sediments, especially in Cenozoic and Cretaceous deposits (Wolfe *et al.* 2016). As a precious cultural relic, amber was exchanged between the East and West on the 'Amber Road' in ancient Europe and along the 'Silk Road' in China. Amber is also a fascinating time capsule for natural history (Ross *et al.* 2010) because it often preserves palaeontological, palaeogeographical and palaeoecological information that researchers can use to explore the ecosystems that existed tens of millions of years ago (Bechtel *et al.* 2016; Xing *et al.* 2018; Jarzembowski *et al.* 2020).

The original source of amber is tree exudate (resin) that was secreted by gymnosperms and angiosperms. The exudate consisted of a viscous liquid made up of a complex mixture of components that can be divided into two groups: volatile and non-volatile substances. The former mainly consist of monoterpenes, sesquiterpenes and some diterpenes, and the latter are usually composed of unsaturated carboxylic diterpene acids and some triterpene acids (Langenheim 1969; Winkler *et al.* 2001). There are two main steps in the conversion of the original resin to amber: (1) the polymerisation (or stabilisation) stage causing a transformation from plant resin to copal resin; and (2) the devolatilisation stage resulting in the transformation of copal resin to amber terpene components. Most of the volatile components evaporate during the first (stabilisation) process, and then the remaining non-volatile fraction converts

into fossilised resin under the appropriate burial conditions (Grimaldi 2009). The fossilisation process, which involves gradually increasing maturity, includes progressive oxidation, polycondensation and polymerisation (Langenheim & Beck 1965). This very lengthy process from resin to amber formation is influenced not only by the properties of the original plant resin (such as its composition and viscosity) but also by environmental conditions such as sunlight, humidity, pressure, temperature, etc. 'Maturity' represents the degree of resin fossilisation; for example, the maturity of copal is lower than that of amber. It is influenced by time, geological processes and the composition of the original resin.

So-called *blue amber* is a particularly rare variety that mainly originates from the Dominican Republic, but also comes from Mexico, Indonesia and Myanmar (Yang & Wang 2010). Dominican blue amber (Figure 1) is recognised by many to be the most desirable variety, especially the 'sky-blue' colour (Figure 1c). The quality and market value of blue amber are mainly determined by the purity of its blue colouration, although it is generally accompanied by a secondary green hue. Variations in the colour appearance of blue amber from different sources are mainly due to differences in their fluorescence spectra. In addition, Jiang *et al.* (2014) found that variations in the fluorescence colour and intensity of blue amber from the Dominican Republic, Mexico and Myanmar corresponded to differences in their Fourier-transform infrared (FTIR) spectra (see also Wang *et al.* 2015). Although the blue colour of amber is related to its fluorescence, researchers are still trying to determine the actual fluorescence mechanism (Zhang *et al.* 2021).

One possible source of the blue fluorescence in Dominican amber is the aromatic hydrocarbon perylene ($C_{20}H_{12}$), a compound that displays fluorescence emissions similar to those of amber in the 430–530 nm range (Bellani *et al.* 2005). Liu *et al.* (2014) found that, because wavelengths below 460 nm were strongly absorbed by amber, the blue fluorescence could only be excited on the surface. Chekryzhov *et al.* (2014) studied lignite-hosted amber from the Russian Far East in which the fluorescence of blue samples resembled that of Dominican blue amber. They also proposed perylene as the cause of blue fluorescence and suggested that

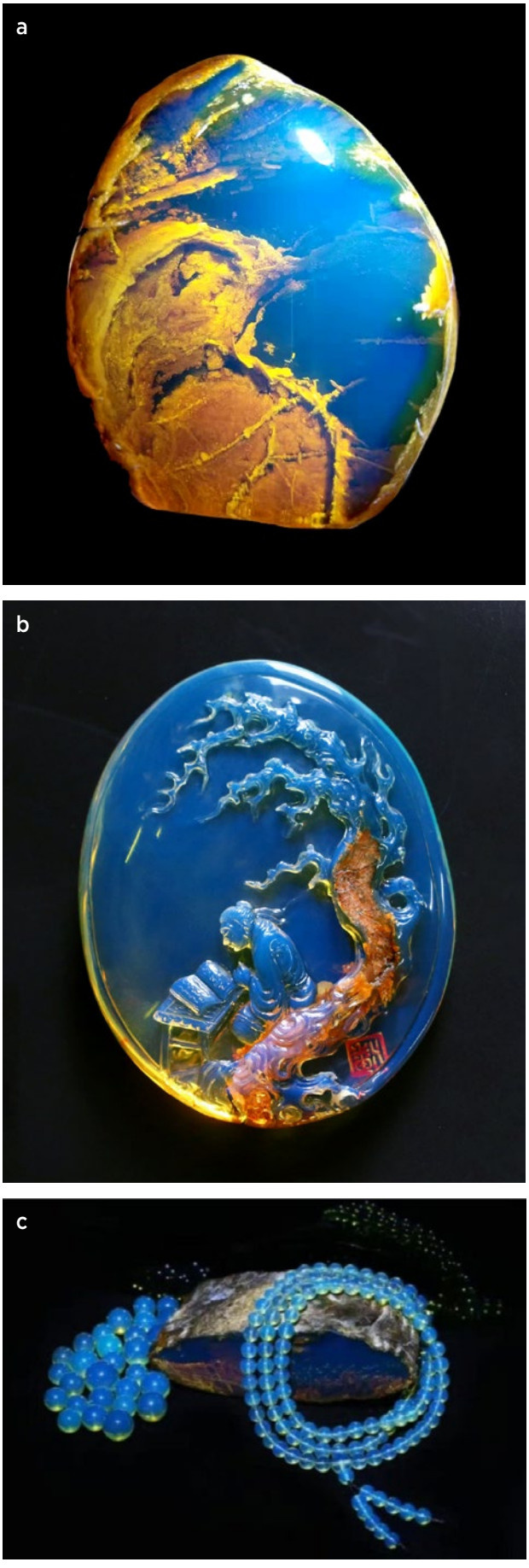


**Figure 1:** Dominican blue amber samples are shown here on a black background and viewed with D65 daylight illumination. They include (**a**) an *objet d'art* that incorporates some bark-like weathered 'skin' (30 × 40 mm); (**b**) an oval pendant carved with the Chinese motif signifying 'knowledge is boundless' (20 × 30 mm); and (**c**) high-quality 'sky-blue' beads (7 mm average diameter). Photos by Yamei Wang (a, c) and Liangzhao Pan (b).

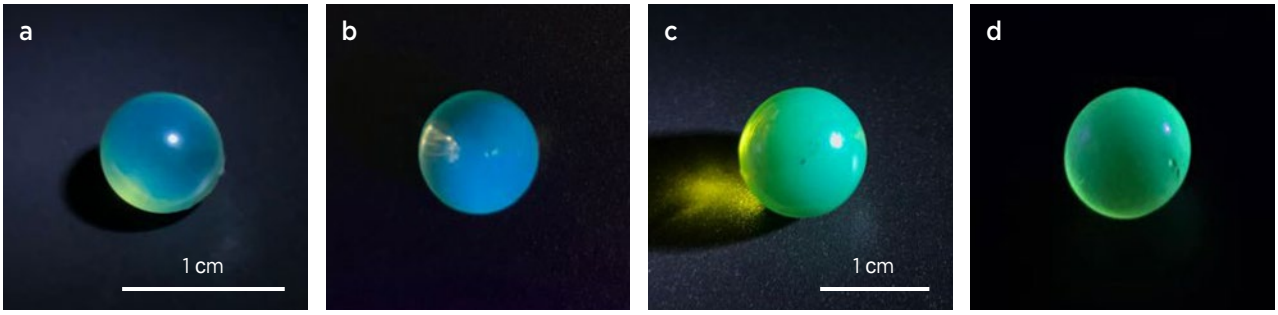


**Figure 2:** Beads of so-called blue amber from the Dominican Republic displaying blue or green colouration are shown in D65 daylight (**a** and **c**) and under 365 nm UV radiation (**b** and **d**). Photos by Chenxing Xin.

the FTIR band of perylene was probably undetectable because it was obscured by other absorptions. However, subsequent gas chromatography-mass spectrometry analysis indicated that hydrocarbon fractions (including perylene) could not be the cause of the blue fluorescence of Russian amber, and that common methods of determining the hydrocarbon composition could not provide direct data (Bechtel *et al*. 2016).

The blue to greenish blue (or even green) colour appearance of blue amber is best seen when samples are viewed with daylight-equivalent illumination (using a D65 or 6500 K colour temperature lamp) over a black background, and such material also shows strong fluorescence when exposed to UV radiation (Figure 2). Notably, some of this blue amber displays distinctive green spots and colour zones when observed over a black background in D65 daylight or under UV radiation (Figure 3). The Dominican Republic is the only locality that yields blue amber displaying this blue and green patchy appearance, and in the Chinese gem trade it is called *colour-jumping blue amber*. The irregular distribution of patchy blue and green colouration within a single piece adds beauty and mystery to this special type of amber, unlike the evenly distributed colouration of ordinary blue amber.

Nevertheless, amber showing this patchy colour phenomenon may be confused with reconstructed amber, and this misunderstanding could hinder the development of the blue amber market. In order to address this issue and explain the mechanism of this unusual colour phenomenon, we performed a systematic investigation of five samples of Dominican amber, including an analysis of their gemmological properties, luminescence characteristics, patchy colouration and degree of maturity by routine gemmological tests, three-dimensional (3D) fluorescence spectroscopy, FTIR spectroscopy and scanning electron microscopy (SEM). The results provide implications for exploring the relationship between amber maturity and its formation during geological diagenesis, and they may also be applicable to determining the geographic origin of Dominican amber.

## LOCATIONS AND GEOLOGY

Dominican amber originates from plant resin produced by the extinct tree species *Hymenaea protera* (Fabaceae family; Langenheim 1995). Unlike *in situ* fossil resins that are hosted by strata containing abundant lignite, coal and plant fossils, Dominican amber-bearing deposits

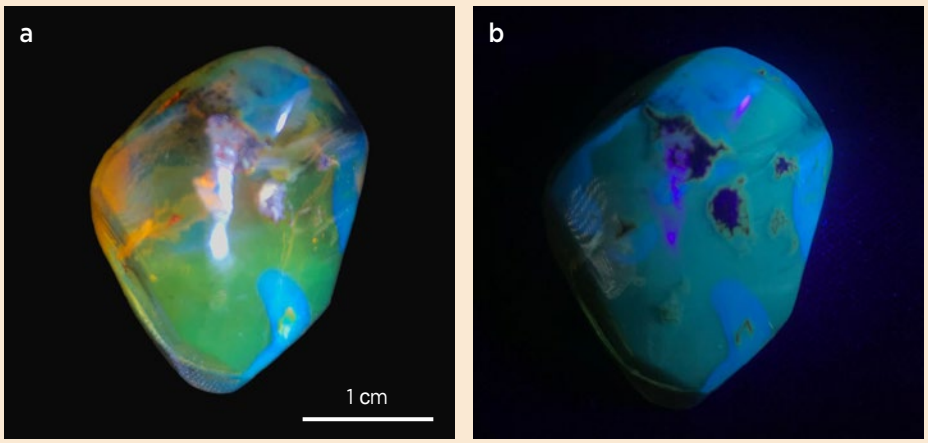


**Figure 3:** This Dominican amber sample shows patchy blue and green colouration, as seen in D65 daylight (**a**) and under UV radiation (**b**). Photos by Chenxing Xin.


**Figure 4:** Most amber mining in the Dominican Republic takes place in underground workings. (**a**) Local miners rest near a typical shaft that is more than 10 m deep. (**b**) One of the authors (GS) joins a local miner at the bottom of a shaft. Photos by Guanghai Shi (a) and Yongqiao Wu (b).

are predominantly secondary in origin and are found within sediments of various facies (from subaerial to deep marine). The original plant resin was transported along river channels by flash floods before eventually being deposited into a sedimentary basin (Grund 2006; Wang *et al.* 2019). After the resin was buried under a sedimentary pile (perhaps more than 1,000 m deep), it underwent diagenetic changes (Iturralde-Vinent 2001). Based on carbon-14 dating and studies of microfossils and foraminifera, the age of the oldest Dominican amber is estimated to range from the Lower Miocene to Middle Oligocene (23–30 Ma; Grimaldi 1995).

Commercially exploitable quantities of amber are found in two areas of the Dominican Republic: north of Santiago in the Cordillera Septentrional (the northern amber deposits), and north-east of Santo Domingo in the margin of the Cordillera Oriental (the eastern amber deposits; Iturralde-Vinent & MacPhee 1996, Liu *et al.* 2014). Mining is commonly carried out in underground workings that attain several metres or more in depth (e.g. Figure 4).

The amber showing the patchy green and blue colouration is not very common, and originates only from the eastern deposits. The eastern mining area yields the youngest resinites in Dominica, some of which may only be several hundred to several thousand years old (Grimaldi 1995). Therefore some of the resinites from this area are not completely petrified.

The surface of rough Dominican amber from both the eastern and northern deposits often possesses a brown to brownish yellow weathered 'skin' of varying thickness, or a corrugated, crust-like texture (e.g. Figure 5). The amber usually displays uniform fluorescence when observed in D65 daylight or under UV radiation, but it is difficult to predict whether after cutting it will display inhomogeneous or irregular patchy green fluorescence. A small window can be polished on the rough amber (again, see Figure 5), but it may not necessarily show the patchy green colouration, which may only appear during the cutting and polishing process.

## MATERIALS AND METHODS

Analyses were conducted primarily on five pieces of Dominican blue amber (Figure 6). Two of these—samples DM-1 and DM-2 (Figure 6a, b)—were used for destructive analyses, in which the blue and green areas were carefully separated, and data were obtained from amber of each colour on freshly exposed surfaces to avoid the influence of oxidation. The sample shown in Figures 6e and 6f displayed patchy colour on both its front and back sides, and it was mainly used for observation under cross-polarised light. In addition, some of the observations noted in the Results and Discussion section were from client stones previously examined at the China University of

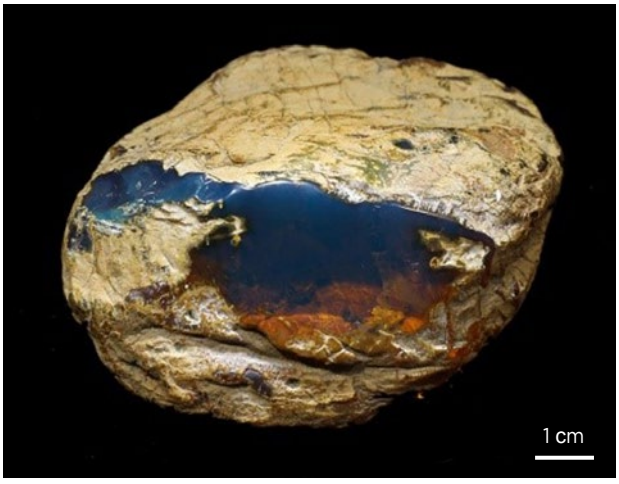


**Figure 5:** Rough Dominican amber often has a crust-like skin. A window has been polished on this specimen to check its quality and colouration. Photo by Yamei Wang.

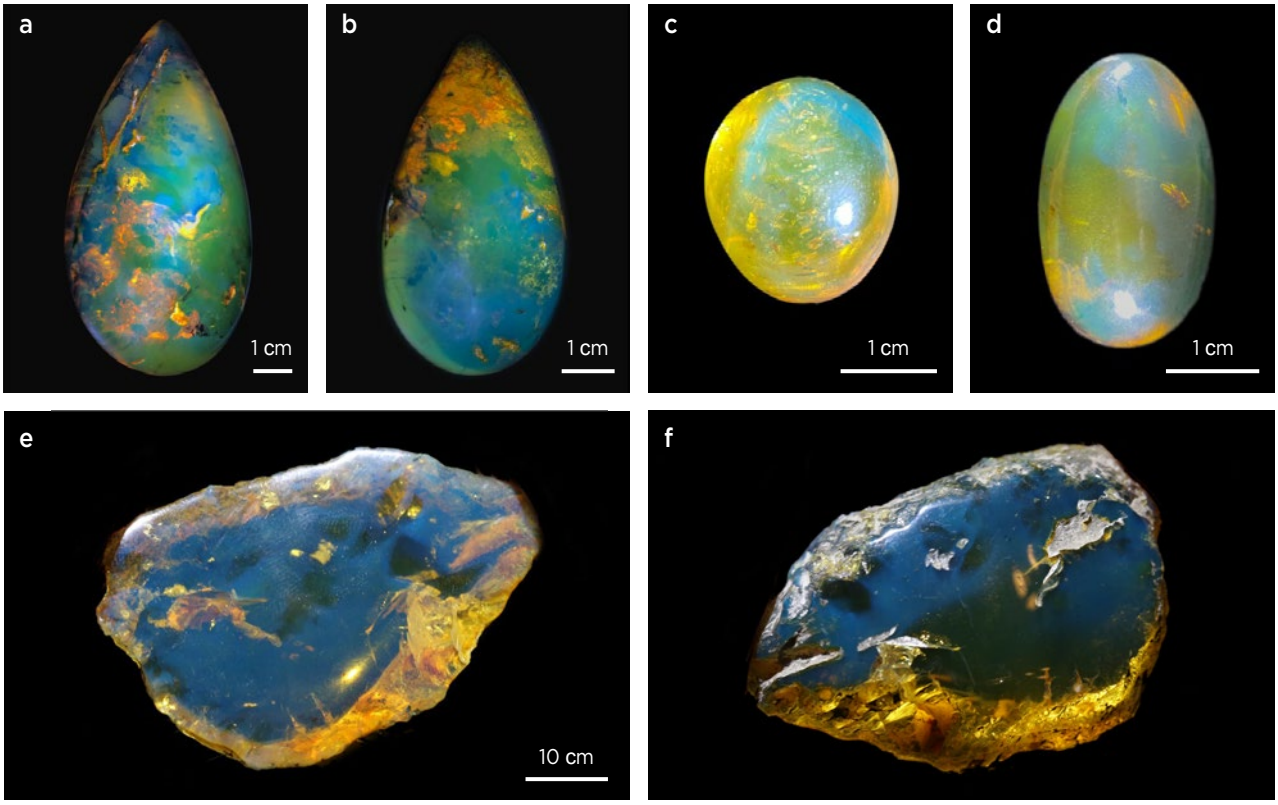


**Figure 6:** Five specimens of Dominican blue amber with patchy green and blue colouration were characterised for this study, and are shown here in D65 daylight. The samples include (**a**) DM-1, (**b**) DM-2, (**c**) DM-3, (**d**) DM-4, and another piece, shown from the front and back (**e**, **f**), that was used primarily for examination with cross-polarised light. Photos by Chenxing Xin.

Geosciences Gem Testing Centre in Guangzhou, China.

A standard D65 light source (16 W, manufactured by Zhejiang Lingchen Technology Co. Ltd) was used for daylight illumination, and a 365 nm long-wave UV lamp (5 W, Warsun R838) was employed for fluorescence observations of samples DM-1 to DM-4. A Fable FGR-002A refractometer was used for spot-RI measurements of DM-1 and DM-2; each sample was tested three times. The hydrostatic SG values of DM-1 and DM-2 were determined using a Sartorius balance (BSA 223S). Microscopic observations of DM-1 and DM-2 were performed with a Leica M205 A optical microscope using both darkfield and brightfield illumination. A polarisation unit on the microscope provided cross-polarised light for observing the samples.

Emission, excitation and 3D fluorescence spectra were collected for samples DM-1 to DM-4 using a Jasco FP-8500 3D fluorescence spectrometer equipped with a continuously adjustable xenon light source. Green and blue areas of DM-1 and DM-2 were analysed separately. The spectroscopy was performed using excitation and emission wavelengths of 220–600 nm and 240–750 nm, respectively, with a bandwidth of 5 nm. The test interval was 1 nm and the scanning speed was 2000 nm/min, performed at room temperature.

To simulate the formation of the patchy colouration in blue amber, ultraviolet-visible (UV-Vis) spectroscopy was performed on sample DM-2 using a PerkinElmer Lambda 650S spectrometer in transmission mode. The measurement range was 250–800 nm with a bandwidth of 1 nm. KeyShot Luxion ApS software (www.keyshot.com) was used for the colour simulation experiments. It can deliver real-time 3D rendering results, thus reducing the time needed to create realistic images.

The microstructure and chemical composition of the fresh cross-sections of amber samples DM-1 and DM-2 were studied with a Hitachi SU8000 scanning electron microscope using an electron-beam accelerating voltage of 20 kV and an energy-dispersive spectrometer (EDS) for chemical analysis. The samples were coated with gold and observed at room temperature.

A Bruker Vertex 80 FTIR spectrometer was used to assess the functional groups, maturity, hydrocarbon structure and geographic origin (cf. Wang *et al*. 2015) of the amber. The blue and green areas of samples DM-1 and DM-2 were powdered and mixed with KBr using a mass-fraction ratio of approximately 1:150 to prepare four pressed pellets for analysis. Spectra were collected from 4000 to 400 $cm^{-1}$ in reflectance mode, with an aperture of 1.5 mm and a resolution of 10 $cm^{-1}$.

## RESULTS AND DISCUSSION

### *Gemmological Properties*

All the specimens displayed the typical yellow body colour of amber without obvious colour variations when viewed over a white background (e.g. Figure 7a, f). However, obvious blue and green areas were seen when the samples were viewed over a black background in D65 daylight or exposed to UV radiation. The boundaries between these areas were vague in D65 daylight (Figure 7b, g) but much more apparent under UV radiation (Figure 7c, h). Specimen DM-1 (SG = 1.10, RI = 1.55) displayed an intertwined, flow-like banding of blue and green, while sample DM-2 (SG = 1.10, RI = 1.54) mainly showed two distinct areas of blue and green.

To perform a more detailed investigation of the fluorescence patterns and avoid interference from inclusions, we sawed each of these two samples into two slices of about 3.0 mm thickness (Figure 7d, e and Figure 7i, j). Comparison of the UV images of these four slices with those of the original amber samples (Figure 7c, h) revealed that the luminescence of the green areas was weaker than that of the blue areas. These slices also demonstrated that the component(s) responsible for the fluorescence showed uneven distribution and were mixed with other chemical constituents of the blue amber. As a result, the fluorescence exhibited an irregular flow pattern.

### *Internal Features*

During the secretion of tree resin, the exudate accumulates on the bark surface or in wood cavities. Various biotic and abiotic inclusions may be trapped by this viscously flowing liquid, such as the plant debris, dark impurities and filamentous plant material that we observed as typical features in our samples (Figure 8a–c). We also noted flow-like striations showing a syrupy-agitated structure (Figure 8d), which indicate the flow path of the resin. The inclusions in our patchy-coloured samples were of the same types as those seen in typical Dominican amber, indicating that the amber with patchy colour distribution also formed naturally without the introduction of any artificial inclusions (as, for instance, in reconstructed amber).

Microscopic observation of the patchy colour areas with D65 daylight showed green spots or colour blocks distributed in blue regions, sometimes with a clear boundary (Figure 9a) and sometimes interspersed with one another in which the blue colour was distributed in flat or banded shapes (Figure 9b). While the green

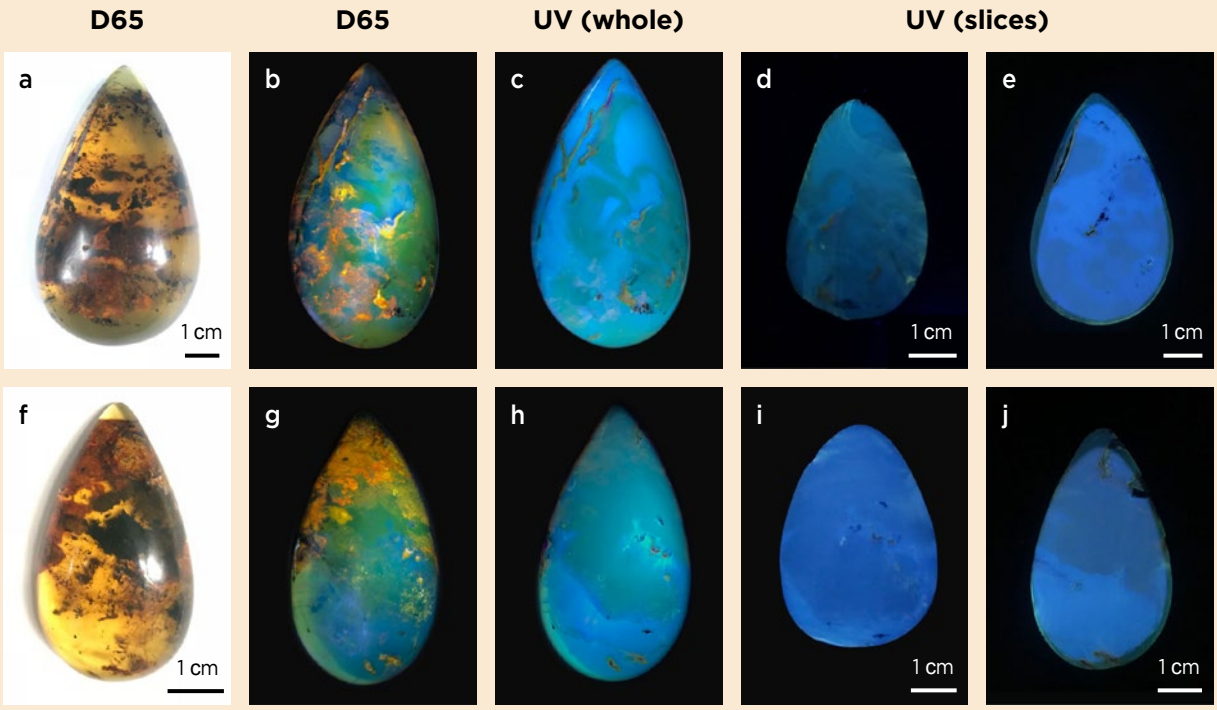


**Figure 7:** Images of Dominican blue amber samples DM-1 (top row; **a**–**e**) and DM-2 (bottom row; **f**–**j**) were taken in different conditions. The specimens are shown in D65 daylight over a white background (a, f) and over a black background (b, g), and also under UV radiation with some incident D65 daylight (c, h). Each sample was then cut into two thin slices (d and e, and i and j), which are shown under UV radiation within a light box to eliminate incident light. Photos by Chenxing Xin.

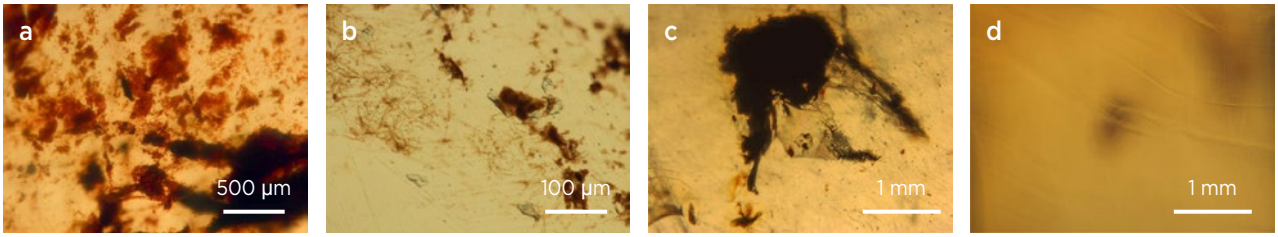


**Figure 8:** Representative internal features in the Dominican blue amber samples include plant debris and filaments (**a**–**c**) and flow patterns (**d**). Photomicrographs by Chenxing Xin.

colour appeared to penetrate into the interior, the blue colour was clearly visible only on the surface, which is consistent with the blue fluorescence being a surface phenomenon (Liu *et al*. 2014). In addition, microscopic observation under UV radiation showed that the blue and greenish blue fluorescence was clearly visible on the surface (Figure 9d, c). The flow-like distribution of fluorescence indicates that the fluorescent component in the amber is accompanied by other substances secreted in the original plant resin. Thus it is reasonable to conclude that there is no particular regularity in the flow patterns of the blue and green regions.

Due to the fluidity of plant resins, most amber materials retain abundant flow patterns during their geological evolution and such a syrupy-like appearance was common in our samples (Figure 10a, b). When viewed with cross-polarised light, colourful flow patterns were seen, with interference colours of yellow-brown, black to grey and orange-red (Figure 10c–e). Notably, the flow pattern in the blue-coloured areas of the amber was very smooth and fluid-like (Figure 10a, c), while in the green areas it was intensely disordered (Figure 10b, d). Resin secretion is a continuous process, and there might be a chronological order to its components, which is reflected in the viscosity and flow structure of the resin. These differences in the flow patterns of the blue and green coloured areas illustrate obvious variations in the chemical components of the amber.

Although the patchy-coloured amber could be mistaken for a reconstructed product, the flow patterns in reconstructed amber are discontinuous, blocky and have obvious boundaries when viewed with cross-polarised light (Figure 10f; see also Li *et al*. 2016). By comparison, the flow transitions in the patchy blue-green amber are continuous and smooth, without obvious boundaries (Figure 10e). Also, the flow pattern distribution was unpredictable in our samples. In some areas, the chaotic and fluid-like areas were completely separated, while in others they were wrapped together or intermeshed, consistent with the distribution of the blue and green colours. The characteristics of the flow patterns indicate that the blue amber with patchy colouration formed naturally.

## *Fluorescence Spectra*

The fluorescence of amber is essentially related to emission from polycyclic aromatic hydrocarbons and heterocyclic hydrocarbons. The variety of fluorescence colours in sedimentary organic matter is largely controlled, for instance, by the concentration of fluorophores, the relative proportions of saturated aromatic hydrocarbons and the degree of thermal evolution of the polycyclic aromatic hydrocarbon components (Bertrand *et al*. 1986; Khorasani 1987). However, it is difficult to accurately determine the structure of the fluorophores through comparison with the typical fluorescent characteristics of a single aromatic hydrocarbon component.

The characteristics of the fluorescence spectra of the blue and green samples (Figures 11 and 12, respectively) were roughly the same, but the fluorescence intensity in the green region was much weaker. The

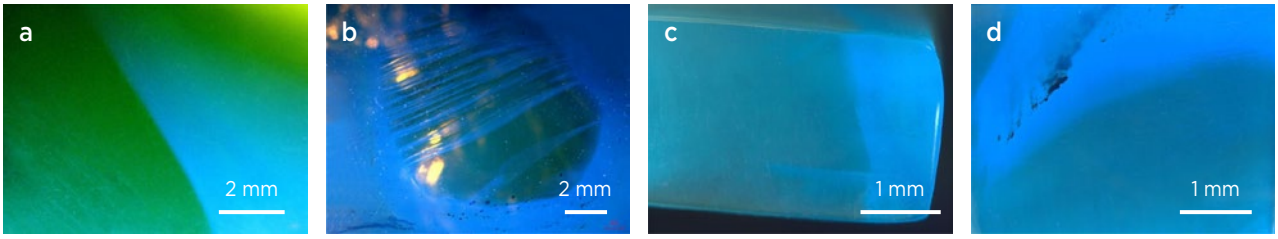


**Figure 9:** Viewed with a microscope in D65 daylight, the blue fluorescence seems to float on the surface while the green colour appears more internal, and the boundary between the two colours may be clear (**a**) or interspersed (**b**). Under UV radiation (with some incident D65 daylight) the blue and greenish blue fluorescence shows irregular distribution (**c**, **d**). Photomicrographs by Yamei Wang (a, b) and Chenxing Xin (c, d).

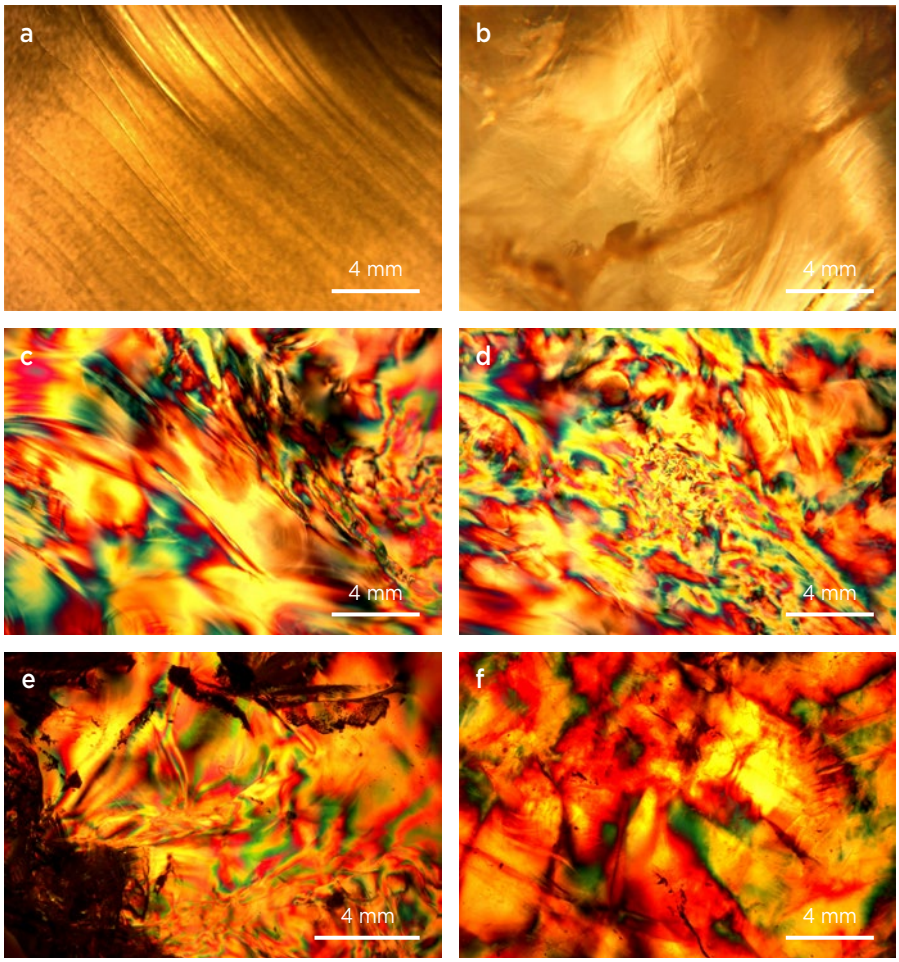


**Figure 10:** Swirl-like flow patterns appear in the (**a**) blue and (**b**) green regions of the amber, but the pattern is more fluid in the blue areas. Viewed with cross-polarised light, the blue regions (**c**) again appear more fluid than the green areas (**d**). At slightly higher magnification, it can be seen that the smooth and disordered areas in the amber are not always distinct (**e**). Nevertheless, by comparison reconstructed amber has a more fragmented and vague flow pattern with domains separated by obvious boundaries (**f**). Photomicrographs by Yamei Wang.

3D fluorescence spectrum of the blue area displayed three distinct luminous centres. However, in the green area there were only two obvious luminous centres, which may be due to the lower fluorescence intensity. Based on the literature (Bellani *et al*. 2005), the emission wavelengths were set at 447, 474 and 508 nm to acquire the excitation spectra (again, see Figures 11 and 12). The excitation spectra were nearly the same for the blue and green regions, except that a small peak at 392 nm appeared only in the blue area.

Based on the excitation spectra, the excitation wavelengths for the emission spectra were set at 417 and 440 nm. The emission spectra of the blue and green samples (again, see Figures 11 and 12) were similar and dominated mainly by peaks at approximately 448–450, 475 and 505–507 nm. The fluorescence colour was determined mainly by the 448–450 and 475 nm peaks in the blue range of the spectrum. This indicates that both the blue and green areas emit blue fluorescence and that the main fluorescent substances are probably the same in both regions. However, the fluorescence intensity is much greater in the blue areas than in the green regions; the higher the intensity, the more obvious the blue colour and the more abundant the fluorescence-causing substance(s). The shapes and locations of the main peaks in the emission spectra were also consistent with a previous study of blue amber, in which the fluorescence emission curves were similar to those of perylene, an aromatic hydrocarbon (Bellani *et al*. 2005).

## Colour Simulation

According to the complementary superposition principle of colours, blue and yellow together can appear green. In order to verify whether the patchy green colouration in Dominican blue amber follows this principle, KeyShot software was used to simulate the formation of the green colour. First, UV-Vis spectroscopy was performed on one of the same samples (DM-2) that was used for fluorescence spectroscopy.

The UV-Vis transmittance spectrum (Figure 13a) displayed typical characteristics of those collected with a long-wavelength-pass filter, showing a half-pass wavelength at about 530 nm and a cut-off at about 450 nm. Therefore, only wavelengths longer than 450 nm could

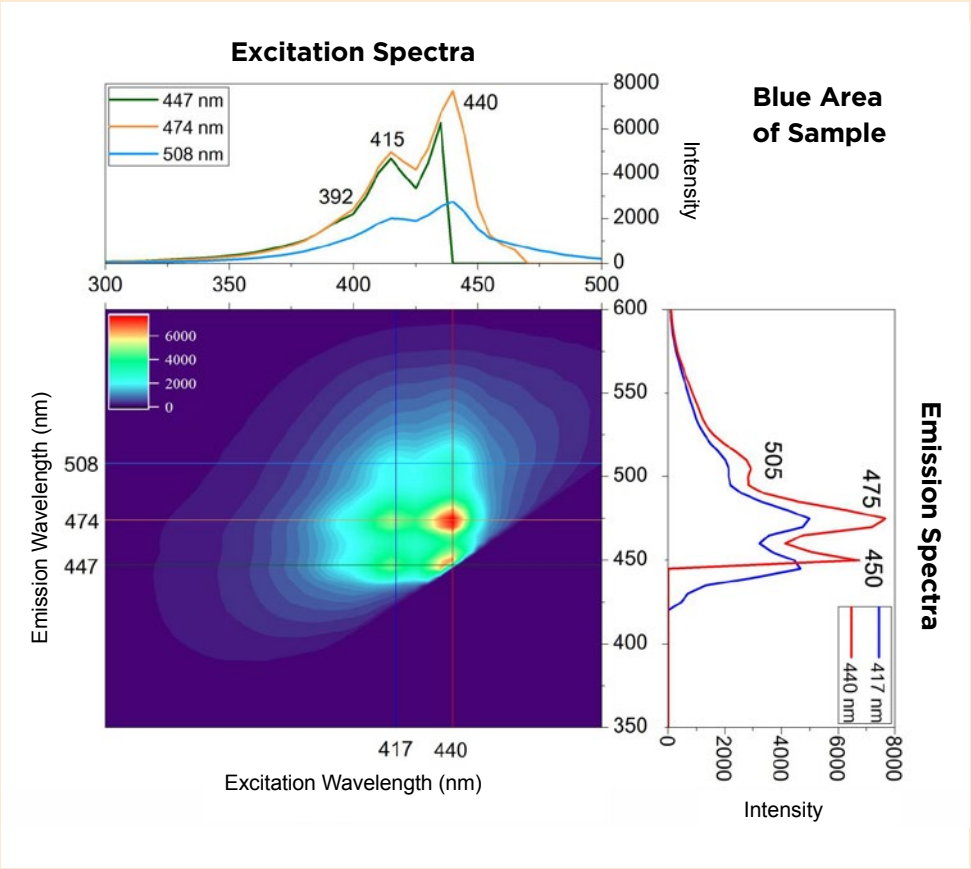


**Figure 11:** The 3D fluorescence spectrum of a blue area of Dominican blue amber sample DM-2 is shown here with its associated excitation and emission spectra. The excitation spectra were obtained with three emission wavelengths (447, 474 and 508 nm), and the emission spectra were collected using two excitation wavelengths (417 and 440 nm).

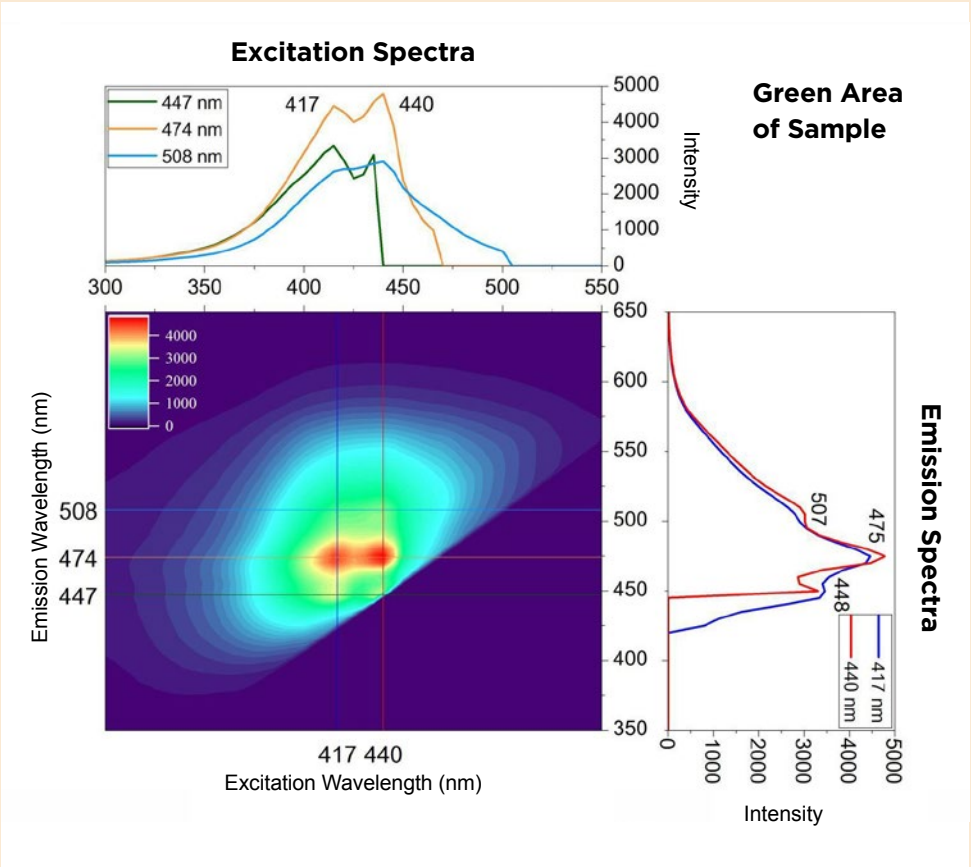


**Figure 12:** The 3D fluorescence spectrum of a green area of Dominican blue amber sample DM-2 is shown here with its associated excitation and emission spectra. The emission and excitation wavelengths are the same as in Figure 11.

partially pass through the amber. The slope of the spectrum was steep until approximately 530 nm and then increased more gradually. The fluorescence emission spectra in Figures 13b and 13c show the classic features for Dominican blue amber, with main fluorescence peaks at 445, 474 and 505 nm, but with different intensities. In the blue region, the intensities of the peaks at 445 and 474 nm were almost the same, but the situation was quite different for the green region: the intensity at 474 nm was much greater than at 445 nm (Figure 13b, c). In addition, although the fluorescence was much stronger in the blue region than in the green area, the intensity at 505 nm was nearly the same in both regions.

With the aid of the QTCCOLOR colour management tool (www.qtccolor.com/tool/spectrum.aspx), the fluorescence spectra of the blue and green areas were translated into colour data and expressed as RGB colour coordinates. The blue area had coordinates R = 0, G = 75 and B = 170, and the green area had coordinates R = 0, G = 124 and B = 161 (represented by the colour swatches in Figure 13b, c). The light-yellow body colour of the amber was also translated, and had coordinates R = 246, G = 224 and B = 85 (Figure 13a). These results support the spectral features noted above. Because 474 nm is close to the green range of the visible spectrum, and 505 nm is in the green range, in terms of colour composition the RGB value of the green area of DM-2 was closer to that of a green hue when compared to the RGB value of the blue area.

Figure 13d displays a simulation of the patchy colour phenomenon of the blue amber. The left side of the virtual sample shows the strong blue fluorescence colour on the surface without any superimposed yellow body colour. On the right side, the weaker blue fluorescence combines with the yellow body colour, resulting in a green colour showing through the transparent amber. This kind of greenish blue colour is quite common in blue amber. The inhomogeneous intensity of the blue fluorescence is therefore responsible for the patchy blue and green colouration.

We also saw this colour superposition effect when the UV radiation component of D65 daylight excited the blue fluorescence of the amber, which was seen together with its yellow body colour. When the fluorescence intensity was weak, the superposition of the surface blue fluorescence on the yellow body colour yielded a green colour (Figure 7c, h, and Figure 9c, d). This corresponded to our observations of the samples under pure long-wave UV radiation within a light box (which eliminated visible light), by showing that the different colour regions emitted blue fluorescence with different intensities (see, e.g., the four slices in Figure 7d, e, i, j), which is consistent with the fluorescence spectra.

In summary, the uneven distribution of a blue-fluorescing substance in Dominican blue amber causes inhomogeneous fluorescence intensities within a single specimen. Where differences in fluorescence intensity are not too strong, the amber appears greenish blue (as seen in most blue amber), but where the differences are stronger, a patchy colour appearance is seen.

## SEM Characterisation

SEM analysis was done to explore the microstructure of the blue and green regions and to investigate any differences in their chemical composition. Regardless of their colour appearance, almost all of the fresh cross-sections we

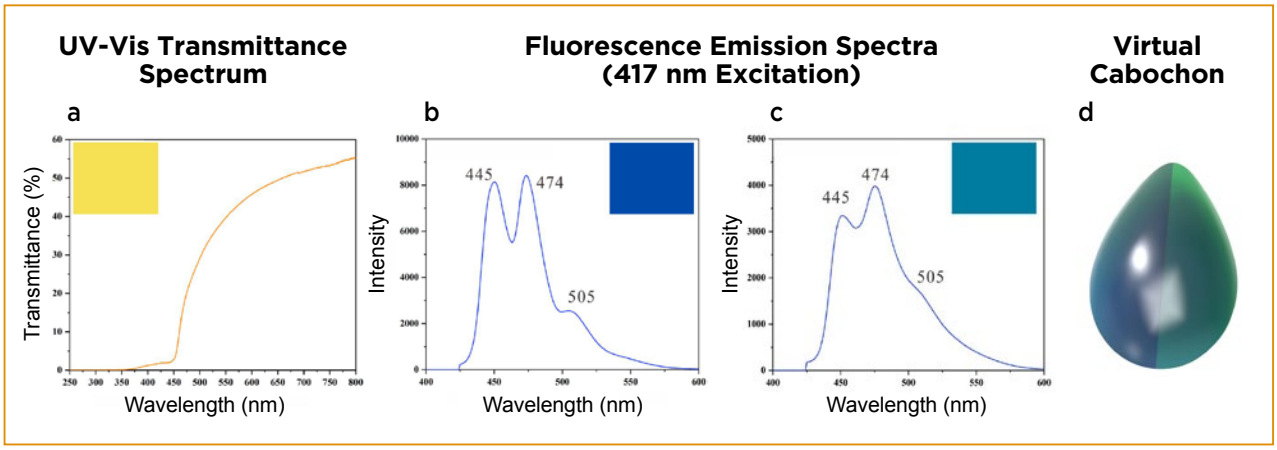


**Figure 13:** (**a**) The UV-Vis transmittance spectrum of sample DM-2 is shown alongside the translated colours and emission spectral traces for the (**b**) blue and (**c**) green regions of DM-2, as seen under long-wave UV radiation. From these translated colours, a simulation of the colour superposition effect in D65 daylight is shown in a virtual cabochon (**d**). Where the blue fluorescence is strong (left side of the virtual sample), the effect of the amber's body colour is minimal, but where the blue fluorescence is weaker (right side), the underlying yellow body colour of the amber contributes to a greenish appearance.

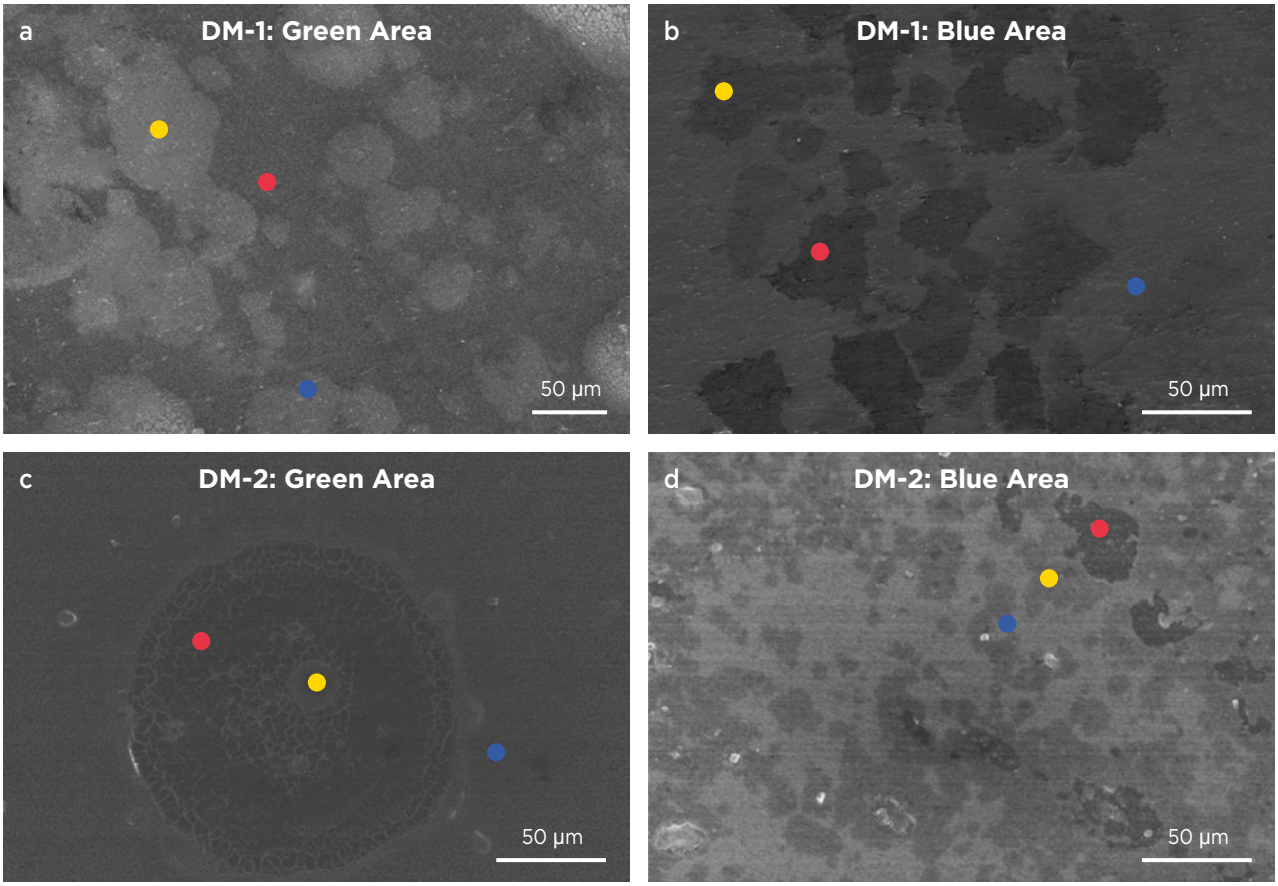


**Figure 14:** Coloured dots on these SEM images indicate where EDS analyses were performed on Dominican amber specimens DM-1 and DM-2. The darkest domains (red points) contained relatively higher amounts of O and lower C. The lighter domains (yellow and blue points) had relatively higher C and lower O (see Table I).

tested revealed non-identical microstructures, sometimes even within the same colour regions. In general, the SEM images showed at least two or three different domains, which appeared grey, darker grey or black (Figure 14). The different grey regions were irregularly distributed, with distinct to blurred boundaries.

Chemical composition was measured on three areas per sample that corresponded to the different shades of grey (again, see Figure 14). The results in Table I show that all areas consisted of oxygen and carbon, the main chemical components of amber (hydrogen cannot be detected by EDS analysis). Overall, C contents were uniform in both the blue and green areas, with local variations reflected by the tonal differences in the SEM images, which reflect differences in average atomic number. (In the working principle of the SEM, the secondary electron emission yield, as a whole, changes with atomic number, and when the atomic number difference in various phases is large enough then the secondary-electron image may reveal compositional contrasts; see Li *et al.* 2011.) The darkest areas (red points in Figure 14) consistently contained higher amounts of O and lower amounts of C. On the other hand, the lighter grey areas (yellow and blue points)

**Table I:** Semi-quantitative chemical composition of the different areas shown in Figure 14a–d, obtained by EDS analysis.

| Area (and amber colour) in Figure 14 | | C (wt.%) | O (wt.%) | C/O ratio |
|---|---|---|---|---|
| 14a (Green) | Red point | 88.7 | 11.3 | 7.8 |
| | Yellow point | 93.9 | 6.1 | 15.4 |
| | Blue point | 91.7 | 8.3 | 11.0 |
| 14b (Blue) | Red point | 91.0 | 9.0 | 10.1 |
| | Yellow point | 94.6 | 5.4 | 17.5 |
| | Blue point | 93.6 | 6.4 | 14.6 |
| 14c (Green) | Red point | 89.3 | 10.3 | 8.7 |
| | Yellow point | 91.4 | 8.7 | 10.5 |
| | Blue point | 92.3 | 7.8 | 11.8 |
| 14d (Blue) | Red point | 91.3 | 8.7 | 10.5 |
| | Yellow point | 93.3 | 6.8 | 13.7 |
| | Blue point | 94.7 | 5.3 | 17.9 |

showed higher C and lower O. This suggests that, due to the varying composition of the original resin, differences in C content exist at the micro level. These reflect variations in amber maturity, as shown in the FTIR analyses below (Grimaldi 2009; Langenheim & Beck 1965). The maturation process involves progressive oxidation, polycondensation and polymerisation in addition to devolatilisation, which is reflected by changes in carbon content.

## *FTIR Spectroscopy and Degree of Amber Maturation*

The curve shapes and main band positions in the FTIR spectra of the blue and green regions were generally the same (Figure 15), confirming the specimens were natural amber and that both of the different-coloured areas originated from the same plant resin. The spectra mainly showed the presence of aliphatic groups (3000–2800 $cm^{-1}$ and 1480–1350 $cm^{-1}$) and oxygenated groups (1800–1600 $cm^{-1}$). All samples displayed bands at 2922 and 2851 $cm^{-1}$ attributed to methyl groups (Seyfullah *et al.* 2015). Two other bands are ascribed to alkyl groups: one at 1459 $cm^{-1}$ associated with $CH_2$ and $CH_3$ bending, and the other at 1382 $cm^{-1}$ due to $CH_3$ bending (Angelini & Bellintani 2005). Furthermore, the stretching band at 1241 $cm^{-1}$ is dominated by carboxylic acid carbon-oxygen (van der Werf *et al.* 2016).

In some fossil resins with a labdane skeleton, it is quite common to detect bands at 1642 and 1459 $cm^{-1}$, which are usually regarded as indicators of higher maturity (Yang & Wang 2010). In some other immature resins, such as copal, the 1642 $cm^{-1}$ band shows greater intensity (Angelini & Bellintani 2005), and with the consumption of C=C bonds in the formation of $CH_2$ and $CH_3$ during oxidation the 1459 $cm^{-1}$ peak increases. This was also reflected in both the green and blue areas, which had a greater intensity at 1459 $cm^{-1}$, while the peak at 1642 $cm^{-1}$ was more obvious in the green zone. Exocyclic alkenes in diterpenoid compounds are represented by a band at 888 $cm^{-1}$ caused by exocyclic methylene, which also indicates amber maturity (Cotton *et al.* 2017). The 888 $cm^{-1}$ absorption related to C=C in the green portion was significantly greater than in the blue region (Figure 15). This might be related to the differentiation of the components of the original resin, that is, the terpenes in the green area were higher than in the blue area. Clearly, the blue colour region has a relatively higher maturity.

Dominican amber is the best-known Class Ic terpenoid amber (Yang & Wang 2010). It lacks succinic acid and is commonly associated with labdatriene (diterpenoid) carboxylic acids. In the original plant resin, an abundance of mono-, sesqui-, di- and tri-terpenoids mix together to comprise the dominant and the fluorescent substances (Iturralde-Vinent & MacPhee 1996; Grimaldi 2009). After experiencing complex oxidative cross-linking processes, the plant resin evolved into fossil resin. Since the fluorescence-producing substance is accompanied by other components, the flow pattern and irregular distribution are both visible in the fluorescence pattern of the amber (e.g. Figure 9b).

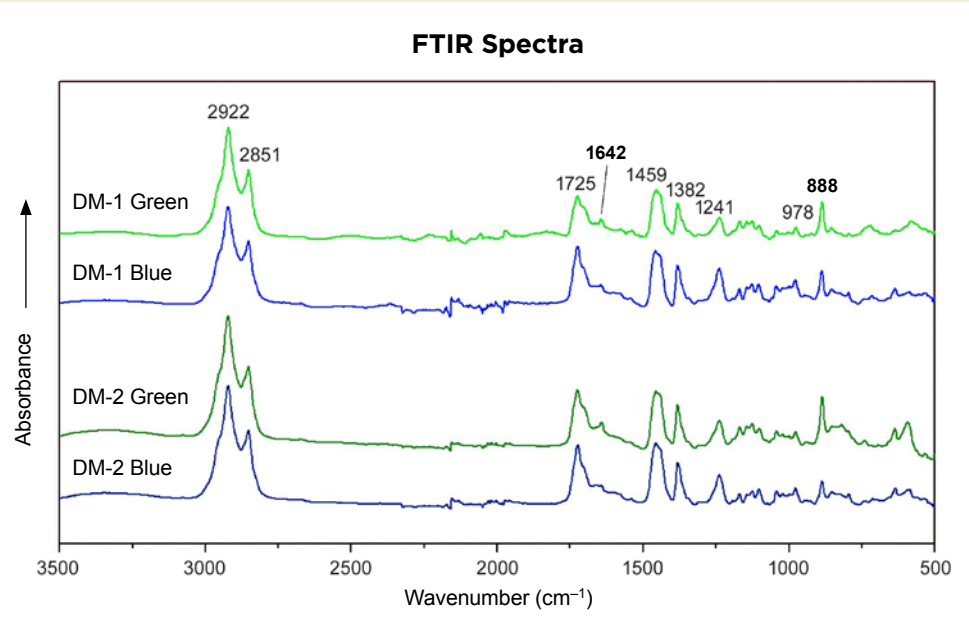


**Figure 15:** FTIR spectra of the green and blue regions of Dominican amber indicate that both areas came from similar plant resin. The features at 1642 and 888 $cm^{-1}$ are considered indicators of maturity, and show that the blue amber is more mature than the green amber.

Because the formation of plant resin is a continuous process, there are variations in the composition of the resin that lead to differences in volatile contents and fluorescent substances. While experiencing the same diagenetic process during burial, variations in the amounts of volatile matter might result in different degrees of maturity in separate regions of a single specimen. The uneven distribution of fluorescent substances is the main reason for the relatively large differences in fluorescence intensity within a specimen displaying patchy blue and green colouration. Nevertheless, it is challenging to interpret the complicated formation process of amber under geological conditions in order to understand the compositional variation of amber and interpret the evolution of its fluorescence with increasing maturity.

## CONCLUSIONS

This study reports on Dominican blue amber showing interesting patchy blue and green colouration. It can be easily distinguished from reconstructed amber by its flow patterns visible with cross-polarised light, as well as by its spectral characteristics and, as previously documented for amber in general, by inclusions such as organic debris. The blue fluorescence colour is dominated by emissions at around 447 and 474 nm (in the blue range), and the blue appearance of the amber is caused by the strong intensity of these features. A green colour appearance results from weaker blue fluorescence that is superimposed on the amber's yellow body colour. This could also explain why most 'blue amber' has a greenish hue.

The intensity of blue luminescence also shows a positive correlation with the degree of amber maturity: the greater the maturity, the stronger the luminescence. The uneven colour distribution—and the differences in maturity degree that it indicates—is related to the uneven distribution of the fluorescent component(s) in the original plant resin during its successive secretion process.

This research on Dominican amber suggests that further investigations of the fluorescence intensities and luminescent characteristics of blue amber could yield helpful information for origin determination, and could shed light on the process of formation and the compositions of luminescent components.

## REFERENCES


Angelini, I. & Bellintani, P. 2005. Archaeological ambers from northern Italy: An FTIR-DRIFT study of provenance by comparison with the geological amber database. *Archaeometry*, **47**(2), 441–454, https://doi.org/10.1111/j.1475-4754.2005.00212.x.

Bechtel, A., Chekryzhov, I.Y., Nechaev, V.P. & Kononov, V.V. 2016. Hydrocarbon composition of Russian amber from the Voznovo lignite deposit and Sakhalin Island. *International Journal of Coal Geology*, **167**, 176–183, https://doi.org/10.1016/j.coal.2016.10.005.

Bellani, V., Giulotto, E., Linati, L. & Sacchi, D. 2005. Origin of the blue fluorescence in Dominican amber. *Journal of Applied Physics*, **97**(1), article 016101 (2 pp.), https://doi.org/10.1063/1.1829395.

Bertrand, P., Pittion, J. & Bernaud, C. 1986. Fluorescence of sedimentary organic matter in relation to its chemical composition. *Organic Geochemistry*, **10**(1–3), 641–647, https://doi.org/10.1016/0146-6380(86)90061-6.

Chekryzhov, I.Y., Nechaev, V.P. & Kononov, V.V. 2014. Blue-fluorescing amber from Cenozoic lignite, eastern Sikhote-Alin, Far East Russia: Preliminary results. *International Journal of Coal Geology*, **132**, 6–12, https://doi.org/10.1016/j.coal.2014.07.013.

Cotton, L.J., Vollrath, F., Brasier, M.D. & Dicko, C. 2017. Chemical relationships of ambers using attenuated total reflectance Fourier transform infrared spectroscopy. *Geological Society, London, Special Publications*, **448**, 413–424, https://doi.org/10.1144/sp448.22.

Grimaldi, D. 2009. Pushing back amber production. *Science*, **326**(5949), 51–52, https://doi.org/10.1126/science.1179328.

Grimaldi, D.A. 1995. The age of Dominican amber. *In*: Anderson, K.B. & Crelling, J.C. (eds) *Amber, Resinite, and Fossil Resins*. American Chemical Society, Washington DC, USA, 203–217, https://doi.org/10.1021/bk-1995-0617.ch011.

Grund, M. 2006. Chironomidae (Diptera) in Dominican amber as indicators for ecosystem stability in the Caribbean. *Palaeogeography, Palaeoclimatology, Palaeoecology*, **241**(3–4), 410–416, https://doi.org/10.1016/j.palaeo.2006.04.005.

Iturralde-Vinent, M.A. 2001. Geology of the amber-bearing deposits of the Greater Antilles. *Caribbean Journal of Science*, **37**(3), 141–167.

Iturralde-Vinent, M.A. & MacPhee, R.D.E. 1996. Age and paleogeographical origin of Dominican amber. *Science*, **273**(5283), 1850–1852, https://doi.org/10.1126/science.273.5283.1850.

Jarzembowski, E.A., Wang, B. & Zheng, D. 2020. The first notocupedin beetle in mid-Cretaceous amber of northern Myanmar (Insecta: Coleoptera: Archostemata). *Cretaceous Research*, **106**, article 104225 95 pp.), https://doi.org/10.1016/j.cretres.2019.104225.

Jiang, W.Q., Nie, S.F. & Wang, Y.M. 2014. Fluorescence spectral characteristic of blue amber from Dominican

Republic, Mexico and Myanmar. *Journal of Gems and Gemmology*, **19**(2), 1–8, https://doi.org/10.15964/j.cnki.027jgg.2017.02.001 (in Chinese with English abstract).

Khorasani, G.K. 1987. Novel development in fluorescence microscopy of complex organic mixtures: Application in petroleum geochemistry. *Organic Geochemistry*, **11**(3), 157–168, https://doi.org/10.1016/0146-6380(87)90019-2.

Langenheim, J.H. 1969. Amber: a botanical inquiry. *Science*, **163**(3872), 1157–1169, https://doi.org/10.1126/science.163.3872.1157.

Langenheim, J.H. 1995. Biology of amber-producing trees: Focus on case studies of *Hymenaea* and *Agathis*. *In*: Anderson, K.B. & Crelling, J.C. (eds) *Amber, Resinite, and Fossil Resins*. American Chemical Society, Washington DC, USA, 1–31, https://doi.org/10.1021/bk-1995-0617.ch001.

Langenheim, J.H. & Beck, C.W. 1965. Infrared spectra as a means of determining botanical sources of amber. *Science*, **149**(3679), 52–54, https://doi.org/10.1126/science.149.3679.52.

Li, P., Bao, S., Zhang, D., Zhuang, L. & Ma, L. 2011. Application of secondary electron composition contrast imaging method in microstructure studies on cathode materials of TWT. *Materials Science Forum*, **689**, 255–259, https://doi.org/10.4028/www.scientific.net/MSF.689.255.

Li, H., Liang, J., Lu, T., Zhang, J. & Zhou, J. 2016. Identification of reconstructed amber from different periods. *Journal of Gemmology*, **35**(4), 320–328, https://doi.org/10.15506/JoG.2016.35.4.320.

Liu, Y., Shi, G. & Wang, S. 2014. Color phenomena of blue amber. *Gems & Gemology*, **50**(2), 134–140, https://doi.org/10.5741/gems.50.2.134.

Ross, A., Mellish, C., York, P. & Crighton, B. 2010. Burmese amber. *In*: Penney, D. (ed) *Biodiversity of Fossils in Amber from the Major World Deposits*. Siri Scientific Press, Manchester, 208–235.

Seyfullah, L.J., Sadowski, E.-M. & Schmidt, A.R. 2015. Species-level determination of closely related araucarian resins using FTIR spectroscopy and its implications for the provenance of New Zealand amber. *PeerJ*, **3**, article e1067 (17 pp.), https://doi.org/10.7717/peerj.1067.

van der Werf, I.D., Fico, D., De Benedetto, G.E. & Sabbatini, L. 2016. The molecular composition of Sicilian amber. *Microchemical Journal*, **125**, 85–96, https://doi.org/10.1016/j.microc.2015.11.012.

Wang, Y., Shi, G., Shi, W. & Wu, R. 2015. Infrared spectrum identification characteristics of amber from three major producing areas (Dominican Republic, Mexico and Myanmar). *Spectroscopy and Spectral Analysis*, **35**(8), 2164–2169, https://doi.org/10.3964/j.issn.1000-0593(2015)08-2164-06 (in Chinese with English abstract).

Wang, Y., Li, Y., Liu, F. & Chen, Q. 2019. Characteristics of hydrothermally treated beeswax amber. *Gems & Gemology*, **55**(3), 370–387, https://doi.org/10.5741/gems.55.3.370.

Winkler, W., Kirchner, E.C., Asenbaum, A. & Musso, M. 2001. A Raman spectroscopic approach to the maturation process of fossil resins. *Journal of Raman Spectroscopy*, **32**(1), 59–63, https://doi.org/10.1002/1097-4555(200101)32:1%3C59::aid-jrs670%3E3.0.co;2-d.

Wolfe, A.P., McKellar, R.C., Tappert, R., Sodhi, R.N.S. & Muehlenbachs, K. 2016. Bitterfeld amber is not Baltic amber: Three geochemical tests and further constraints on the botanical affinities of succinite. *Review of Palaeobotany and Palynology*, **225**, 21–32, https://doi.org/10.1016/j.revpalbo.2015.11.002.

Xing, L., Caldwell, M.W., Chen, R., Nydam, R.L., Palci, A., Simões, T.R., McKellar, R.C., Lee, M.S.Y. *et al*. 2018. A mid-Cretaceous embryonic-to-neonate snake in amber from Myanmar. *Science Advances*, **4**(7), article eaat5042 (8 pp.), https://doi.org/10.1126/sciadv.aat5042.

Yang, Y., & Wang, Y. 2010, Summary on organic components and relevant spectral characteristics of amber and copal. *Journal of Gems & Gemology*, **12**(1), 16–22, https://doi.org/10.15964/j.cnki.027jgg.2010.01.005 (in Chinese with English abstract).

Zhang, Z., Jiang, X., Wang, Y., Kong, F. & Shen, A.H. 2021. Fluorescence characteristics of blue amber from the Dominican Republic. *Gems & Gemology*, **56**(4), 484–496, https://doi.org/10.5741/gems.56.4.484.

## The Authors

**Chenxing Xin[1], Dr Yan Li[1], Dr Yamei Wang[1, 2] and Dr Guanghai Shi[3]**

[1] Gemmological Institute, China University of Geosciences, Wuhan 430074, China

[2] China University of Geosciences Gem Testing Centre, Guangzhou 510080, China

[3] State Key Laboratory of Geological Processes and Mineral Resources, China University of Geosciences, Beijing 100083, China

Emails: yanli@cug.edu.cn; wangym@cug.edu.cn

## Acknowledgements

The authors thank all who have contributed to this project, especially Prof. Andy H. Shen, Jiang Jie and Fanglin Lv for their great support and fruitful discussions. The thoughtful and constructive comments by the reviewers and editors are gratefully acknowledged. This research was financially supported by grant no. 2018YFF0215400 from the National Key R&D Program of China and grant no. CIGTXM-02-202001 from the Hubei Province Gemstone Technology Engineering Research Centre. This paper is CIGT contribution CIGTWZ-2020001.

# Liberation of Emeralds from Micaceous Host Rock Using Electric-Pulse Disaggregation Versus Conventional Processing

Vishnu Dasari, Anirudh Sharma, Etienne Marvillet, Prahalad Singh, Vladimir Rudashevsky, Oleg Alikin and Urja Zaveri

**ABSTRACT:** In ore processing, electric-pulse disaggregation (EPD) is used for the liberation of mineral crystals from host rocks. Since 2019, EPD technology has been used exclusively to recover emeralds produced from the Kagem mine in Zambia. This article compares the differences in the recovery of emeralds from micaceous schist host rock at the Kagem mine by EPD technology versus the conventional hand-cobbing method. The amount of emeralds obtained using both methods was similar, but EPD had numerous advantages in terms of liberation speed, ease of performing the process and the characteristics of the liberated emeralds.

*The Journal of Gemmology*, **37**(7), 2021, pp. 716–724, https://doi.org/10.15506/JoG.2021.37.7.716


**Figure 1:** Emerald crystals are recovered from micaceous host rocks at the Kagem mine in Zambia. The gems must be extracted from the micaceous material prior to sorting and quality assessment. Photo © Gemfields Ltd, 2021.

**Figure 2:** Kagem is considered the world's largest emerald mining area. This photo shows one of the currently active pits. Photo © Gemfields Ltd, 2021.

In the gem industry, the size and quality of rough material play a crucial role in its pricing. Thus, one of the primary goals during mining and recovery is the liberation of the rough stones without any breakage that reduces their size or diminishes transparency. This is particularly important for gem material that is 'frozen' within host rock rather than crystallising in open cavities or 'pockets'. An excellent example of this is provided by emeralds that form in schist-type deposits (e.g. Figure 1) and must be liberated from their host rock before they can be sorted and cut into gemstones.

Electric-pulse disaggregation (EPD) is a mineral-processing technology developed as an alternative to mechanical crushing to liberate mineral grains and crystals from any rock type, regardless of its lithology or grain-size distribution (Cabri *et al*. 2008). Additional terms for this technique include *electrical fragmentation, electrical disintegration, high-voltage pulsed-power fragmentation* and *high-voltage breakage* (or *high-voltage pulse breakage*). EPD technology replaces the compressive force used for mechanical crushing with tension caused by the shearing effect of a localised explosion. During the EPD process, rock material is immersed in a water bath, where it undergoes fragmentation when subjected to high-voltage pulses that are greater than 50 kV. The high voltage causes the rock to break along zones of weakness, usually represented by grain boundaries. As a result, mineral crystals are mostly liberated in their original sizes and shapes (Andres 1995; Cabri *et al*. 2008; van der Wielen *et al*. 2014). In addition, the EPD technique can be used to 'pre-weaken' ores before conventional processing (Wang *et al*. 2011).

In this study, we focus on emerald liberation using the EPD Spark-2 device installed at the Kagem mine in Zambia (Figure 2), in comparison to the conventional hand-cobbing approach. The use of EPD Spark-2 equipment to process different types of geological samples for the extraction of gems, diamonds, and precious and rare metals was reviewed by Cabri *et al*. (2008) and Rudashevsky *et al*. (2018). This study specifically explores the effectiveness of this device for liberating emerald grains greater than 2.8 mm in size from their micaceous matrix and compares the performance of this technique to conventional mechanical hand cobbing that is more commonly used for the recovery of gem material at similar deposits.

## BACKGROUND

### *Use of EPD in Geoscience and Gem Applications*

An extensive database of peer-reviewed publications on different applications of EPD in geosciences is available at www.mineralogy.online, and various studies have revealed its applications and advantages as compared to mechanical crushing for the comminution of ores

(Lastra *et al*. 2003; Ito *et al*. 2009; Matko 2020) and the recovery of gem materials (Rudashevsky *et al*. 2018). EPD is used in process mineralogy (analysis of relationships between ore and gangue or accessory minerals in order to optimise the recovery of target elements), mineral processing (treating ores and mineral products in order to separate the valuable minerals from the gangue) and as a sample preparation technique for:

- Extraction of grains of precious metals such as silver, gold and platinum-group metals from ore material (Cabri *et al*. 2008; Rudashevsky *et al*. 2018)
- Extraction and concentration of diamond-indicator minerals, microdiamonds and various accessory minerals from kimberlite and other matrix rocks (Cabri *et al*. 2008; Rudashevsky *et al*. 2018; Matko 2020)
- Recovery of gem rough from host rock as undamaged crystals (Cabri *et al*. 2008; Rudashevsky *et al*. 2018)
- Recovery of fossils and microfossils from rocks (Saini-Eidukat & Weiblen 1996; Beasley *et al*. 2020)

Some specific gem applications of EPD technology include recovering emeralds at the Sandawana mine in Zimbabwe and diamonds elsewhere in Zimbabwe (Andres 1995). The EPD Spark-2 device, in particular, has been used at the Korkodino demantoid mine (Cabri *et al*. 2008), and it is presently employed at the Poldnevskoy demantoid mine in Russia. In addition, since 2019 the EPD Spark-2 device has been used at the Kagem emerald mine in Zambia.

### *Kagem Emerald Mine*

The Kagem emerald mine (Figure 2) is operated by Gemfields Ltd, one of the world's leading suppliers of coloured stones. Kagem emeralds most commonly occur in micaceous rocks adjacent to quartz veins and pegmatites that caused hydrothermal alteration of the talc-chlorite-tremolite-magnetite schist host rocks (Zwaan *et al*. 2005; Cook 2009).

Gemfields acquired the Kagem mine in 2008, in partnership with the Zambian government through the Industrial Development Corporation, and has provided a steady supply of emeralds to the gem trade. Today, the Kagem mine produces about one-third of the world's emeralds by volume and is reportedly the world's largest producing emerald mine, covering 41 km$^2$. The Kagem mine aims to positively impact local communities, in alignment with the United Nations' Division for Sustainable Development Goals (see https://sdgs.un.org/goals). In addition, Kagem provides funds for conservation initiatives aimed at protecting Africa's wildlife.

### *EPD Technology at the Kagem Mine*

The EPD Spark-2 device at the Kagem mine (Figure 3) was developed by CNT Instruments LLC (St Petersburg, Russia) and is housed in a separate facility beside the sorting house. The equipment includes a 2.5 × 2.5 × 2.5 m Faraday cage and separate high-voltage grounding. A specially designed power supply and control board are connected to a Marx generator, which consists of ten impulse capacitors connected in parallel to allow the build-up of high voltage that can exceed 250 kV. An array of spark gaps (spherical electrodes separated by an adjusted distance) is triggered in the air, closing the circuit so that the discharge occurs in a series arrangement. The inductance coils in the circuit regulate the timing of the discharges. Due to a sudden increase of electric current in the expanding discharge channel filled by high-density plasma, a physical tensile force is exerted on the rock, resulting in its explosive breakdown below the electrode inside the water-filled chamber (Figure 4; see also Andres 1995; Cabri *et al*. 2008).

## MATERIALS AND METHODS

Samples of emerald-bearing micaceous schist from Kagem's run-of-mine product were used for this study. They were pre-tumbled to remove some of the mica and other easily detachable gangue and to provide roughly equivalent-sized pieces for the experiments. Two batches were prepared to yield a similar composition, quality and quantity (Figure 5) to test emerald extraction using EPD vs conventional hand cobbing:

- Batch 1 (for EPD): 26 pieces with a total weight of 755.0 g and an average mass of 29.0 g/piece
- Batch 2 (hand cobbing): 21 pieces with a total weight of 750.0 g and an average mass of 35.7 g/piece

The procedures used for each processing technique are described below and summarised in Figure 6. The following were noted individually for each batch:

- Weight of the material produced
- Characteristics of the material produced
- Amount of time taken
- Ease of performing the process

Batch 1 was processed by the EPD Spark-2 device using a 16 mm sieve for 1 minute at 1 Hz frequency with a 25 mm distance between the electrode and the sieve (again, see Figure 4), using an output voltage of over 250 kV in a 40 L chamber filled with tap water.

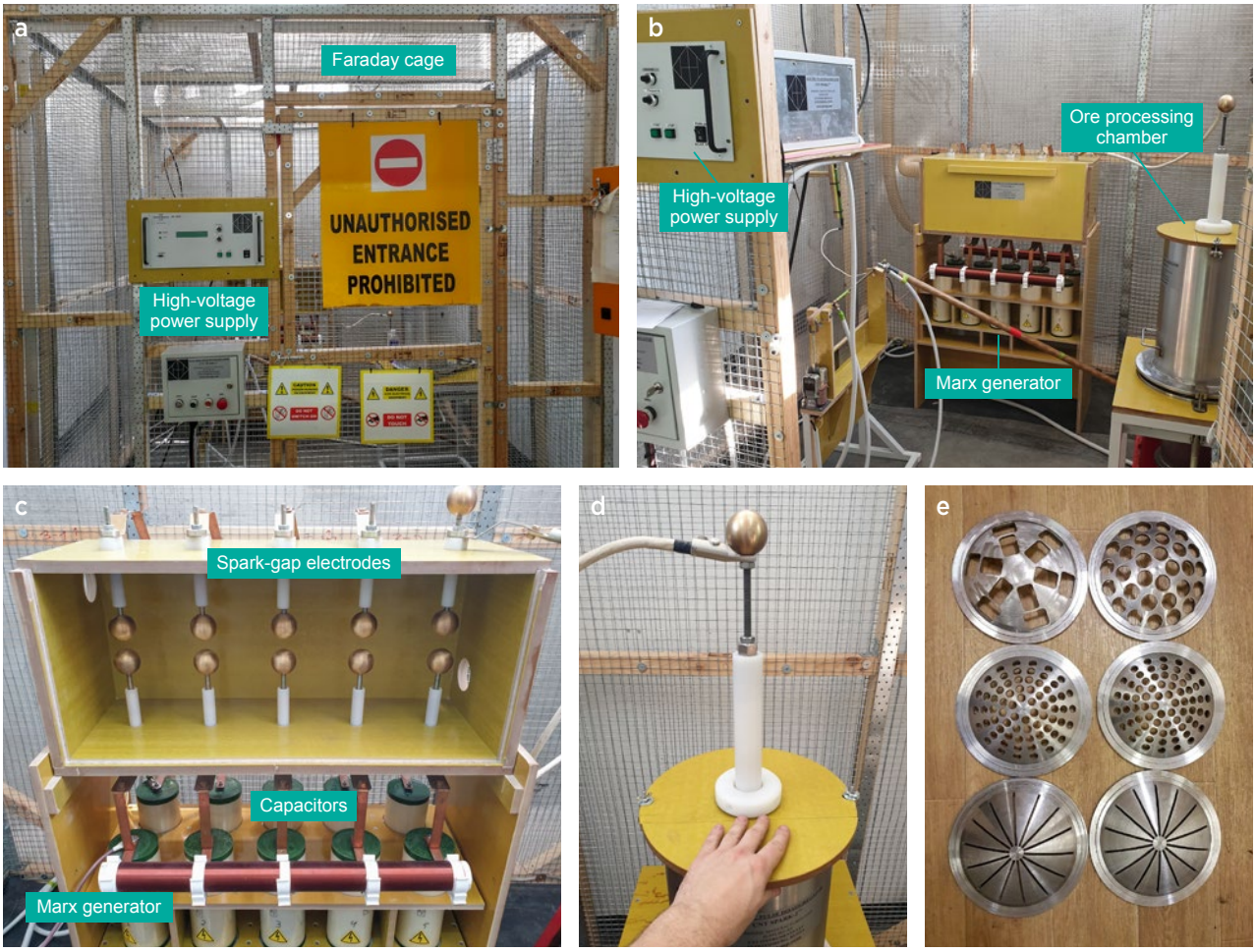


**Figure 3:** The EPD Spark-2 device was installed at the Kagem mine in 2019. (**a**) The equipment is housed inside a Faraday cage. (**b**) The components include a high-voltage power supply (left), Marx generator (centre) and the ore processing chamber (right). (**c**) The Marx generator consists of a series of impulse capacitors and associated spark electrodes. (**d**) Ore material is processed in a cylindrical chamber (located under a wooden lid) that is filled with water. (**e**) Sieves of various sizes can be used to suspend the ore material within the sample chamber. Photos by V. Rudashevsky and O. Alikin.

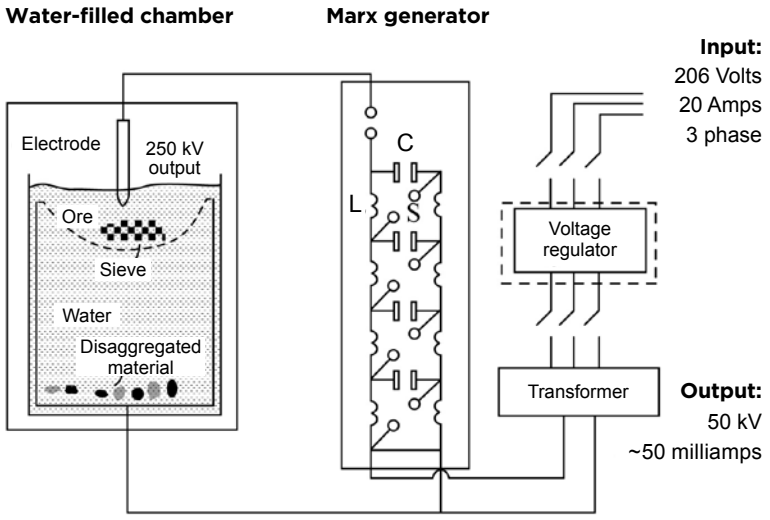


**Figure 4:** This simplified circuit diagram for an EPD device (adapted from Cabri *et al.* 2008) shows how the incoming current passes through a voltage regulator and then to a transformer that creates high voltage, which is then routed to a Marx generator to increase the voltage further and release it in pulses. The current is discharged into ore material that is placed on a sieve directly underneath the electrode within a water-filled container. The disaggregated material falls through the sieve and is collected in a plastic bag. Abbreviations: C = capacitor, L = inductance coil and S = spark gap.


**Figure 5:** For the experiments in this study, pieces of pre-tumbled emerald-bearing micaceous schist were separated into Batch 1 (left, for EPD processing) and Batch 2 (right, for hand cobbing). Photos by V. Rudashevsky and O. Alikin.

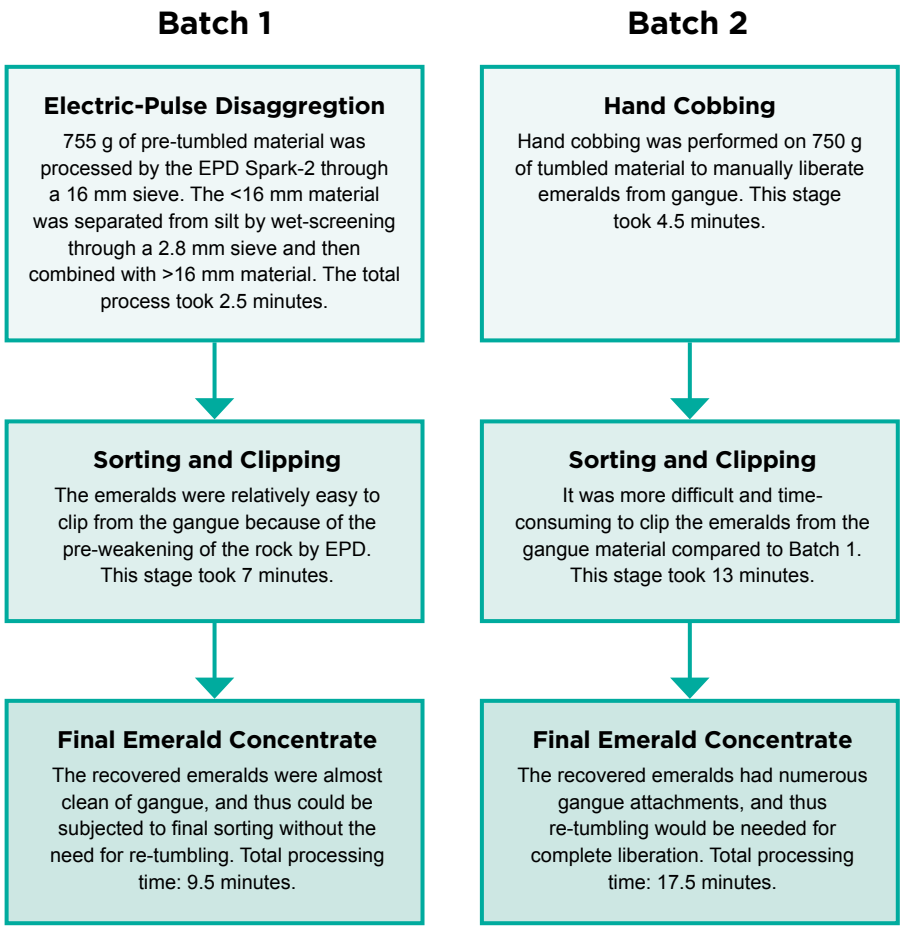


**Figure 6:** This flowchart summarises the different stages in the experiments to recover emeralds using EPD technology vs the conventional hand-cobbing approach.

**Figure 7:** Conventional hand cobbing is accomplished using a hammer in order to recover emeralds from micaceous schist. Photo by V. Rudashevsky and O. Alikin.

The processing was done using a batch mode with a plastic bag used to catch the disaggregated material. The resulting product was wet-sieved and sorted, and then prominent areas of host rock that remained attached to the emeralds were removed by manual clipping using nippers. The various fractions were then weighed.

Batch 2 was subjected to conventional hand cobbing using a hammer (Figure 7), followed similarly by sorting, clipping and weighing. The clipping was performed by the same individual who clipped the EPD-processed material to provide, as much as possible, an accurate time comparison.

## RESULTS

The final weights of the emerald concentrate and gangue material (tailings) obtained by each processing technique are reported in Table I.

### *Batch 1: EPD Processing*

After EPD processing of 755.0 g of ore material, 295 g remained on top of the 16 mm sieve, including at least four liberated emeralds that were primarily free of gangue. The smaller disaggregated fragments passed through the sieve into the plastic bag below. This material was then wet-screened using a 2.8 mm sieve to remove fine material (Figure 8), which was dried for weighing. The total time for this part of the process was 2.5 minutes. The portions captured by the 16 mm and 2.8 mm sieves were then combined for hand sorting to remove any visible emeralds

**Table I:** Results of processing emerald ore with EPD and hand-cobbing techniques.

| Batch no. | Processing method | Initial ore quantity | Emerald concentrate | Tailings (>2.8 mm) | Tailings (<2.8 mm) | Material loss | Processing time |
|---|---|---|---|---|---|---|---|
| 1 | EPD | 755.0 g | 120.7 g | 532.3 g | 102.0 g | 0 g | 9.5 min |
| 2 | Hand cobbing | 750.0 g | 134.1 g | 614.9 g | na* | 1.0 g | 17.5 min |

* Abbreviation: na = not applicable, since the tailings from hand cobbing did not undergo any screening.

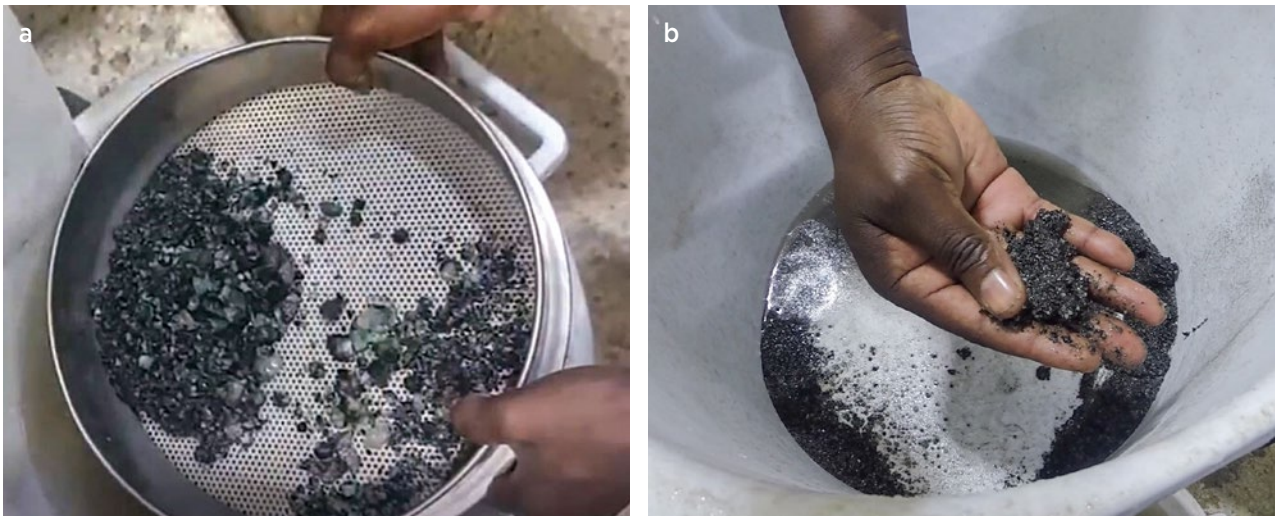


**Figure 8:** Disaggregated material that passed through the 16 mm sieve during EPD processing is then wet-screened using a 2.8 mm sieve (**a**) to remove waste silt (**b**). Photos by V. Rudashevsky and O. Alikin.

**Figure 9:** Emeralds are hand-picked from the disaggregated material after EPD processing, including some relatively large crystals. Photo by V. Rudashevsky and O. Alikin.

(Figure 9). Finally, clipping of the remaining host rock from the emerald pieces took 7 minutes. This part of the process was relatively quick and easy due to the pre-weakening of the matrix caused by EPD processing.

Overall, the emeralds were relatively clean and would not require re-tumbling prior to further sorting (Figure 10a). Thus, the total time for the complete processing of Batch 1 was 9.5 minutes.

### *Batch 2: Hand Cobbing*

During hand cobbing, several flakes were observed to fly out of the workspace, but most of them were recovered. The weight of any lost material was calculated from the final weight obtained for this batch (Table I). Hand cobbing took 4.5 minutes and clipping took 13 minutes. Clipping of attached matrix material was more time consuming than after EPD processing because of the difficulty separating the emeralds from the host rock. Even after clipping, the manually liberated emeralds still had significant quantities of host rock attached to them (Figure 10b). This 'final' product would therefore need to undergo re-tumbling before further sorting. The total time for the processing of Batch 2 was 17.5 minutes (not including the need for further tumbling).

## DISCUSSION

Based on this study, we make the following observations:

1. The weights of emerald concentrate liberated by each processing technique were similar, but the EPD-processed batch contained fewer broken crystals of emerald along with a lower retention of the micaceous matrix compared to the conventionally processed batch (Figure 10).
2. Although the amount of emerald concentrate recovered by hand cobbing was greater than for EPD processing (120.7 g/755.0 g = 16.0% vs 134.1/750.0 g = 17.9%), the emeralds obtained by EPD were more completely liberated from the matrix and had less gangue attached compared to the hand-cobbed material.

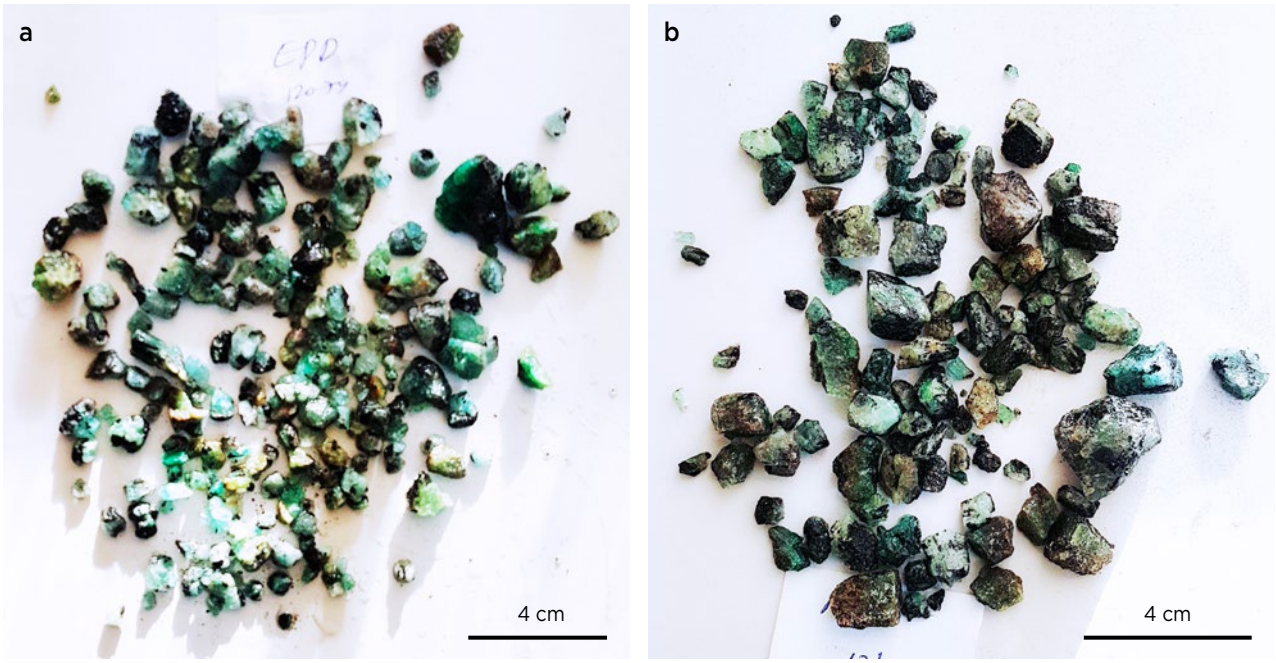


**Figure 10:** These photos show the final emerald concentrates recovered (**a**) after EPD processing and (**b**) after conventional hand cobbing. The EPD-liberated emeralds have very little residual micaceous schist material compared to those obtained by hand cobbing. Photos by V. Rudashevsky and O. Alikin.

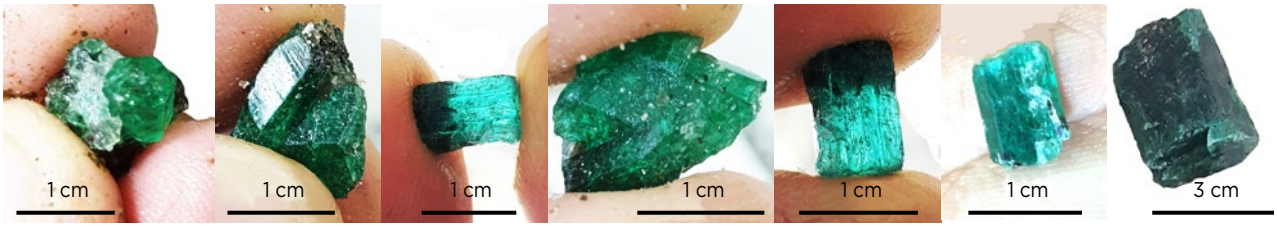


**Figure 11:** Close-up images are shown of some emeralds recovered by the EPD process. Photos by V. Rudashevsky and O. Alikin.

3. As expected from the commonly fractured nature of schist-hosted emeralds (due to geological forces and mining), the concentrate obtained by EPD processing was composed of emerald fragments as well as well-preserved unfractured crystals (Figures 10 and 11).

4. Since hand-cobbed material had much fewer completely liberated crystals and most of the emeralds had multiple gangue attachments (Figure 10b), it needed to be re-tumbled, which is time consuming and often rounds the crystals (thus reducing weight).

5. Overall, EPD processing took 8 minutes less than hand cobbing. Not only was the EPD processing quicker, but a further benefit was the pre-weakening of the micaceous gangue material, which made the clipping process easier and also eliminated the need for any further tumbling, saving additional time.

Another factor to consider is that the conventional hand method depends on the skill and experience of the person doing the cobbing, whereas EPD is non-operator-dependent technology. Moreover, an additional benefit of EPD processing is the prevention of theft that could more easily occur during the conventional hand-cobbing method. Thus, this technology has high potential for replacing on-site manual operations for the recovery of emeralds (Figure 12) and other gems.

## CONCLUSION

The comparative experiments described in this article revealed that recovery of the emeralds from micaceous host rock by EPD technology had several advantages over the conventional hand-cobbing method. Specifically, EPD processing was faster, and any remaining gangue material could be clipped more easily due to

**Figure 12:** These faceted emeralds (approximately 5–8 ct) from the Kagem mine were cut from rough material recovered by EPD processing. Photo © Gemfields Ltd, 2021.

the pre-weakening effect, thus removing the need for re-tumbling of the emerald concentrate. In addition, the EPD-processed emeralds were less fragmented, and in some cases complete crystals were preserved. Moreover, since the processed material was captured inside plastic bags, there was no loss of any pieces, thus ensuring accurate monitoring of concentrates/tailings and helping to prevent theft.

Based on these advantages, we conclude that EPD processing holds the potential to become standard technology for the liberation and recovery of gems that are 'frozen' within their host rocks.

## REFERENCES


Andres, U. 1995. Electrical disintegration of rock. *Mineral Processing and Extractive Metallurgy Review*, **14**(2), 87–110, https://doi.org/10.1080/08827509508914118.

Beasley, C., Parvaz, D.B., Cotton, L. & Littler, K. 2020. Liberating microfossils from indurated carbonates: Comparison of three disaggregation methods. *Journal of Micropalaeontology*, **39**(2), 169–181, https://doi.org/10.5194/jm-39-169-2020.

Cabri, L.J., Rudashevsky, N.S., Rudashevsky, V.N. & Oberthür, T. 2008. Electric-pulse disaggregation (EPD), hydroseparation (HS) and their use in combination for mineral processing and advanced characterization of ores. *40th Annual Meeting of the Canadian Mineral Processors*, Ottawa, Ontario, Canada, 22–24 January, Paper 14, 211–235.

Cook, R.B. 2009. Collector's Note: Zambian emeralds, a recent find. *Rocks & Minerals*, **85**(1), 74–78, https://doi.org/10.1080/00357520903458210.

Ito, M., Owada, S., Nishimura, T. & Ota, T. 2009. Experimental study of coal liberation: Electrical disintegration versus roll-crusher comminution. *International Journal of Mineral Processing*, **92**(1–2), 7–14, https://doi.org/10.1016/j.minpro.2009.02.007.

Lastra, R., Cabri, L.J. & Weiblen, P. 2003. Comparative liberation study by image analysis of Merensky Reef samples comminuted by electric-pulse disaggregation and by conventional crusher. *XXII International Mineral Processing Conference*, Cape Town, South Africa, 29 September–3 October, 251–260.

Matko, M. 2020. *Ore liberation and characterization using electric pulse disaggregation and other novel techniques*. MS thesis, University of Minnesota, Duluth, Minnesota, USA, xv + 247 pp.

Rudashevsky, V.N., Rudashevsky, N. & Antonov, A.V. 2018. The universal technology of mineralogical investigations of bedrocks, ores and processed products. *Regional Geology and Metallogeny*, No. 73, 88–102 (in Russian with English abstract).

Saini-Eidukat, B. & Weiblen, P.W. 1996. A new method of fossil preparation, using high-voltage electric pulses. *Curator*, **39**(2), 139–144, https://doi.org/10.1111/j.2151-6952.1996.tb01085.x.

van der Wielen, K.P., Weh, A., Giese, H. & Kaeppeler, J. 2014. High voltage breakage: A review of theory and applications. *In*: Yianatos, J., Doll, A., Gomez, C. & Kyvenhoven, R. (eds.) *XXVII International Mineral Processing Congress – IMPC 2014*, Santiago, Chile, 20–24 October, 78–86.

Wang, E., Shi, F. & Manlapig, E. 2011. Pre-weakening of mineral ores by high voltage pulses. *Minerals Engineering*, **24**(5), 455–462, https://doi.org/10.1016/j.mineng.2010.12.011.

Zwaan, J.C., Seifert, A.V., Vrána, S., Laurs, B.M., Anckar, B., Simmons, W.B., Falster, A.U., Lustenhouwer, W.J. *et al.* 2005. Emeralds from the Kafubu area, Zambia. *Gems & Gemology*, **41**(2), 116–148, https://doi.org/10.5741/gems.41.2.116.



### The Authors

**Vishnu Dasari, Anirudh Sharma and Prahalad Singh**
Kagem Mining Ltd, P.O. Box 21657, Plot 6374, Corner Dr Aggrey Ave. and Kariba Road, Light Industrial Area, Kitwe, Zambia
Email: vishnu.dasari@gemfields.com

**Etienne Marvillet**
Gemfields Ltd, 1 Cathedral Piazza, London SW1E 5BP, United Kingdom

**Dr Vladimir Rudashevsky, Oleg Alikin and Urja Zaveri FGA**
Centre for New Technologies (CNT Instruments LLC), Shosse Revolutsii, 69 Lit I, St Petersburg 195279, Russia
Email: info@cnt-mp.com



### Acknowledgements

This study was supported by CNT Instruments LLC (www.cnt-mp.com). In addition, we are grateful to Gemfields Ltd and Kagem Mining Ltd (Lufwanyama, Zambia) for providing samples and images for this study.

# An innovator in gemstone reporting

• Identification of colored gemstones • Country of origin determination • Full quality and color grading analysis

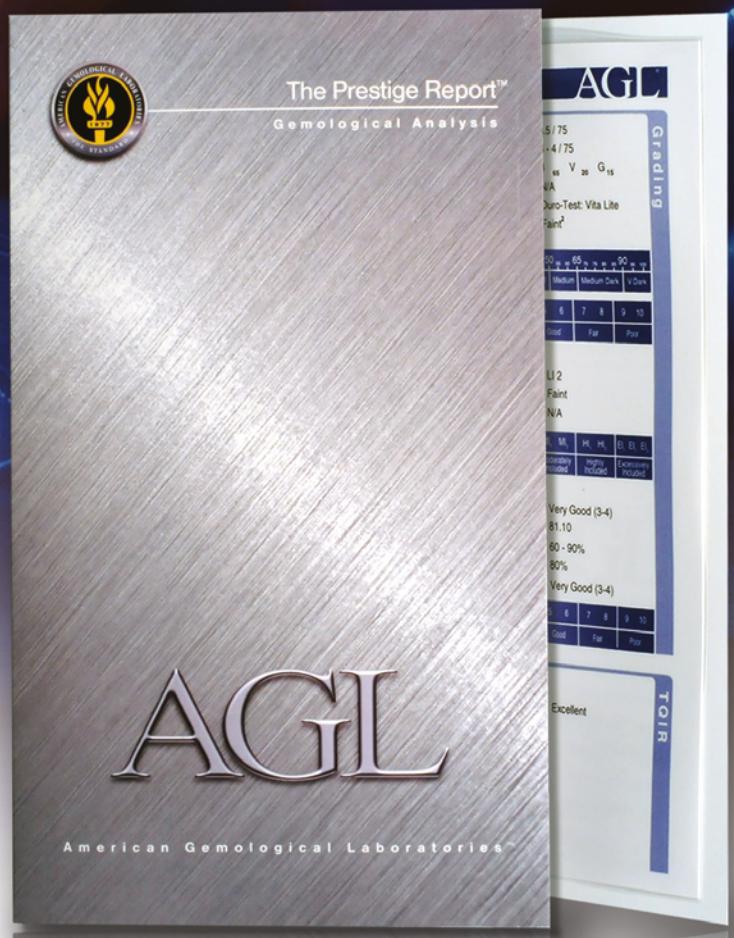


AMERICAN GEMOLOGICAL LABORATORIES AGL

580 5th Ave • Suite 706 • New York, NY 10036, USA
www.aglgemlab.com • +1 (212) 704 - 0727

**Figure 1:** Co-bearing spinel ranging from bright blue to violet-blue and dark blue was discovered near Pakistan's Hunza Valley in 2019. The faceted stones shown here weigh 0.41–0.57 ct. Photo by K. Schollenbruch.

# Cobalt-Blue Spinel from Northern Pakistan

Klaus Schollenbruch, Dudley Blauwet, Anna-Kathrin Malsy and Vera Bosshard

**ABSTRACT:** Blue spinel coloured by cobalt was recently found near the Hunza Valley of northern Pakistan. Characterisation of 35 samples showed that hue variations ranging from bright blue to violet-blue to dark blue are due to variable relative concentrations of the colour-causing elements Co, Fe and Cr. Most of the spinels were semi-transparent and contained abundant internal features, including fractures, twin lamellae and growth structures, as well as distinctive iridescent geometric sectors. Solid inclusions consisted of rutile, zircon, apatite, phlogopite and calcite; fluid inclusions were rare. Samples displaying bright blue colouration typical of so-called Co-spinel had strong absorptions due to $Co^{2+}$ along with subordinate $Fe^{2+}$ features in their UV-Vis spectra, and contained relatively low ratios of Fe/Co (<110) and Cr/Co (<4).

*The Journal of Gemmology*, **37**(7), 2021, pp. 726–737, https://doi.org/10.15506/JoG.2021.37.7.726


Few gemstones can boast such an exceptional range of colour as spinel. Red and pink spinels are among the best-known and most valuable colour varieties of this mineral, probably as a result of their resemblance to pink sapphires and rubies. Indeed, it was not until 1783 that spinel was identified as a separate mineral from corundum (Holden 1991). Until relatively recently, spinels of other colours were often marginalised commercially and were better known to collectors. This changed in the late 1970s to early 1980s, when blue spinel coloured by cobalt (hereafter, termed *Co-spinel*) was recognised by the gem trade (e.g. Mitchell 1977; Fryer 1982; Shigley & Stockton 1984). In general, most blue spinels are coloured by Fe, which causes a steely, slightly greyish hue. However, small amounts of cobalt (in the absence of elevated Fe) can yield a bright, intense, almost 'electric' blue colour (e.g. Palke & Sun 2018). Co-spinel is one of the rarest varieties of this magnesium aluminium oxide (Figure 1).

Localities for Co-spinel include Sri Lanka (e.g. Shigley

& Stockton 1984; Harder 1986; Lomthong *et al*. 2019), Vietnam (e.g. Blauwet 2011; Chauviré *et al*. 2015; Sokolov *et al*. 2019), Canada (Belley & Groat 2019) and Greece (Taran *et al*. 2009), but only Sri Lanka and Vietnam are commercially important sources. However, because Co-spinel falls in the same price range as ruby, sapphire and emerald (Peretti *et al*. 2015), currently lesser-known mining sites or localities that are difficult to access might become commercially attractive in the future. Co-bearing spinel from one such deposit—in northern Pakistan—is described in this article.

Northern Pakistan is known for producing various gem materials, such as emerald, aquamarine, ruby and spinel (e.g. Gübelin 1982; Kazmi & O'Donoghue 1990; Clanin 2008; Malkani 2020). One area hosting different gem varieties is the Hunza Valley (Figure 2), which became accessible in the 1970s with the construction of the Karakorum Highway. Soon after, gems and mineral specimens from this region appeared on the international market and were described in the literature (e.g. Piat 1974; Okrusch *et al*. 1976). Pegmatitic deposits at Chumar Bakhoor are particularly famous for producing aquamarine mineral specimens (e.g. Lyckberg 2011), but the Hunza region is also a source of small amounts of ruby, sapphire and spinel that are mined from marble-hosted deposits.

Most of the Hunza Valley spinels are pink to red to brownish red and violet to greyish blue (Gübelin 1982). The host marbles consist of carbonate sediments with detrital inputs that were metamorphosed during the collision between the Indian and the Eurasian plates starting 53 million years ago (Garnier *et al*. 2004). The marble bands can attain thicknesses up to 10 m and alternate with garnetiferous mica schists (Okrusch *et al*. 1976; Gübelin 1982). Ruby and spinel formed as a result of amphibolite-facies metamorphism at temperatures of approximately 600–790°C and pressures up to 7 kbar (Garnier *et al*. 2008). The marbles also contain several other minerals, such as amphibole, diopside, chlorite, margarite and muscovite (Okrusch *et al*. 1976). Geologically, the ruby and spinel deposits of Myanmar and Hunza are similar, and this is reflected in their inclusion scenes.

The potential of the Hunza Valley as a source of gem material has been reinforced by recent findings of Co-blue spinels of various shades, including some unusually brightly coloured ones discussed in this article. The samples in this study were acquired by the authors in October 2019 from local miners in Ganish village (on the south side of Karimabad), and reportedly came from the high-altitude Shispare region located north-west of Karimabad (Figure 3). The deposit is 17 hours' walking distance from Karimabad and is positioned close to the Shispare glacier in the western part of the Karakoram mountain range. This article describes the gemmological properties, internal features, absorption spectra and chemical characteristics of these spinels, and also discusses the origins of their colouration.

## MATERIALS AND METHODS

From a parcel of several hundred, mostly very small crystal fragments, 35 samples (0.02–1.3 g) were selected for testing and divided into three groups: violet-blue,


**Figure 2:** This view looking down the Hunza Valley to the south-west shows the entrance to Shispare Valley, where the spinel deposit is located. The tallest mountain in the cloud to the left of centre is Rakaposhi (elevation 7788 m). Photo by K. Schollenbruch.

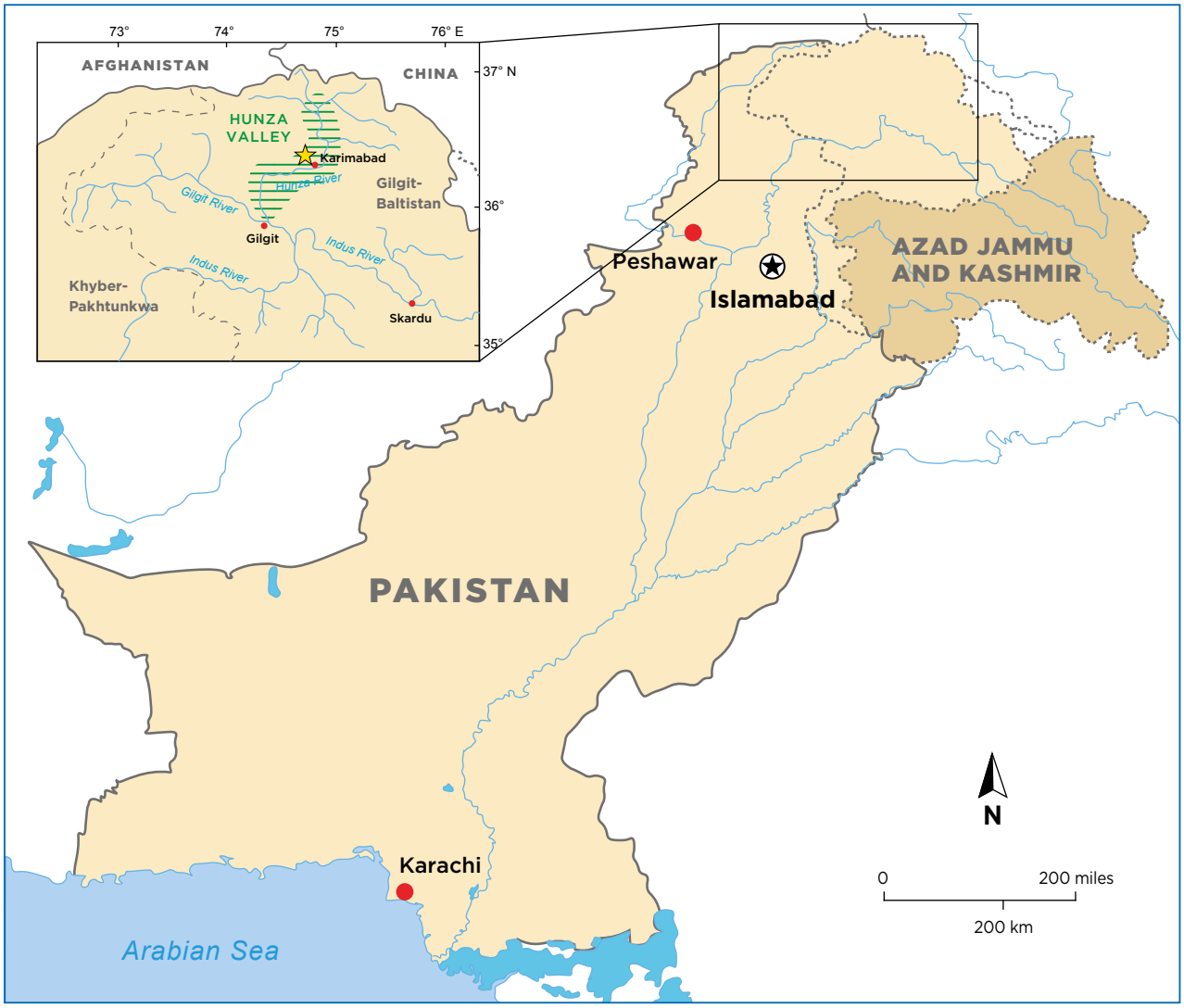


**Figure 3:** The Hunza Valley is located in the far north of Pakistan. The yellow star in the inset map indicates the approximate location of the spinel deposit.

bright blue and dark blue (Figure 4). Windows were polished on 21 samples, and three specimens from each colour group were faceted (0.19–0.79 ct). In addition, we examined one matrix specimen (Figure 5) consisting of marble containing several bright blue spinels reaching a few millimetres in size, along with several brown phlogopite crystals, tiny pyrite crystals and a few tiny pink sapphires in the coarse white marble matrix.

Standard gemmological testing was done with a refractometer for RI and a hydrostatic balance for SG. Fluorescence was observed with a 4 W long- and short-wave UV lamp. The specific tests done on each sample—and the data obtained—are shown in Appendix Table A-1. All samples were inspected with a GIA DLScope Professional trinocular microscope, and inclusion photos were taken with a Canon EOS 6D camera. For greater depth of field, image stacking of selected photomicrographs was done with Helicon Focus 7.6.1 software.

Mineral inclusions were identified in selected samples using a Renishaw InVia Raman microscope with a resolution of approximately 1 $cm^{-1}$. The analyses were done confocally in the range 150–1500 $cm^{-1}$ using a 514 nm diode-pumped solid-state green laser (100 mW power), with a grating of 1800 lines/mm. To increase resolution, two scans per measurement were performed for most samples. Ultraviolet-visible-near infrared (UV-Vis-NIR) spectroscopy was performed on all samples with a Varian Cary 5000 spectrophotometer in the range of 280–880 nm with a slit size of 0.1 mm and scan rate of 3 nm/sec. Chemical analyses of all samples were obtained by laser ablation inductively coupled plasma mass spectrometry (LA-ICP-MS) using an NWR193UC excimer laser-ablation system coupled to an Agilent 8800 triple-quadrupole mass spectrometer. The power of the 193 nm laser was set at 65% and the frequency was 20 Hz. The ablation spots were 50 µm in diameter.

**Figure 4:** The spinel study samples were separated into the three colour groups: violet-blue (left), bright blue (centre) and dark blue (right). The faceted stones weigh 0.19–0.79 ct. Photo by K. Schollenbruch.

Before and after each measurement, NIST SRM 612 glass reference material was analysed. Data were processed with the GLITTER software.

## RESULTS AND DISCUSSION

### *Gemmological Properties*

Highly transparent areas of the spinel were rare, and most samples were quite fractured. Their colours ranged from bright blue to a dark grey-blue to violet-blue (again, see Figure 4). The bright blue samples were mostly of medium tone and were intense blue without another hue modifier. The violet-blue group ranged from violet to violetish blue, in light to dark tones. The dark blue samples were greyish blue and ranged from dark to very dark. Roughly 50% of the samples in the original parcel of several hundred pieces belonged to the dark blue group, and the rest were approximately equally distributed between the bright blue and violet-blue categories. Among the 35 samples selected for testing, 12 were bright blue, 12 were violet-blue and 11 were dark blue.

SG values were 3.53–3.69, consistent with those expected for gem spinel. The RI ranged from 1.714 to 1.720, with darker stones showing higher values than the lighter ones. The fluorescence observed with long-wave UV radiation appeared mostly patchy and ranged from inert to weak pink-red (Figure 6); most of the samples were inert (rarely faint red) under short-wave UV radiation. The colour-change behaviour that has been described for some Co-spinels from Vietnam (Senoble 2010; Krzemnicki 2014; Chauviré *et al.* 2015) was not observed.

**Figure 5:** This matrix specimen (approximately 6.3 cm wide) consists mainly of coarse calcite marble that contains several bright blue spinel fragments. Smaller brown phlogopite crystals are also seen in this view. Photo by K. Schollenbruch.

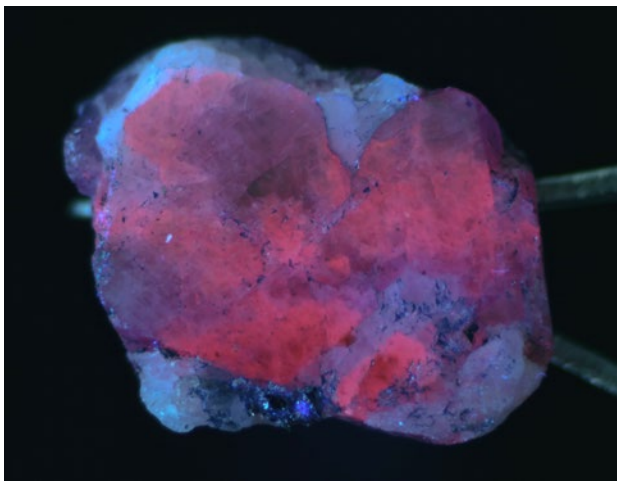

**Figure 6:** The spinel in this sample (no. 20, approximately 9.7 mm wide) shows patchy red fluorescence under long-wave UV radiation, while areas of the marble host rock are inert. Photo by K. Schollenbruch.

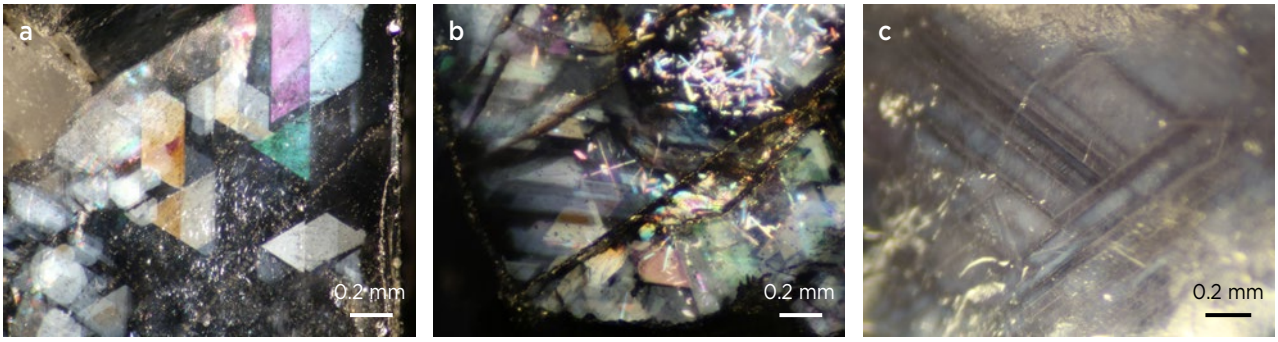


**Figure 7:** (**a**) Iridescent geometric areas are present in most of the spinel samples when viewed with the microscope. (**b**) Iridescent rutile inclusions are also common, and most of them are oriented parallel to the directions shown by iridescent geometric areas. (**c**) The phase forming the whitish clouds and needles within the geometric sectors of this spinel was too small to be identified by Raman analysis, but may consist of very fine-grained rutile. The cloudy zones are reminiscent of 'silk' inclusions and follow complex growth structures in the spinel, resulting in a milkiness that causes reduced transparency. Photomicrographs by K. Schollenbruch; darkfield illumination.

## *Internal Features*

A variety of internal features were seen with the microscope and are presented below according to type: structural characteristics, mineral inclusions and fluid inclusions.

**Structural Characteristics.** Most stones were dominated by small to large fractures with reflective surfaces. Depending on their abundance, they reduced transparency in some samples. The fractures were decorated with dendritic structures in some cases. In addition, clearly visible growth structures were present in some samples, mostly as short growth lines or sectors oriented in one or two directions. Also observed were twin lamellae, either as single twin planes or as lamellar twinning.

The most striking structural feature, observed in most samples from all three colour groups, consisted of iridescent geometric sectors subdivided into complex smaller areas displaying various colouration (Figure 7a). These areas commonly had triangular shapes or showed combinations of trigonal shapes, indicating a relationship to the {111} planes of spinel. Most were visible only from a certain angle with reflected lighting from a fibre-optic lamp. The iridescent sectors were often separated by thin, non-iridescent bands. Superimposed on some of these sectors were small iridescent particles and clusters of short needles and platelets (Figure 7b). The iridescence of the sectors may be related to the presence of oriented cloud-like particles that are reminiscent of rutile 'silk' (Figure 7c). So far, similar iridescent sectors are known only for some Co-free blue spinels (e.g. from Morogoro, Tanzania; Figure 8).

**Mineral Inclusions.** The tested samples showed a large variety of solid inclusions. Very common were the iridescent particles, needles and irregular-shaped platelets mentioned above (Figure 7b; see also Figure 9a). These were present within clearly defined areas, forming dense bands or clusters, and mostly were oriented parallel to growth structures. Raman analysis identified some of the larger needles and platelets as rutile. Rutile also formed medium to large, dark brown to black metallic, rounded to elongate crystals (Figure 9b). Most appeared singly, but some loose clusters of rutile were also observed. In some spinels, the rutile grains were surrounded by brownish halos (Figure 9c). Raman analysis of such a halo yielded a spectrum that did not match any of those in our spectral library or in the RRUFF database.

Also present were colourless zircon crystals (identified by Raman spectroscopy), usually as individuals (Figure 10a) or sometimes grouped into small clusters (Figure 10b). They were oval to round and sometimes were associated with small tension halos. Other mineral

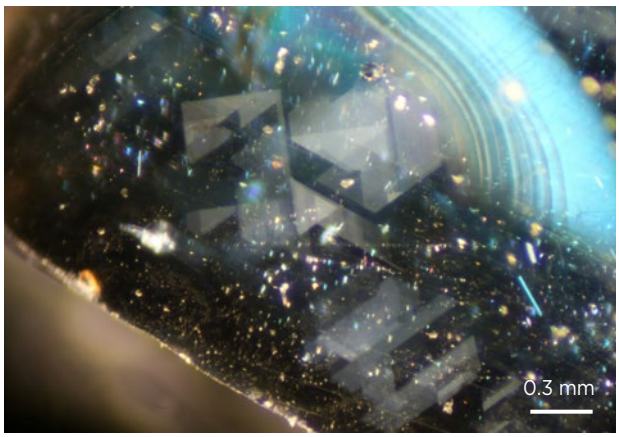


**Figure 8:** The inclusion scene in this dark blue (Fe-coloured, Co-free) Tanzanian spinel from Gübelin Gem Lab's reference collection shows features similar to those seen in the Pakistani spinels in Figure 7. Also prominent is a curved iridescent fracture in the upper-right portion of the image. Photomicrograph by K. Schollenbruch; reflected fibre-optic lighting.

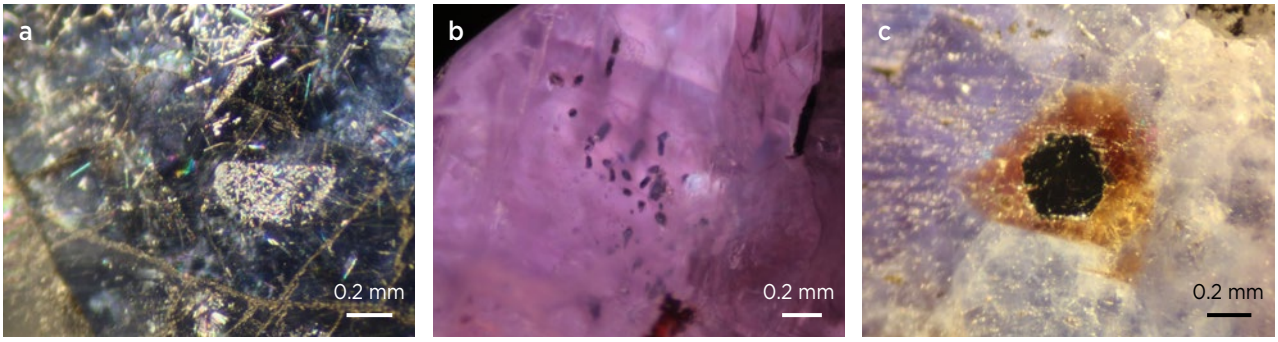


**Figure 9:** Rutile inclusions in the Pakistani spinels have various forms, including (**a**) oriented clusters of iridescent short needles and irregular-shaped platelets; (**b**) a cluster of small rounded crystals; and (**c**) a large black crystal (which appeared metallic in reflected light) surrounded by a brown halo. Photomicrographs by K. Schollenbruch; reflected fibre-optic lighting.

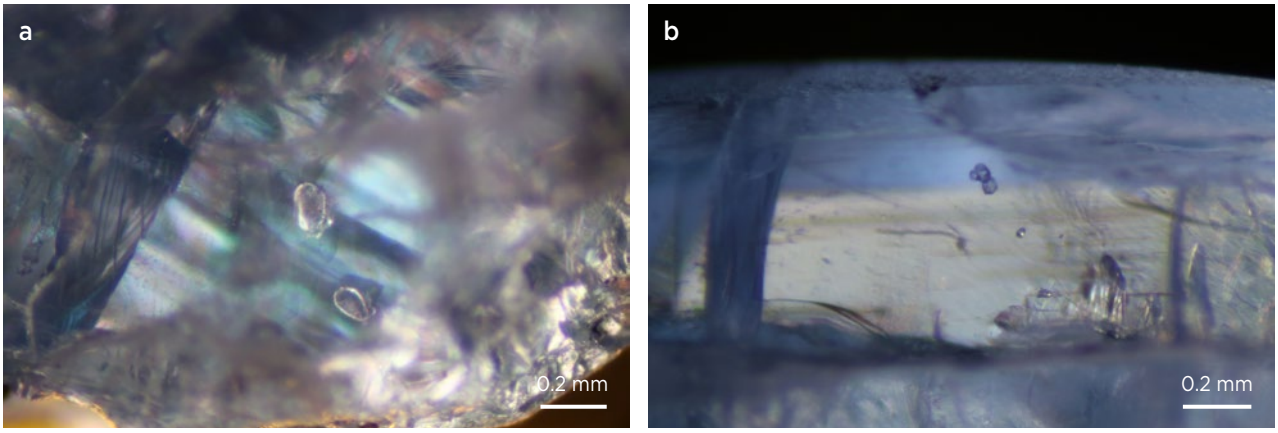


**Figure 10:** Zircon crystals in the Pakistani spinels form (**a**) as rounded colourless individuals or (**b**) in small clusters. Photomicrographs by K. Schollenbruch; darkfield illumination.

inclusions, often slightly larger than the zircons but also colourless, were identified by Raman spectroscopy as apatite. They appeared as rounded subhedral crystals, accompanied by grainy, transparent brownish minerals which could not be identified. In general, they were less common than the zircon inclusions.

Large, light brown mica platelets were identified by Raman analysis as phlogopite (Figure 11). Even larger, anhedral inclusions consisting of calcite (Figure 12; identified by Raman spectroscopy) were present in most of the samples.

**Fluid Inclusions.** Partially healed fissures were not common and were rather small. They consisted of tiny

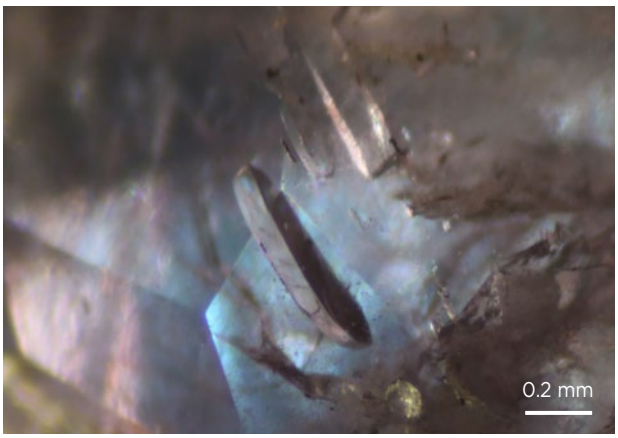


**Figure 11:** The large, platy, slightly brownish inclusion in this spinel was identified as phlogopite. Photomicrograph by K. Schollenbruch; darkfield illumination.

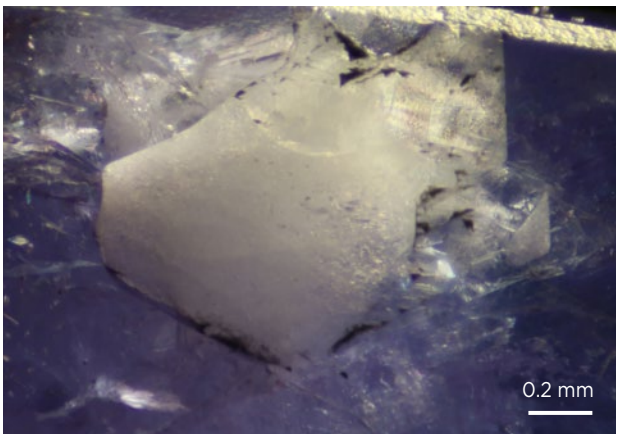


**Figure 12:** Calcite is quite common in the Pakistani spinels, occurring mostly as slightly milky anhedral masses. Photomicrograph by K. Schollenbruch; reflected fibre-optic lighting.

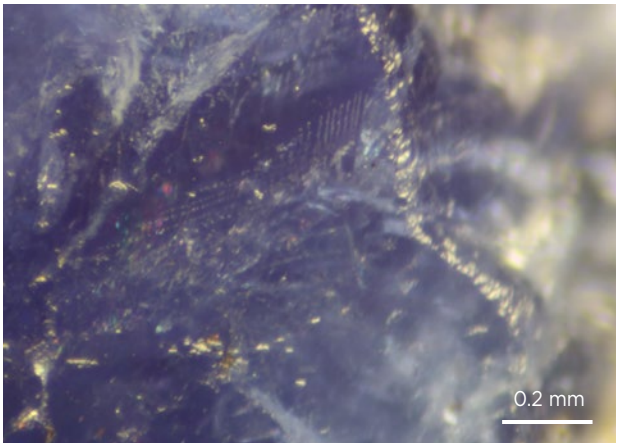


**Figure 13:** Rarely seen in the spinels are partially healed fissures. They are characterised by a geometric arrangement of tiny fluid inclusions, as is typical for spinel in general. Photomicrograph by K. Schollenbruch; reflected fibre-optic lighting.

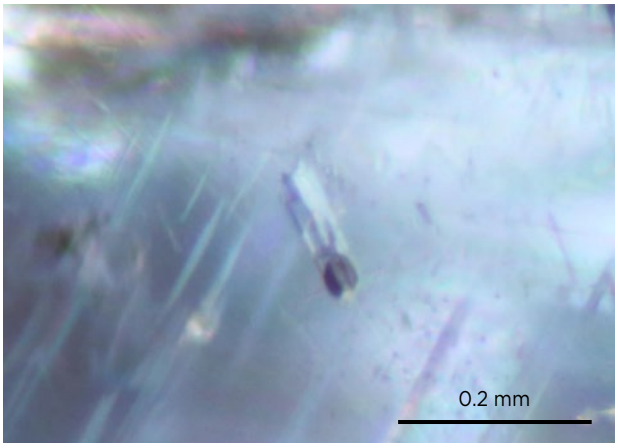


**Figure 14:** The rare three-phase inclusion seen here (in spinel sample no. 4) consists of a negative crystal containing a dark-appearing gas bubble and a colourless mineral within a fluid. Photomicrograph by K. Schollenbruch; darkfield illumination.

fluid inclusions that were arranged in rough geometric patterns (Figure 13). One sample contained a three-phase inclusion consisting of a dark-appearing gas bubble together with a slightly rounded colourless crystal suspended in a colourless fluid (Figure 14).

## *UV-Vis Spectroscopy*

The UV-Vis spectra of the spinels show two complex areas of absorption at approximately 370–480 nm and 540–640 nm (Figure 15). The first region consists primarily of various absorptions related to $Fe^{2+}$ (e.g. Gaffney 1973; Dickson & Smith 1976; Muhlmeister *et al.* 1993; Chauviré *et al.* 2015; D'Ippolito *et al.* 2015). The second area consists mainly of absorptions associated with $Co^{2+}$ substituting for $Mg^{2+}$ (e.g. Wherry 1929; Shigley & Stockton 1984; D'Ippolito *et al.* 2015), plus $Fe^{2+}$ in tetrahedral coordination (see references for $Fe^{2+}$ listed above).

Although the perceived colour of a gem depends on several additional factors—such as inclusions, transparency and size—the hue range of these spinels mainly correlated with the intensities of $Fe^{2+}$ and $Co^{2+}$ absorptions. The bright blue spinels all showed

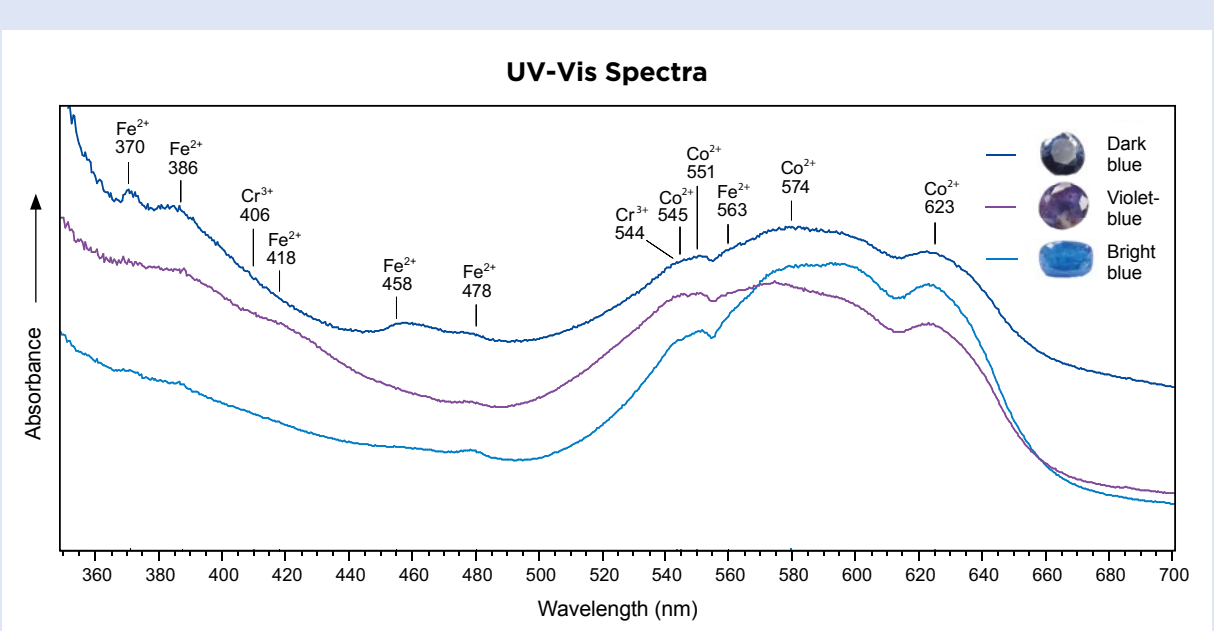


**Figure 15:** UV-Vis absorption spectra of representative spinel samples from the three different colour groups show corresponding differences in the relative abundance of the chromophores $Fe^{2+}$, $Co^{2+}$ and $Cr^{3+}$. The bright blue spinel shows the lowest Fe absorption, whereas Fe-related features are more prevalent in the violet-blue and dark blue samples.

strong absorption between 540 and 640 nm, and less pronounced absorption in the 350–500 nm range compared to the violet-blue and dark blue spinels. The dark blue samples also had pronounced absorption caused by Co, but this was accompanied by more prominent bands due to $Fe^{2+}$ (i.e. equal to or greater than the intensity of the $Co^{2+}$-related bands). The violet-blue spinels showed a slightly distorted Co-absorption triplet, with somewhat stronger relative absorption between 545 and 550 nm. The cause of the violet hue could be complex. Purplish shades have been ascribed to the presence of tetrahedrally coordinated $Fe^{2+}$ as the dominant iron species (D'Ippolito *et al.* 2015). Another factor could be the additional absorption caused by $Cr^{3+}$ at approximately 544 nm (Schmetzer *et al.* 1989; Malsy & Klemm 2010), which overlaps one of the $Co^{2+}$ bands (again, see Figure 15).

## LA-ICP-MS Analysis

Chemical data are summarised for each spinel colour group in Table I, and a full set of the analyses are available in *The Journal*'s data depository (Table DD-1). The indication from the spectral data that Fe and Co are mainly responsible for the blue-to-violet hues was supported by the chemical compositions of the samples. A comparison of the data for the bright blue, violet-blue and dark blue spinels provides some general trends. The bright blue and violet-blue spinels generally contained <25,000 ppm Fe together with >200 ppm Co on average. The main difference between the bright blue and violet-blue spinels was their Cr content, which was higher in the violet-blue samples (average 2180 ppm), whereas most bright blue and dark blue spinels had lower Cr contents (average 476 and 803 ppm, respectively). Overall, the relative amounts of Co, Fe and Cr roughly correlated with the three different colour groups (Figure 16).

Other elements that were consistently present in significant (albeit trace) amounts in the samples were Zn, Li, Ni, V, Ga, Ti, Mn and Be (again, see Table I).

## Causes of Colour

The main colouring elements in the tested spinels are Co and Fe. However, the meaning of the term *Co-spinel* is not clearly defined, and different definitions appear in the literature. Chauviré *et al.* (2015) defined the bright blue colour in terms of chemical analysis by calculating molar absorptivity to investigate the exact Fe/Co ratio in which Co became the main contributor to the blue hue. D'Ippolito *et al.* (2015) determined that Co concentrations of more than 10 ppm can have an effect on the spinel colouration. All investigated samples in the

**Table I:** Chemical data for the tested spinel samples by colour group.*

| Element (ppmw) | Bright blue | Violet-blue | Dark blue |
|---|---|---|---|
| Li | 67.3–561 (335) | 130–525 (347) | 7.9–248 (113) |
| Be | 14.8–78.0 (37.7) | 11.8–49.2 (26.3) | 14.0–74.2 (37.7) |
| Ti | 3.0–435 (88.0) | 13.2–1100 (156) | 17.6–405 (110) |
| V | 49.6–293 (129) | 58.2–329 (179) | 85.4–918 (267) |
| Cr | 117–1200 (476) | 814–4950 (2180) | 108–2220 (803) |
| Mn | 32.5–78.9 (44.6) | 48.3–98.0 (73.6) | 63.9–193 (142) |
| Fe | 10110–22760 (14650) | 13480–19110 (15700) | 16870–47170 (32830) |
| Co | 249–359 (302) | 151–420 (251) | 62.4–268 (119) |
| Ni | 167–336 (265) | 44.1–218 (118) | 19.6–181 (81.0) |
| Zn | 1610–3710 (2320) | 1870–5570 (2560) | 2180–7520 (4020) |
| Ga | 68.5–156 (99.5) | 80–225 (109) | 91.5–258 (187) |
| Sn | 0.83–4.22 (1.84) | 0.98–722 (52.5) | 0.82–4.80 (1.70) |
| Pb | 0.086–3.32 (0.42) | 0.095–173 (14.3) | 0.086–1.10 (0.28) |
| Bi | 0.026–0.027 (0.027) | 0.025–0.21 (0.078) | 0.025–0.057 (0.035) |

* Average values are shown in parentheses; typically three spots per sample were analysed.

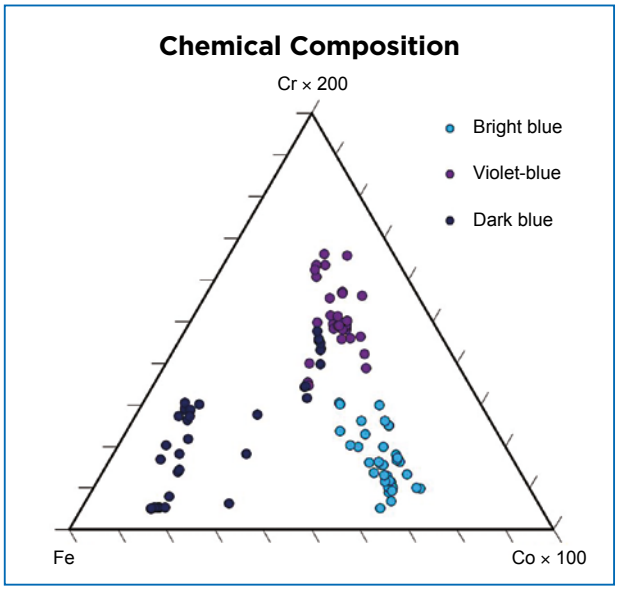


**Figure 16:** A triangular plot of the Co, Fe and Cr contents of the three spinel colour groups shows consistent trends with some overlap. Higher Cr contents correlate to the violet samples and greater Fe corresponds with dark blue colouration. The bright blue samples tend to contain relatively low amounts of both Fe and Cr and higher amounts of Co.

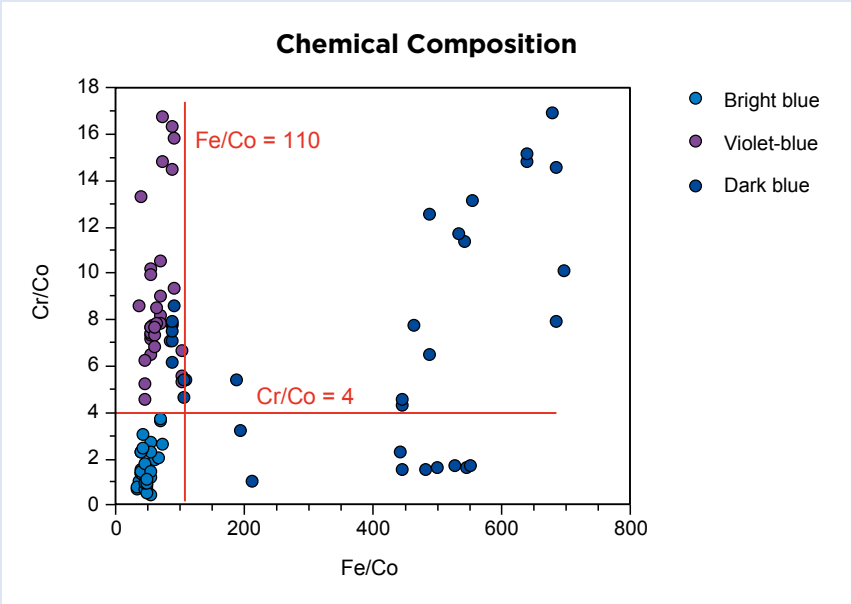


**Figure 17:** The bright blue samples have the lowest ratios of both Fe/Co (<110) and Cr/Co (<4), and therefore correlate with a chemical definition for Co-spinel from this locality. The violet samples have higher Cr/Co and low Fe/Co values, while the dark blue samples show relatively high Fe/Co ratios and variable (but typically elevated) Cr/Co values.

present study likewise contained >10 ppm Co. However, only some of our specimens displayed bright blue colour (e.g. comparable to some Co-spinels from Vietnam). We found that the hue is mainly determined by the relative amounts of Fe, Co and Cr. In general, a high Fe content causes a dark greyish blue appearance, independent of the amounts of Co and Cr. Spinels with low Fe could be separated into Co-rich + Cr-rich and Co-rich + Cr-poor compositions, and only the latter showed the desirable bright blue colour. By contrast, the Co-rich + Cr-rich samples were all violet to violet-blue.

Until now, efforts to define Co-spinel have been focused only on the Co and Fe contents (Peretti *et al.* 2015; Palke & Sun 2018; Sokolov *et al.* 2019). We feel that Cr should also be taken into consideration because it has a clear impact on the visible colour of spinel. Even with low Fe and high Co concentrations, Co-bearing spinels containing significant Cr will not have the appealing blue colour. Although the most convenient method to estimate the proportions of Fe and Co affecting spinel colouration is UV-Vis spectroscopy, the influence of $Cr^{3+}$ absorption is not straightforward because the two main peaks at 406 and 544 nm overlap those of $Fe^{2+}$ and $Co^{2+}$, respectively. Chemical data for amounts or ratios of the main chromophores (Fe and Co) have been used in various attempts to define Co-spinel. Peretti *et al.* (2015) suggested a minimum Co content of 40–60 ppm, and Sokolov *et al.* (2019) proposed an Fe/Co ratio of between 10 and 110. From the samples analysed in the present study, we found a consistent Fe/Co ratio of <110 in our bright blue spinels, but with an additional limitation of a Cr/Co ratio of <4 (Figure 17).

Nevertheless, in addition to taking into account any chemical or spectroscopic requirements, the definition of Co-spinel in the gem trade should also require that a stone possess an appealing bright blue colour.

## CONCLUSION

A new spinel deposit in northern Pakistan has yielded stones containing Co that show a variety of blue to violet hues (e.g. Figure 18). Those samples showing bright blue colouration commonly associated with the term *Co-spinel* in the gem trade had ratios of Fe/Co < 110 and Cr/Co < 4.

**Figure 18:** Crystals of violetish blue Co-spinel embedded in marble host rock were found recently in northern Pakistan. The specimen shown here is approximately 5 cm wide. Photo by K. Schollenbruch.

Together with recently discovered Co-spinels in Canada (Belley & Groat 2019), it is apparent that more sources for this rare variety of blue spinel are being found. This could lead to a demand for the origin determination of Co-spinels. The internal features in the stones from Pakistan might serve as one criterion to distinguish them from Co-spinels from other origins. Notably, the iridescent geometric patterns we observed in the Pakistan spinels have not yet been reported for Co-spinels from elsewhere, although they have been documented in some Co-free blue spinels (containing Fe), such as those from Morogoro, Tanzania.

Whether the Co-spinels from Pakistan will have a significant impact on the international market will depend largely on the amount and quality that are produced. Although the Pakistan material looks promising, currently it cannot compete with the quality and size of Co-spinels from Vietnam and Sri Lanka. The deposit is located in a very remote and high-elevation part of the Karakorum Mountains (Figure 19), and mining is only possible during the summer months. However, as the Co-spinels from Pakistan are a relatively new find, better quality might be produced as mining continues.

**Figure 19:** This view from Pakistan's Hunza Valley is looking north from Karimabad, in the direction of the Shispare Valley where the spinel deposit is located (behind the mountains shown here). Photo by K. Schollenbruch.

## REFERENCES


Belley, P.M. & Groat, L.A. 2019. Metacarbonate-hosted spinel on Baffin Island, Nunavut, Canada: Insights into the origin of gem spinel and cobalt-blue spinel. *Canadian Mineralogist*, **57**(2), 147–200, https://doi.org/10.3749/canmin.1800060.

Blauwet, D. 2011. Gem News International: Spinel from northern Vietnam, including a new mine at Lang Chap. *Gems & Gemology*, **47**(1), 60–61.

Chauviré, B., Rondeau, B., Fritsch, E., Ressigeac, P. & Devidal, J.-L. 2015. Blue spinel from the Luc Yen District of Vietnam. *Gems & Gemology*, **51**(1), 2–17, https://doi.org/10.5741/gems.51.1.2.

Clanin, J. 2008. Gemstone and mineral mining in Pakistan's mountains. *InColor*, No. 7, 19–21, 24–25.

D'Ippolito, V., Andreozzi, G.B., Hålenius, U., Skogby, H., Hametner, K. & Günther, D. 2015. Color mechanisms in spinel: Cobalt and iron interplay for the blue color. *Physics and Chemistry of Minerals*, **42**(6), 431–439, https://doi.org/10.1007/s00269-015-0734-0.

Dickson, B.L. & Smith, G. 1976. Low-temperature optical absorption and Mössbauer spectra of staurolite and spinel. *Canadian Mineralogist*, **14**(2), 206–215.

Fryer, C. 1982. Lab Notes: Spinel and sapphire, colored by cobalt (?). *Gems & Gemology*, **18**(4), 231–233.

Gaffney, E.S. 1973. Spectra of tetrahedral $Fe^{2+}$ in $MgAl_2O_4$. *Physical Review B*, **8**(7), 3484–3486, https://doi.org/10.1103/PhysRevB.8.3484.

Garnier, V., Giuliani, G., Ohnenstetter, D., Bakhsh, K.A., Vinh, H.Q., Trinh, P.T. & Long, P.V. 2004. Les gisements de rubis du Pakistan et du Viêt-nam. *Revue de Gemmologie A.F.G.*, No. 150, 1–7.

Garnier, V., Giuliani, G., Ohnenstetter, D., Fallick, A.E., Dubessy, J., Banks, D., Vinh, H.Q., Lhomme, T. *et al.* 2008. Marble-hosted ruby deposits from Central and Southeast Asia: Towards a new genetic model. *Ore Geology Reviews*, **34**(1–2), 169–191, https://doi.org/10.1016/j.oregeorev.2008.03.003.

Gübelin, E.J. 1982. Gemstones of Pakistan: Emerald, ruby, and spinel. *Gems & Gemology*, **18**(3), 123–139, https://doi.org/10.5741/gems.18.3.123.

Harder, H. 1986. Natürliche kobaltblaue Spinelle von Ratnapura, Sri Lanka. *Neues Jahrbuch für Mineralogie, Monatshefte*, No. 3, 97–100.

Holden, M. 1991. *The Encyclopedia of Gemstones and Minerals*. Facts on File, New York, New York, USA, 303 pp.

Kazmi, A.H. & O'Donoghue, M. 1990. *Gemstones of Pakistan: Geology and Gemmology*. Gemstone Corporation of Pakistan, Peshawar, Pakistan, 146 pp.

Krzemnicki, M.S. 2014. Blue cobalt spinel from Vietnam. *Facette Magazine*, No. 21, 14.

Lomthong, P., Schwarz, D., Zoyza [*sic*], G., Yanyu, C. & Liu, Y. 2019. Spinels from Sri Lanka. *InColor*, No. 43, 40–52.

Lyckberg, P. 2011. Edelstein-Pegmatite in Pakistan: Chumar Bakhoor. *Mineralien-Welt*, No. 4, 67–77.

Malkani, M.S. 2020. Mineral resources of Gilgit Baltistan and Azad Kashmir, Pakistan: An update. *Open Journal of Geology*, **10**(6), 661–702, https://doi.org/10.4236/ojg.2020.106030.

Malsy, A. & Klemm, L. 2010. Distinction of gem spinels from the Himalayan mountain belt. *CHIMIA International Journal for Chemistry*, **64**(10), 741–746, https://doi.org/10.2533/chimia.2010.741.

Mitchell, R.K. 1977. African grossular garnets; blue topaz; cobalt spinel; and grandidierite. *Journal of Gemmology*, **15**(7), 354–358, https://doi.org/10.15506/JoG.1977.15.7.354.

Muhlmeister, S., Koivula, J.I., Kammerling, R.C., Smith, C.P., Fritsch, E. & Shigley, J.E. 1993. Flux-grown synthetic red and blue spinels from Russia. *Gems & Gemology*, **29**(2), 81–98, https://doi.org/10.5741/gems.29.2.81.

Okrusch, M., Bunch, T.E. & Bank, H. 1976. Paragenesis and petrogenesis of a corundum-bearing marble at Hunza (Kashmir). *Mineralium Deposita*, **11**(3), 278–297, https://doi.org/10.1007/bf00203079.

Palke, A.C. & Sun, Z. 2018. What is cobalt spinel? Unraveling the causes of color in blue spinels. *Gems & Gemology*, **54**(3), 262.

Peretti, A., Günther, D. & Haris, M.T.M. 2015. GRS Alert: New spinel treatment discovered involving heat and cobalt-diffusion. GRS Gemresearch Swisslab, www.gemresearch.ch/news/2015/05/22/grs-alert-new-spinel-treatment-discovered-involving-heat-and-cobalt-diffusion, 22 May, accessed 20 June 2021.

Piat, D. 1974. Le rubis himalayen d'Hunza. *Bulletin de l'Association Française de Gemmologie*, No. 41, 5–7.

Schmetzer, K., Haxel, C. & Amthauer, G. 1989. Colour of natural spinels, gahnospinels and gahnites. *Neues Jahrbuch für Mineralogie, Abhandlungen*, **160**(2), 159–180.

Senoble, J.B. 2010. Beauty and rarity – A quest for Vietnamese blue spinels. *InColor*, No. 14, 18–23.

Shigley, J.E. & Stockton, C.M. 1984. 'Cobalt-blue' gem spinels. *Gems & Gemology*, **20**(1), 34–41, https://doi.org/10.5741/gems.20.1.34.

Sokolov, P., Kuksa, K., Marakhovskaya, O. & Gussiås, G.A. 2019. In search of cobalt blue spinel in Vietnam. *InColor*, No. 43, 60–65.

Taran, M.N., Koch-Müller, M. & Feenstra, A. 2009. Optical spectroscopic study of tetrahedrally coordinated $Co^{2+}$ in natural spinel and staurolite at different temperatures and pressures. *American Mineralogist*, **94**(11–12), 1647–1652, https://doi.org/10.2138/am.2009.3247.

Wherry, E.T. 1929. Mineral determination by absorption spectra. II. *American Mineralogist*, **14**(9), 323–328.

## The Authors

**Dr Klaus Schollenbruch, Dr Anna-Kathrin Malsy and Vera Bosshard**
Gübelin Gem Lab Ltd, Maihofstrasse 102, CH-6006 Lucerne, Switzerland
Email: klaus.schollenbruch@gubelingemlab.com

**Dudley Blauwet**
Dudley Blauwet Gems, PO Box 695, Louisville, Colorado 80027, USA

## Acknowledgements

Without the help of Aziz Azullah, and Shahid Ali and his team, it would not have been possible to reach the Hunza Valley and acquire these samples. Klemens Link kindly helped with performing LA-ICP-MS measurements and data interpretation. Pierre Hardy is thanked for English corrections and valuable input.

# APPENDIX

**Table A-1:** Standard gemmological data and other testing on Co-bearing spinels from Pakistan.*

| Sample | Colour group | Type | Weight (ct) | RI | SG | Long-wave UV fluorescence | Short-wave UV fluorescence | Raman | UV-Vis | LA-ICP-MS |
|---|---|---|---|---|---|---|---|---|---|---|
| 1 | Bright blue | Windowed | 0.30 | 1.719 | 3.53 | Inert | Inert | ✓ | ✓ | ✓ |
| 2 | Bright blue | Windowed | 0.65 | - | - | Inert | Inert | ✓ | ✓ | ✓ |
| 3 | Bright blue | Rough | 0.49 | - | - | Inert | Inert | - | ✓ | ✓ |
| 4 | Bright blue | Windowed | 0.73 | 1.716 | 3.57 | Inert | Inert | - | ✓ | ✓ |
| 5 | Bright blue | Windowed | 1.52 | 1.716 | - | Faint red | Inert | ✓ | ✓ | ✓ |
| 6 | Violet-blue | Windowed | 1.74 | 1.718 | - | Faint red | Inert | ✓ | ✓ | ✓ |
| 7 | Violet-blue | Rough | 1.74 | 1.718 | - | Faint red | Inert | - | ✓ | ✓ |
| 8 | Violet-blue | Windowed | 1.17 | 1.719 | - | Weak red | Inert | - | ✓ | ✓ |
| 9 | Violet-blue | Windowed | 2.37 | 1.718 | - | Faint red | Inert | ✓ | ✓ | ✓ |
| 10 | Violet-blue | Windowed | 1.48 | 1.719 | - | Faint red | Inert | ✓ | ✓ | ✓ |
| 13 | Bright blue | Rough | 0.09 | - | 3.69 | Faint red | Inert | - | ✓ | ✓ |
| 14 | Bright blue | Windowed | 0.87 | 1.717 | - | Faint red | Faint red | ✓ | ✓ | ✓ |
| 15 | Bright blue | Rough | 0.98 | 1.719 | - | Faint red | Inert | - | ✓ | ✓ |
| 16 | Dark blue | Windowed | 1.19 | 1.720 | - | Inert | Inert | - | ✓ | ✓ |
| 17 | Dark blue | Windowed | 1.43 | 1.719 | - | Inert | Inert | - | ✓ | ✓ |
| 18 | Dark blue | Windowed | 1.44 | 1.720 | 3.59 | Inert | Inert | ✓ | ✓ | ✓ |
| 19 | Dark blue | Windowed | 1.90 | 1.719 | - | Inert | Inert | - | ✓ | ✓ |
| 20 | Violet-blue | Windowed | 2.11 | 1.719 | - | Weak red | Faint red | - | ✓ | ✓ |
| 21 | Violet-blue | Windowed | 2.14 | 1.719 | - | Faint red | Faint red | ✓ | ✓ | ✓ |
| 22 | Violet-blue | Rough | 2.23 | 1.719 | - | Inert | Inert | - | ✓ | ✓ |
| 23 | Dark blue | Windowed | 6.61 | 1.720 | - | Inert | Inert | - | ✓ | ✓ |
| 24 | Bright blue | Windowed | 2.47 | 1.718 | - | Faint red | Inert | - | ✓ | ✓ |
| 25 | Dark blue | Windowed | 3.43 | 1.720 | - | Inert | Inert | ✓ | ✓ | ✓ |
| 26 | Dark blue | Windowed | 3.28 | 1.720 | - | Inert | Inert | ✓ | ✓ | ✓ |
| 27 | Dark blue | Windowed | 4.11 | 1.720 | - | Inert | Inert | - | ✓ | ✓ |
| 28 | Violet-blue | Windowed | 5.82 | - | - | Faint red | Inert | - | ✓ | ✓ |
| 29 | Violet-blue | Faceted | 0.51 | 1.717 | 3.59 | Faint red | Inert | ✓ | ✓ | ✓ |
| 30 | Violet-blue | Faceted | 0.48 | 1.717 | - | Weak red | Faint red | ✓ | ✓ | ✓ |
| 31 | Violet-blue | Faceted | 0.40 | 1.717 | 3.59 | Weak red | Faint red | - | ✓ | ✓ |
| 32 | Bright blue | Faceted | 0.48 | 1.716 | 3.59 | Inert | Inert | ✓ | ✓ | ✓ |
| 33 | Bright blue | Faceted | 0.57 | 1.716 | 3.58 | Faint red | Inert | - | ✓ | ✓ |
| 34 | Bright blue | Faceted | 0.41 | 1.714 | 3.55 | Inert | Inert | ✓ | ✓ | ✓ |
| 35 | Dark blue | Faceted | 0.24 | 1.720 | 3.57 | Inert | Inert | - | ✓ | ✓ |
| 36 | Dark blue | Faceted | 0.19 | 1.720 | - | Inert | Inert | ✓ | ✓ | ✓ |
| 37 | Dark blue | Faceted | 0.79 | 1.720 | 3.56 | Inert | Inert | ✓ | ✓ | ✓ |

* Samples 11 and 12 were not included in this study since they were pink and therefore fell outside of the three colour groups.

# Gem-A Notices

## COVID-19 NOTICE FROM GEM-A CEO ALAN HART

Now that coronavirus restrictions are steadily being relaxed across the country, the temptation to imagine a return to normal life in the months to come is greater than ever. Although there is much cause for hope, we are not yet entirely out of the woods, and the ramifications of the virus are—for most of us—still very significant here.

Although Gem-A has been as affected by the pandemic as many of you have, the shoots of recovery are finally beginning to sprout through. We are currently in the process of completing our audit for 2020, and we're excited to be planning our next Annual General Meeting, which will be announced soon. Following on from the success of the last AGM, we have taken the decision to host the next one online to give our valued international Members the chance to attend and contribute.

In another nod to optimism, we're thrilled to announce that we are planning to host a graduation ceremony in person on Monday 8 November at London's historic Church House. We are keen to have an opportunity to come together and network after what has been a tough 18 months for all of us. As many international restrictions remain in place, we have opted for a hybrid event, meaning you can follow proceedings online if you are not able to attend in person. I hope you can, as I'm very excited to catch up with our knowledgeable and passionate graduates and Members!

As always, I would like to acknowledge and thank our Members for their ongoing support throughout this challenging period; it reminds me what a great, compassionate community we are part of. Here's to seeing old faces—and meeting new ones—in the months to come!

## GIFTS TO THE ASSOCIATION

Gem-A is most grateful to the following for their generous donations that will support continued research and teaching:

**Mary and Alan Burland**, United Kingdom, for donating Mary's entire collection of *The Journal of Gemmology* back issues to Gem-A's library.

**Prof. Dr Henry A. Hänni**, Switzerland, for an original set of ornamental gem materials used in his *Journal* article titled 'An investigation of grinding hardness of some ornamental stones' (Vol. 37, No. 6, 2021).

**Prof. Dongsheng Li**, China, for six synthetic moissanite and nine cubic zirconia gemstones for Gem-A's diamond teaching sets.

## GEM-A CONFERENCE

The 2021 Gem-A Conference will take place on Sunday 7 November. Due to ongoing uncertainty regarding COVID-19 and the associated restrictions, we have opted to hold this year's conference online. This is an exciting opportunity to offer tailored sessions and round-tables to our valued Members around the world. Further details will be published in due course.

## GEM-A GRADUATION AND PRESENTATION OF AWARDS

This year, we look forward to holding a combined 2020/2021 Gem-A Graduation and Presentation of Awards at London's Church House on 8 November 2021. Further details will be published soon.

## A WEBINAR WITH THE EDITOR

Go behind the scenes at *The Journal of Gemmology* by tuning in to the next instalment of our ongoing webinar series with Editor-in-Chief Brendan Laurs FGA, on 6 October 2021 at 17:00 GMT. Join us as we hear Brendan discuss the current issue of *The Journal* with Gem-A's CEO Alan Hart FGA DGA, explaining how the issue was developed and focusing in greater detail on some of the fascinating feature articles and Gem Notes. To register your place, head to: https://linktr.ee/gemaofgb. Did you miss our last session of Gem-A Live with Brendan? Head to Gem-A's YouTube channel and watch it now: www.youtube.com/c/GemAOfficialChannel.

# Over 110 years of experience in gemmology education

**Our FGA and DGA Members are located around the world – join them by studying with Gem-A in one of three ways**

**AT GEM-A HQ**
London

**WORLDWIDE**
at one of our ATC's

**ONLINE**
with in-person practical lab classes

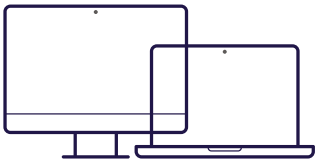

**Find out more by contacting: education@gem-a.com**

## Buy Gem-A Instruments online


**OVER 100 PRODUCTS AVAILABLE**

View the full collection and offers at: **shop.gem-a.com**

Gem-A
THE GEMMOLOGICAL ASSOCIATION OF GREAT BRITAIN

Gem-A, 21 Ely Place, London, EC1N 6TD, UK
+44 (0)20 7404 3334 www.gem-a.com.
Registered charity no. 1109555

CREATING GEMMOLOGISTS SINCE 1908

# Learning Opportunities

*Note*: Event dates and formats are subject to change depending on the COVID-19 situation.

## CONFERENCES AND SEMINARS

**Geological Society of America Annual Meeting (GSA Connects 2021)**
10–13 October 2021
Portland, Oregon, USA (hybrid online)
https://community.geosociety.org/gsa2021/home
*Session of interest*: Gemological Research in the 21st Century—Gem Minerals and Localities

**Canadian Gemmological Association (CGA) Conference**
23 October 2021
Online
https://canadiangemmological.com/2021-cga-conference

**2021 American Society of Appraisers (ASA) International Conference**
24–26 October 2021
Las Vegas, Nevada, USA (hybrid online)
www.appraisers.org/Education/events/asa-international-conference

**CIBJO Congress 2021**
1–4 and 15–18 November 2021
Online
www.cibjo.org/congress2021

**GAC-MAC London 2021 Joint Annual Meeting**
1–5 November 2021
London, Ontario, Canada (hybrid online)
https://gacmac2021.ca
*Session of interest*: Diamonds in Cratons, Diamond-bearing Rocks and Mantle Xenoliths

**2021 Gem-A Conference**
7 November 2021
London
https://gem-a.com
*Note*: The Gem-A Graduation and Presentation of Awards will take place on 8 November 2021.

**2021 International Gems & Jewelry Academic Conference**
November 2021 (exact dates TBA)
Beijing, China
Email: ngtcyjb@ngtc.com.cn

**23rd Federation for European Education in Gemmology (FEEG) Symposium**
29–30 January 2022
Paris, France
www.feeg-education.com/symposium

**NAJA 57th Ace© It Winter Conference**
30–31 January 2022
Tucson, Arizona, USA
https://najaappraisers.com/event/57th-aceit-winter-conference-tucson-az

**AGTA GemFair Tucson**
1–6 February 2022
Tucson, Arizona, USA
https://agta.org/agta-gem-fair-tucson
*Note*: Includes a seminar programme

**7th International Gem & Jewelry Conference (GIT 2021)**
2–3 February 2022
Chanthaburi, Thailand
www.git.or.th/index_en.html

**Tucson Gem and Mineral Show**
10–13 February 2022
Tucson, Arizona, USA
www.tgms.org/show
*Note*: Includes a seminar programme

**Inhorgenta Munich**
11–14 February 2022
Munich, Germany
www.inhorgenta.com/en
*Note*: Includes a seminar programme

**Hasselt Diamond Workshop 2022: SBDD XXVI**
9–11 March 2022
Hasselt, Belgium
www.uhasselt.be/SBDD

**34th Annual Santa Fe Symposium**
22–25 May 2022
Albuquerque, New Mexico, USA
www.santafesymposium.org

**Sainte-Marie-aux-Mines Mineral & Gem Show**
June 2022 (exact dates TBA)
Sainte-Marie-aux-Mines, France
www.sainte-marie-mineral.com

*Note*: Includes workshops on stone cutting and micro-minerals

**International Colored Gemstone Association (ICA) Congress**
September 2022 (exact dates TBA)
Shenzhen, China
www.gemstone.org/ica-congresses

**13th Annual Portland Jewelry Symposium**
October 2022 (exact dates TBA)
Portland, Oregon, USA
https://portlandjewelrysymposium.com

## OTHER EDUCATIONAL OPPORTUNITIES

**Gem-A Workshops and Courses**
Gem-A, London
https://gem-a.com/education

**Gemstone Safari to Tanzania**
12–29 January 2022 and 6–23 July 2022
www.free-form.ch/tanzania/gemstonesafari.html

**Lectures with Gem-A's Midlands Branch**
Fellows Auctioneers, Augusta House, Birmingham
Email Louise Ludlam-Snook at gemamidlands@gmail.com

- Alan Hodgkinson—Garnets, Gemstones & Lenses
  24 September 2021
- TBA
  29 October 2021
- Beatrix Thadour-Sampson—
  Pearls: Changing Fashions & Meanings Through the Ages
  26 November 2021

**Lectures with The Society of Jewellery Historians**
Society of Antiquaries of London, Burlington House
www.societyofjewelleryhistorians.ac.uk/current_lectures

- Akis Goumas—Learning and Experimenting with Ancient Jewellery of the Aegean Region
  26 October 2021 (online only)
- Ute Decker—Sculptural Minimalism & Fairtrade Gold – Philosophy, Provenance and Process
  23 November 2021
- Tim Schroder—Jewels at the Court of Henry VIII
  25 January 2022
- Rebecca Roberts—Jewellery and Power in Iron Age Kazakhstan
  22 February 2022
- Natasha Awais-Dean—Jewels Captured in Perpetuity: The Jewellery Book of Anne of Bavaria
  22 March 2022
- Gonçalo de Vasconcelos e Sousa—An Aspect of Portuguese Jewellery
  24 May 2022
- Karl Schmetzer—The Late 14th-Century Royal Crown of Blanche of Lancaster
  28 June 2022

# New Media

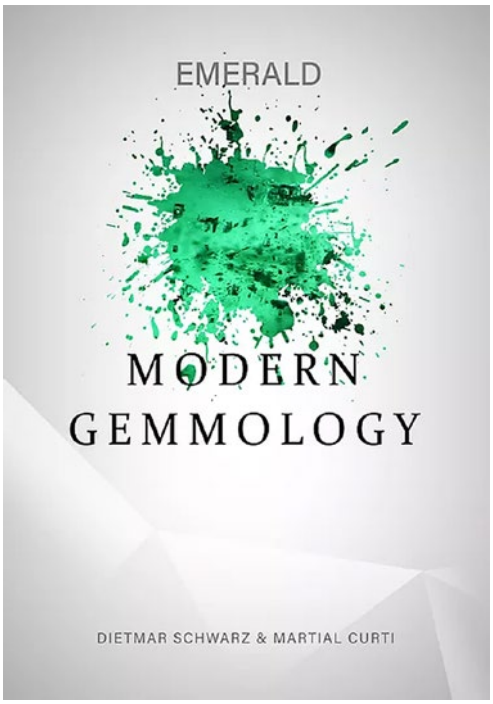


## Emerald Modern Gemmology

**By Dietmar Schwarz and Martial Curti, 2020. Bellerophon Gemlab Ltd, Bangkok, Thailand, www.gemlabanalysis.com/shop, 481 pages, illus., no ISBN. EUR81.00 hardcover or USD49.99 eBook (the latter available in English or Chinese).**

Writing a 481-page reference book on a single gem variety is no small undertaking. It requires years of experience and a significant amount of resources, including gem samples and, perhaps more importantly, ample amounts of time. This publication is intended to serve as a reference primarily for geographic origin determination, and most of the book is dedicated to characterising emeralds from the current commercially significant sources. These include Colombia, Brazil, Russia, Afghanistan and Ethiopia, among many others. Minor sources such as North Carolina, USA, are not included, presumably because they are not commercially relevant.

The first chapter covers the basic characteristics of emerald, such as internal features, trace-element composition, spectra and physical properties. It serves as a good foundation for the later chapters on individual localities, and is particularly useful for gemmologists who do not have access to advanced analytical equipment and who must rely heavily on microscopic observations. Next is a chapter describing geological implications that helps explain the classification of emeralds into two main groups (tectonic-magmatic and tectonic-metamorphic related). The reader is then introduced to how the geographic origin of emeralds is determined using laboratory techniques such as chemical and spectral fingerprinting, and inclusion identification using Raman spectroscopy. The following chapters cover specific emerald deposits and major emerald-producing countries. The coverage of each locality is generally quite comprehensive, with information on its history, maps of mining locations and inclusion galleries, as well as trace-element characteristics and UV-Vis-NIR spectra for emeralds from each deposit.

Much of this book is very professionally done and makes a significant contribution to the gemmological literature. However, there are a few areas that this reviewer feels could have been improved upon. Most notable is that many of the photomicrographs appear oversaturated in green colour, to the extent that this seems to have contributed to a loss of detail in the inclusion features. It appears that the intended colour or appearance could not be reproduced in print, since the image quality in the digital version of the book does not suffer from this same problem. Unfortunately, only some of the images include a magnification factor—key to giving the reader a sense of what would be resolvable with a standard gemmological microscope—and many photomicrographs have no scale information at all. Also, many of the figures appear somewhat grainy and difficult to read in the hardcopy. This is especially true for many of the spectra. Last, the book's binding began to separate during the course of this review, so long-term durability of the print version could be a concern. Of course, this problem could be easily avoided by using the electronic version.

This is an impressive work on emerald that can be appreciated for the vast amount of information it contains. While there are a few small issues with the print edition of the book (which are remedied by the electronic version), this should not discourage those interested in the subject who prefer a print format. Overall this is a great reference work that will appeal to serious gemmologists and those with a particular interest in emeralds. This book will also be valued by the growing crowd of gemmological book collectors.

(*Editor's note*: According to information provided by author DS, he wrote the text of the book, except for the Foreword, Afterword and Acknowledgements, which were prepared by author MC. The photos in the second part of the book were taken at the Bellerophon Lab by MC and Theodor Rozet. All samples in the photos belong to the private 'Emerald Reference and Research Collection' of DS.)

**Nathan D. Renfro**
Gemological Institute of America
Carlsbad, California, USA

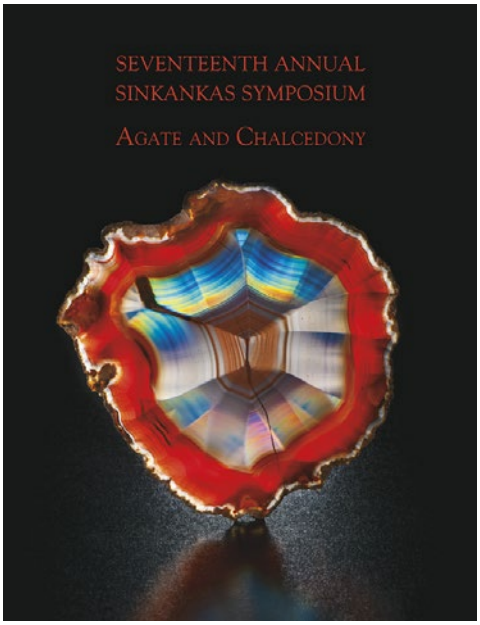


## Seventeenth Annual Sinkankas Symposium—Agate and Chalcedony

**Ed. by Lisbet Thoresen and Stuart Overlin, 2021. Pala International Inc., Fallbrook, California, USA, https://sinkankas.dpidirect.com, 157 pages, illus., ISBN 978-0991532056. USD35.00 softcover or free PDF.**

The Seventeenth Annual Sinkankas Symposium, focusing on agate and chalcedony, was co-sponsored by the Gemological Society of San Diego and the Gemological Institute of America. It was held online as pre-recorded sessions from eight speakers that were available on-demand from 8 April to 7 June 2021. The accompanying proceedings volume contains contributions from most of the speakers, as well as additional content from a few more contributors. It is printed on heavy paper stock and contains 186 colour images and illustrations, with photos by talented photographers Mia Dixon, Harold and Erica Van Pelt, Orasa Weldon and Robert Weldon.

The book opens with a dedication, acknowledgements and programme listing, and these are followed by speaker and author biographies. There is also an obituary for Claren 'Si' Frazier (1933–2020), written by Dona Leicht, which was reprinted from the July–August issue of *Rocks & Minerals* (although not credited as such, but accompanied by different photos). Si was an enthusiastic researcher and collector of quartz-family gems, and he actively participated in previous Sinkankas symposia.

The main portion of this volume consists of informative contributions by various experts on several subjects: agate and chalcedony objects made by Fabergé (by Timothy Adams); the textural complexity of agates (by Dr Peter Heaney); collecting cryptocrystalline quartz (by William Larson); chalcedonies of Anatolia from the Neolithic period to the present (by Dr Çiğdem Lüle); the micro-world of agate and chalcedony (by Nathan Renfro); gem carving in ancient times (by Si and Ann Frazier); agate and quartz carvings crafted by Harold Van Pelt (by Lisbet Thoresen); the challenges of photographing agates (by Robert Weldon); and an article reprinted from the Winter 2017 issue of *Gems & Gemology* titled 'Gem virtuosos: The Drehers and their extraordinary carvings' (by Robert Weldon, Cathleen Jonathan and Rose Tozer). The volume closes with an agate bibliography assembled by Ann Frazier.

The book is attractively laid out, and a nice touch is the spectacular full-page photo that faces the first page of each article. (There is an error in the caption of one such photo, which appears on p. 2, as it indicates a Crazy Lace agate measuring 49.78 mm, whereas the same photo on the back cover is described as a Laguna agate measuring 162.2 mm.) The wide range of topics—from ancient carvings to contemporary fashioned objects, and from microscopic internal features to textural complexities, and finally the particular considerations for collecting and photographing agate and chalcedony—make this a valuable addition to the literature. Gemmologists, enthusiasts, collectors and anyone interested in quartz-family gems will benefit from adding this informative volume to their reference library.

**Brendan M. Laurs FGA**

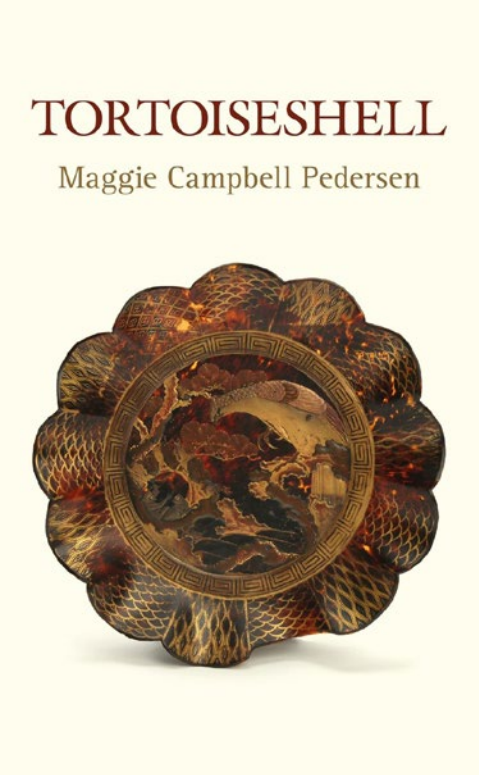


## Tortoiseshell

**By Maggie Campbell Pedersen, 2021. The Crowood Press, Marlborough, Wiltshire, www.crowood.com/products/tortoiseshell-by-maggie-campbell-pedersen, 192 pages, illus., ISBN 978-0719831447. GBP25.00 hardcover.**

I found this book to be excellent for gleaning a better understanding of tortoiseshell. Outside of seeing the material in museums (and the popular plastic imitation of tortoiseshell on eyeglass frames), there is very little direct reference to this material for gemmologists. However, Maggie Campbell Pedersen's passion and scholarship shine brightly in this concise work, starting with pointing out that the title of the book is a misnomer: the shell used comes only from sea turtles, not land tortoises. This misnomer, according to the author, 'may have arisen because early English naturalists called turtles "sea tortoises"', and the name *tortoiseshell* stuck.

The book is amply illustrated with more than 100 colour photographs distributed among its eight chapters. Chapter 1, 'Turtle Species', covers the origin, species and lifecycle of marine turtles. It indicates that the horny plates (known as *scutes*) on the shells of only three sea turtle species have been used as tortoiseshell. Hawksbill turtle shell is most commonly employed due to its colourful quality and patterning. Scutes from green turtles are also used, and loggerhead turtle shell is only occasionally seen.

Chapter 2 covers 'Conservation and the Dangers Faced by Turtles Today'. As the title suggests, the turtles from which tortoiseshell is harvested continue to need protection from extinction. The chapter is well researched and covers the value of human intervention, but the most important fact seems to be the need to learn more.

Chapter 3, 'What is Tortoiseshell?', explains that it consists of a natural polymer, while also covering the formation of the keratinous scutes and their colour. Chapter 4—'Identifying Tortoiseshell and its Simulants'—describes the many materials used historically to imitate tortoiseshell: horn, baleen, celluloid, acrylic, polyester and polyvinyl chloride. It then illustrates, with detailed photos, the visual features that can be used to identify true tortoiseshell and separate it from the many look-alikes. Chapter 5, 'Testing Tortoiseshell', is one of the most important chapters for the gemmologist because it goes into the various basic and advanced gemmological tests that are useful for identifying tortoiseshell.

Chapter 6, 'Treatments and Care', explains how large sheets of tortoiseshell have been assembled together, followed by information on polishing, piqué work, marquetry, backing, dyeing and more. The chapter concludes with information on the care of both tortoiseshell and its imitations.

Chapter 7, 'History', is a well-researched section that begins with ancient times. Tortoiseshell initially became fashionable in ancient Rome, and 'Julius Cesar is said to have had warehouses full of tortoiseshell' (p. 111). The chapter also describes its historic use in many regions—including China, India, Ceylon, the Ottoman Empire, Polynesia, New Zealand, Australia, Mesoamerica and Madagascar—and concludes with a detailed look at Europe and Japan. Amazing photographic examples of cabinets and tables show the intricate detail and exquisite craftsmanship of inlaid tortoiseshell, as well as many *objets d'art*.

Chapter 8, 'Other Keratins Used in the Decorative Arts', covers horn, baleen, hooves, hair and many more. The book concludes with an appendix on the laws and regulatory bodies that protect sea turtles. A second appendix consists of a reference chart with basic identifying characteristics of mottled and 'blond' tortoiseshell, horn and plastics. The book concludes with a glossary, bibliography and index.

This book is a must for any gemmologist who wishes to learn the many aspects of tortoiseshell.

**Bill Larson FGA**
Pala International
Fallbrook, California, USA

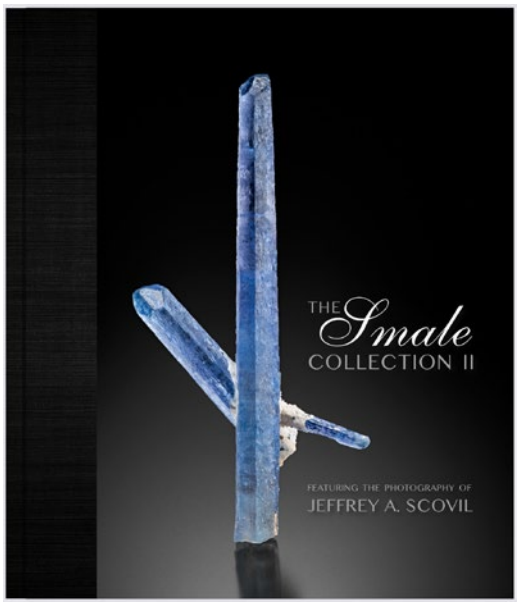


## The Smale Collection II

**Ed. by Gloria Staebler, Dave Bunk and Brittany MacRostie, 2021. Lithographie, Arvada, Colorado, USA, www.lithographie.org/bookshop/the_smale_collection_ii.htm, 176 pages, illus., ISBN 978-1734131024. USD60.00 hardcover.**

This wonderful book contains 165 pages of gorgeous, full-page photos of crystallised mineral specimens from the collection of famous mathematician and mineral collector Steve Smale. It follows a 2006 book titled *The Smale Collection: Beauty in Natural Crystals*, which also featured specimens from his collection, without any particular theme.

The book begins with a preface that describes Smale's mineral collection as a reflection of his life and travels. This is followed on pages 1–116 with photographs featuring specimens from Smale's collection that appeared in advertisements in *The Mineralogical Record*. Next, pages 117–137 are comprised of photos of some crystal specimens from Smale's collection that are included in an online museum of Chinese minerals hosted by the City University of Hong Kong, which depict some of the finest pieces that were mined in China during the past two decades. Then, pages 138–158 feature images of selected specimens from Smale's collection, and pages 159–165 consist of a species and locality index.

The full-page images by photographer Jeff Scovil are printed using a six-colour process that yields the best colour representation I have ever seen for crystallised minerals, making them appear almost lifelike. According to one of the book's editors (GS), the traditional four-colour offset printing process relies on layering four pigments (cyan, magenta, yellow and black, or CMYK), but this cannot recreate the full red-green-blue (RGB) colour gamut. The six-colour process adds two more pigments to the CMYK gamut—orange and green—which dramatically expand the print-colour range. The palette of 'blacks', which are created from a combination of black plus the other pigments, is also expanded in six-colour space, giving images a depth and nuance unobtainable through traditional means. The six-colour process is relatively new, and few presses have the physical capacity to work with the six plates that are necessary for this method of printing.

This book should be of interest to gemmologists because more than half of the pieces are crystal specimens of gem species. And with the new printing process applied to photos of Smale's extraordinary collection, the reader will see tsavorite, aquamarine, demantoid and emerald crystals in a way that will excite anyone. I highly recommend this beautiful book, brought to life with the care of Steve Smale, Jeff Scovil and Gloria Staebler, the last of whom deserves extra recognition for advancing a colour process that should become better known in the field of gemmology.

**Bill Larson FGA**

# Other Book Titles

## COLOURED STONES

**Photoatlas of Inclusions in Bohemian Garnet**
By Radek Hanus, 2019. Self-published, 116 pages, ISBN 978-8075680716. CZK1000 hardcover.

## FAIR TRADE

**Sustainable Luxury and Jewelry**
Ed. by Ivan Coste-Manière and Miguel Ángel Gardetti, 2021. Springer, Singapore, xi + 253 pages, ISBN 978-9811624537 or e-ISBN 978-9811624544, https://doi.org/10.1007/978-981-16-2454-4. USD159.99 hardcover or USD119.00 e-Book.

## GEM LOCALITIES

**Opal Dreaming: A Short History of Coober Pedy**
By Sue Britt, 2020. Coober Pedy Historical Society, Coober Pedy, South Australia, Australia, 62 pages, ISBN 978-1925263480. AUD15.00 softcover.

**Opal Hunters: The Bartrams on the Opal Fields 1936–2021**
By Donald Bartram, 2021. Peacock Publications, Adelaide, South Australia, Australia, 176 pages, ISBN 978-1925263541. AUD50.00 hardcover.

**Type Mineralogy of Brazil: A Book in Progress**
By Daniel Atencio, 2020. Universidade de São Paulo, São Paulo, Brazil, 662 pages, ISBN 978-6586403015, https://doi.org/10.11606/9786586403015. Free PDF at www.livrosabertos.sibi.usp.br/portaldelivrosUSP/catalog/book/540.

## INSTRUMENTATION

**Modern Raman Microscopy: Technique and Practice**
By Alexander Rzhevskii, 2021. Cambridge Scholars Publishing, Newcastle upon Tyne, 392 pages, ISBN 978-1527567849. GBP64.99 hardcover.

**Portable Spectroscopy and Spectrometry (Vol. 1: Technologies and Instrumentation; Vol. 2: Applications)**
Ed. by Richard Crocombe, Pauline Leary and Brooke Kammrath, 2021. John Wiley & Sons Ltd, New York, New York, USA, 608 pages, ISBN 978-1119835578 or e-ISBN 978-1119636489, https://doi.org/10.1002/9781119636489. USD165.00 hardcover or USD132.00 eBook.

## JEWELLERY HISTORY

**Bijoux Anciens (1800–1950) [Antique Jewellery (1800–1950)]**
By Victoire de Castellane, 2021. Flammarion, Paris, France, 128 pages, ISBN 978-2080249890 (in French). EUR15.00 softcover.

**Tadema Gallery London: Jewellery from the 1860s to 1960s**
By Beatriz Chadour-Sampson and Sonya Newell-Smith, 2021. Arnoldsche Art Publishers, Stuttgart, Germany, 328 pages, ISBN 978-3897905986. EUR68.00 hardcover.

## JEWELLERY AND *OBJETS D'ART*

**Diva! Italian Glamour in Fashion Jewellery**
By Alba Cappallieri, 2021. Silvana Editoriale, Milan, Italy, 264 pages, ISBN 978-8836648047 (in English and Italian). EUR50.00 hardcover.

**The Jewellery Box**
By Jorunn Veiteberg, 2021. Arnoldsche Art Publishers, Stuttgart, Germany, 552 pages, ISBN 978-3897906198. EUR38.00 hardcover.

**Modern British Jewellery Designers 1960–1980**
By Mary Ann Wingfield, 2021. ACC Art Books, Woodbridge, Suffolk, 160 pages, ISBN 978-1788841214. GBP25.00 hardcover.

**The Real Thing—Den Ægte Vare—真实之物: Jewellery and Objects by Kim Buck**
By Jorunn Veiteerg, 2021. Arnoldsche Art Publishers, Stuttgart, Germany, 176 pages, ISBN 978-3897906129 (in English, Danish and Chinese). EUR38.00 hardcover.

**The Shape of Matter: Through an Artist's Eye**
By Paula Crevoshay, Martin Bell and Christopher Chavez, 2020. Crevoshay, Albuquerque, New Mexico, USA, 232 pages, ISBN 978-0988672338. USD69.95 hardcover.

**Treasures in Gold & Jade: Masterworks from Taiwan**
Ed. by Peter C. Keller, 2020. Bowers Museum (Santa Ana, California, USA) and Houston Museum of Natural Science (Houston, Texas, USA), 80 pages, ISBN 978-0578695730 (in English and Chinese). USD25.00 hardcover.

**Van Cleef and Arpels: Treasures and Legends**
By Vincent Meylan, 2021. ACC Art Books, Woodbridge, Suffolk, 344 pages, ISBN 978-1788841474. GBP55.00 hardcover.

## PEARLS

**Arnie: Pearls and Luggers in the Torres Strait**
By Arnie Duffield and Lee Duffield, 2021. Xlibris AU, Bloomington, Indiana, USA, 130 pages, ISBN 978-1664105218 softcover, 978-1664105225 hardcover or e-ISBN 978-1664105201. USD16.99 softcover, USD35.99 hardcover or USD4.99 eBook.

**Pearls: A Practical Guide**
By Wendy Graham, 2021. The Crowood Press Ltd, Marlborough, Wiltshire, 96 pages, ISBN 978-1785008122. GBP12.99 softcover.

# Literature of Interest

## COLOURED STONES

**Agate genesis: A continuing enigma.** T. Moxon and G. Palyanova, *Minerals*, **10**(11), 2020, article 953 (26 pp.), https://doi.org/10.3390/min10110953.*

**Characterization of order-disorder transition in $MgAl_2O_4$:$Cr^{3+}$ spinel using photoluminescence.** C. Wang, A.H. Shen and Y. Liu, *Journal of Luminescence*, **227**, 2020, article 117552 (8 pp.), https://doi.org/10.1016/j.jlumin.2020.117552.

**Color and genesis of californite [vesuvianite] from Pakistan: Insights from μ-XRF mapping, optical spectra and X-ray photoelectron spectroscopy.** Z. Lu, X. He, C. Lin, L. Liang, X. Jin and Q. Guo, *Scientific Reports*, **10**, 2020, article 285 (12 pp.), https://doi.org/10.1038/s41598-019-57186-0.*

**Considerations about Bi and Pb in the crystal structure of Cu-bearing tourmaline.** A. Ertl and P. Bačík, *Minerals*, **10**(8), 2020, article 706 (15 pp.), https://doi.org/10.3390/min10080706.*

**Corindons multi-astériés de forme " cacahuète " [Peanut-shaped multi-star corundum].** J.-P. Gauthier, J. Fereire and T.N. Bui, *Revue de Gemmologie A.F.G.*, No. 212, 2021, 4–8 (in French with English abstract).

**Crystallinity and play-of-colour in gem opal with digit patterns from Wegel Tena, Ethiopia.** K. Zhao and F. Bai, *Minerals*, **10**(7), 2020, article 625 (17 pp.), https://doi.org/10.3390/min10070625.*

**Discussing the coloration mechanism of Luodian jade from Guizhou.** L. Wang, J. Lin, T. Ye, J. Tan, B. Wang and L. Yang, *Open Access Library Journal*, **7**(5), 2020, article e6364 (7 pp.), https://doi.org/10.4236/oalib.1106364.*

**Enhydros-Achat aus Brasilien [Enhydro agate from Brazil].** U. Henn and R. Schultz-Güttler, *Gemmologie: Zeitschrift der Deutschen Gemmologischen Gesellschaft*, **70**(1/2), 2021, 61–62 (in German with English abstract).

**The fluorescence spectra of gem-quality hauyne.** F. Lü and A.H. Shen, *Spectroscopy and Spectral Analysis*, **40**(11), 2020, 3468–3471, www.gpxygpfx.com/EN/Y2020/V40/I11/3468 (in Chinese with English abstract).*

**Gemmological characteristic of painite.** J. Guo, R. Liao and Q. Zheng, *Journal of Gems & Gemmology*, **23**(3), 2021, 44–52, https://doi.org/10.15964/j.cnki.027jgg.2021.03.006 (in Chinese with English abstract).

**Gemmological and chemical characteristics of spessartine from Zambia.** H. Zhang, C. Liu, S. Qiruong and A.H. Shen, *Journal of Gems & Gemmology*, **23**(2), 2021, 1–10, https://doi.org/10.15964/j.cnki.027jgg.2021.02.001 (in Chinese with English abstract).

**Gemology, mineralogy, and spectroscopy of an attractive tremolitized diopside anorthosite gem material from the Philippines: A new type of material with similarities to Dushan jade.** X. Ye, F. Bai, M. Li and H. Sun, *Minerals*, **11**(2), 2021, article 152 (18 pp.), https://doi.org/10.3390/min11020152.*

**Hackmanite—The natural glow-in-the-dark material.** C. Agamah, S. Vuori, P. Colinet, I. Norrbo, J.M. de Carvalho, L.K. Okada Nakamura, J. Lindblom, L. van Goethem *et al.*, *Chemistry of Materials*, **32**, 2020, 8895–8905, https://doi.org/10.1021/acs.chemmater.0c02554.*

**The impact of trace metal cations and absorbed water on colour transition of turquoise.** X. Wang and Y. Guo, *Royal Society Open Science*, **8**(2), 2021, article 20110 (20 pp.), https://doi.org/10.1098/rsos.201110.*

**Influence of low-symmetry component of crystal field on gemstones colors: $Cr^{3+}$ in ruby and emerald.** D.W. Yang, M.G. Brik, A.M. Srivastava, C.G. Ma and M. Piasecki, *Journal of Luminescence*, **221**, 2020, article 117061 (4 pp.), https://doi.org/10.1016/j.jlumin.2020.117061.

**Influence of metamictization on the gemological properties of natural zircon: A Raman spectroscopic study of zircons in the gemological collection of Abraham Gottlob Werner.** S. Gao and G. Heide, *Journal of Raman Spectroscopy*, **52**(1), 2021, 71–77, https://doi.org/10.1002/jrs.6041.*

**Intriguing minerals: Corundum in the world of rubies and sapphires with special attention to Macedonian rubies.** M. Jeršek, G. Jovanovski, B. Boev and P. Makreski, *ChemTexts*, **7**(3), 2021, article 19 (23 pp.), https://doi.org/10.1007/s40828-021-00143-0.

**Introducing semi-gem quality blue corundum from the Alvand complex, Hamedan, west Iran.** F.S. Alehashem, M. Moazzen and A. Jahangiri, *Periodico di Mineralogia*, **90**(2), 2021, 195–209, https://doi.org/10.13133/2239-1002/17315.*

**Investigation of recently discovered common green opals from Anosy (Madagascar).** F. Caucia, L. Marinoni, M. Gilio and E.D. Cors, *Periodico di Mineralogia*, **90**(2), 2021, 217–228, https://doi.org/10.13133/2239-1002/16982.*

**L'opale gemme : Une nouvelle fenêtre sur la vie [Gem opal: A new window on life].** B. Chauviré, *Revue de Gemmologie A.F.G.*, No. 212, 2021, 25–28 (in French).

**La luminescence orange des corindons. Une origine pas classique pour les gemmologues ! Partie II [The orange luminescence of corundum. An unconventional origin for gemologists! Part II].** M. Vigier, E. Fritsch and O. Segura, *Revue de Gemmologie A.F.G.*, No. 212, 2021, 13–19 (in French with English abstract).

**Micro-features of spinel.** N.D. Renfro, J.I. Koivula, S.F. McClure, K. Schumacher and J.E. Shigley, *Gems & Gemology*, **57**(1), 2021, 46–49, https://doi.org/10.5741/gems.57.1.46.*

**Mineralogical and spectral characteristics of purple boulder opal from Australia.** X. Gao, M. Wang, S. Ye and Z. Yin, *Journal of Gems & Gemmology*, **23**(3), 2021, 37–43, https://doi.org/10.15964/j.cnki.027jgg.2021.03.005 (in Chinese with English abstract).

**Mineralogy, geochemistry and genesis of agate—A review.** J. Götze, R. Möckel and Y. Pan, *Minerals*, **10**(11), 2020, article 1037 (51 pp.), https://doi.org/10.3390/min10111037.*

**Mineralogy and geochemistry of nephrite jade from Yinggelike deposit, Altyn Tagh (Xinjiang, NW China).** Y. Jiang, G. Shi, L. Xu and X. Li, *Minerals*, **10**(5), 2020, article 418 (22 pp.), https://doi.org/10.3390/min10050418.*

**Mn-bearing purplish-red tourmaline from the Anjanabonoina pegmatite, Madagascar.** F. Bosi, B. Celata, H. Skogby, U. Hålenius, G. Tempesta, M.E. Ciriotti, E. Bittarello and A. Marengo, *Mineralogical Magazine*, **85**(2), 2021, 242–253, https://doi.org/10.1180/mgm.2021.20.*

**New insights for gem-quality Mn-bearing diopside-omphacite, violane variety, from Saint Marcel (Val d'Aosta, Italy): Its trace elements and spectroscopic characterization.** V. Diella, R. Bocchio, F. Caucia, N. Marinoni, A. Langone and E. Possenti, *Minerals*, **11**(2), 2021, article 171 (21 pp.), https://doi.org/10.3390/min11020171.*

**Opals in the Harvard mineral and gem collection.** R. Alonso-Perez, *GemGuide*, **40**(3), 2021, 4–9.

**Optical and luminescence spectroscopy of varicolored gem spinel from Mogok, Myanmar and Lục Yên, Vietnam.** I. Malíčková, P. Bačík, J. Fridrichová, R. Hanus, Ľ. Illášová, J. Štubňa, D. Furka, S. Furka *et al.*, *Minerals*, **11**(2), 2021, article 169 (13 pp.), https://doi.org/10.3390/min11020169.*

**Our friends the inclusions. The detective at the party of inclusions. Tenth episode.** L. Costantini and C. Russo, *Rivista Italiana di Gemmologia/Italian Gemological Review*, No. 12, 2021, 7–21.

**Phase composition and genesis of pyroxenic jadeite from Guatemala: Insights from cathodoluminescence.** C. Lin, X. He, Z. Lu and Y. Yao, *RSC Advances*, **10**(27), 2020, 15937–15946, https://doi.org/10.1039/d0ra01772h.*

**Quality evaluation of tourmaline green appearance based on CIECAM16 color appearance model.** B. Yuan, Y. Guo, Y. Li and H. Jia, *IOP Conference Series: Materials Science and Engineering*, **746**, 2020, article 012005 (14 pp.), https://doi.org/10.1088/1757-899x/746/1/012005.*

**The REE-induced absorption and luminescence in yellow gem-quality Durango-type hydroxylapatite from Muránska Dlhá Lúka, Slovakia.** P. Bačík, J. Fridrichová, J. Štubňa, T. Bancík, Ľ. Illášová, H. Pálková, R. Škoda, T. Mikuš *et al.*, *Minerals*, **10**(11), 2020, article 1001 (21 pp.), https://doi.org/10.3390/min10111001.*

**Silicon-oxygen region infrared and Raman analysis of opals: The effect of sample preparation and**

**measurement type.** N.J. Curtis, J.R. Gascooke and A. Pring, *Minerals*, **11**(2), 2021, article 173 (31 pp.), https://doi.org/10.3390/min11020173.*

**Some encounters with halite and gypsum – Notes on their crystallography and gemmology.** S. Stocklmayer, *Australian Gemmologist*, **27**(5), 2021, 274–282.

**Spectroscopic and crystal-chemical features of sodalite-group minerals from gem lazurite deposits.** N.V. Chukanov, A.N. Sapozhnikov, R.Y. Shendrik, M.F. Vigasina and R. Steudel, *Minerals*, **10**(11), 2020, article 1042 (24 pp.), https://doi.org/10.3390/min10111042.*

**Spectroscopic study of green-yellow and green turquoise associated minerals from Zhushan, Hubei Province.** Y. Ku, M. Yang and Y. Li, *Spectroscopy and Spectral Analysis*, **40**(6), 2020, 1815–1820, www.gpxygpfx.com/EN/Y2020/V40/I06/1815 (in Chinese with English abstract).*

**Spektroskopické štúdium prírodných spodumenov z lokality Kunar, Afganistan [Spectroscopic study of natural spodumene from Kunar, Afghanistan].** I. Malíčková, P. Bačík, J. Fridrichová, Ľ. Illášová and R. Škoda, *Esemestník, Spravodajca Slovenskej mineralogickej spoločnosti [Newsletter of Mineralogical Society of Slovakia]*, **9**(1), 2021, 5–10, https://mineralogickaspolocnost.com/wp-content/uploads/2021/04/esemestnik-2020-1-web.pdf (in Slovak with English abstract).*

**Study of Fe ions in aquamarine and the effect of dichroism as seen using UV–Vis, NIR and X-ray.** N. Bunnag, B. Kasri, W. Setwong, E. Sirisurawong, M. Chotsawat, P. Chirawatkul and C. Saiyasombat, *Radiation Physics and Chemistry*, **177**, 2020, article 109107 (7 pp.), https://doi.org/10.1016/j.radphyschem.2020.109107.

**Study of gemmological characteristics and chemical composition of Zultanite samples to determine their nature.** A.A. Anisimova and G.N. Ivanova, *IOP Conference Series: Earth and Environmental Science*, **408**, 2020, article 012049 (4 pp.), https://doi.org/10.1088/1755-1315/408/1/012049.*

**Study on gemology characteristics of the turquoise from Mongolia.** Q. Chen, H. Wang, X. Liu, C. Qin and D. Bao, *Spectroscopy and Spectral Analysis*, **40**(7), 2020, 2164–2169, www.gpxygpfx.com/EN/Y2020/V40/I07/2164 (in Chinese with English abstract).*

**Study on the relation between the intensity distribution of infrared absorption peak at 3 309 $cm^{-1}$ and trace elements in color zones of Changle sapphire.** C. Chen, T. Shao and A.H. Shen, *Spectroscopy and Spectral Analysis*, **40**(7), 2020, 2138–2142, www.gpxygpfx.com/EN/Y2020/V40/I07/2138 (in Chinese with English abstract).*

**Unravelling the origin of the yellow-orange luminescence in natural and synthetic scapolites.** F. Blumentritt, C. Latouche, Y. Morizet, M.-T. Caldes, S. Jobic and E. Fritsch, *Journal of Physical Chemistry Letters*, **11**(12), 2020, 4591–4596, https://doi.org/10.1021/acs.jpclett.0c00712.

**UV-Vis absorption spectra and 3D fluorescence spectra study of color-change garnet with red fluorescence.** C. Liu, C. Chen, T. Shao, Z. Li and A.H. Shen, *Spectroscopy and Spectral Analysis*, **40**(7), 2020, 2148–2152, www.gpxygpfx.com/EN/Y2020/V40/I07/2148 (in Chinese with English abstract).*

## CULTURAL HERITAGE

**Can the oyster speak? Pearling empires and the marine environments of South India and Sri Lanka, c. 1600–1900.** S. Ostroff, in M. Chaiklin, P. Gooding & G. Campbell, Eds., *Animal Trade Histories in the Indian Ocean World*. Palgrave Macmillan, Cham, Switzerland, 2020, 65–98, https://doi.org/10.1007/978-3-030-42595-1_3.

**A gemmological study of the reliquary crown of Namur, Belgium.** Y. Bruni, F. Hatert, P. George, H. Cambier and D. Strivay, *European Journal of Mineralogy*, **33**(2), 2021, 221–232, https://doi.org/10.5194/ejm-33-221-2021.*

**Historiography and FTIR spectral signatures of beryl crystals from some ancient Roman sites in the Eastern Desert of Egypt.** A.A. Surour and S.A.M. Omar, *Environmental Earth Sciences*, **79**(23), 2020, article 520 (15 pp.), https://doi.org/10.1007/s12665-020-09260-4.

**Western connections of northeast Africa: The garnet evidence from late antique Nubia, Sudan.** J. Then–Obłuska, H.A. Gilg, U. Schüssler and B. Wagner, *Archaeometry*, **63**(2), 2021, 227–246, https://doi.org/10.1111/arcm.12607.

## DIAMONDS

**Application of the entropy method and color difference formula to the evaluation of round brilliant cut diamond scintillation.** F. Liu, Y. Guo, S. Lv and G. Chen, *Mathematics*, **8**(9), 2020, article 1489 (14 pp.), https://doi.org/10.3390/math8091489.*

**Color center in minerals: Taking diamond nitrogen center as an example.** F. Chen, *Acta Mineralogica Sinica*, **41**(2), 2021, 109–119 (in Chinese with English abstract).

**Deciphering the enigmatic origin of Guyana's diamonds.** R. Bassoo, K.S. Befus, P. Liang, S.L. Forman and G. Sharman, *American Mineralogist*, **106**(1), 2021, 54–68, https://doi.org/10.2138/am-2020-7486.

**Diamond with nitrogen: States, control, and applications.** Y. Zheng, C. Li, J. Liu, J. Wei and H. Ye, *Functional Diamond*, **1**(1), 2021, 63–82, https://doi.org/10.1080/26941112.2021.1877021.*

**Diamond's spectral constellation.** M.D. Cowing, *Gemmology Today*, June 2021, 24–31, https://tinyurl.com/u8eda.*

**Diamonds certify themselves: Multivariate statistical provenance analysis.** C.E. McManus, N.J. McMillan, J. Dowe and J. Bell, *Minerals*, **10**(10), 2020, article 916 (12 pp.), https://doi.org/10.3390/min10100916.*

**Distribution of nitrogen-vacancy $NV^-$ centers in cubic diamond crystals from Anabar placers as revealed by ODMR and PL tomography.** S.V. Titkov, V.V. Yakovleva, I.D. Breev, A.N. Anisimov, P.G. Baranov, A.I. Dorofeeva and N.S. Bortnikov, *Doklady Earth Sciences*, **496**(1), 2021, 45–47, https://doi.org/10.1134/s1028334x21010244.

**Infrared, photoluminescence, and electron paramagnetic resonance characteristic features of diamonds from the Aikhal pipe (Yakutia).** A. Komarovskikh, M. Rakhmanova, O. Yuryeva and V. Nadolinny, *Diamond and Related Materials*, **109**, 2020, article 108045 (9 pp.), https://doi.org/10.1016/j.diamond.2020.108045.

**The origin of color of 1330 nm center diamonds.** T. Hainschwang, F. Notari and G. Pamies, *Diamond and Related Materials*, **110**, 2020, article 108151 (14 pp.), https://doi.org/10.1016/j.diamond.2020.108151.

**QUIDDIT - Quantification of infrared active defects in diamond and inferred temperatures.** L. Speich and S.C. Kohn, *Computers & Geosciences*, **144**, 2020, article 104558 (7 pp.), https://doi.org/10.1016/j.cageo.2020.104558.

**Review for frequent characteristics of diamond UV-Vis-MIR spectra.** J. Li, C. Fan, Y. Cheng, X. Liu, Y. Wang, G. Shan, T. Li, G. Li *et al.*, *Journal of Synthetic Crystals*, **50**(1), 2021, 158–166, http://rgjtxb.jtxb.cn/EN/Y2021/V50/I1/158 (in Chinese with English abstract).*

**Speaking the same language – [Grading of] diamonds (part two).** *Gemmology Today*, June 2021, 42–47, https://tinyurl.com/44zv778w.*

**Unusual green type Ib-IaB Dniester-type diamond from Ukrainian placers.** V.M. Kvasnytsya and F.V. Kaminsky, *Mineralogy and Petrology*, **115**(2), 2021, 149–160, https://doi.org/10.1007/s00710-020-00732-w.

## FAIR TRADE

**Provenance Proof – New technologies to track and trace gems in the supply chain.** C. Lawson and M. Simmiss, *Australian Gemmologist*, **27**(5), 2021, 262–271.

**Research on traceability system construction of turquoise from Zhushan, Hubei Province, based on blockchain.** H. Xia and M. Yang, *Journal of Gems & Gemmology*, **23**(2), 2021, 46–52, https://doi.org/10.15964/j.cnki.027jgg.2021.02.006 (in Chinese with English abstract).

## GEM LOCALITIES

**Afghanistan gemstone industry – The calm before the storm.** G.W. Bowersox, *GemGuide*, **40**(4), 2021, 12–14.

**Collecting the King of Kashmir aquamarine [Pakistan].** D. Trinchillo, *Mineralogical Record*, **51**(6), 2020, 755–779.

**Die Diamantvorkommen Namibias [The diamond occurrences of Namibia].** U. Henn, *Gemmologie: Zeitschrift der Deutschen Gemmologischen*

*Gesellschaft*, **70**(1/2), 2021, 3–36 (in German with English abstract).

**Geochemical and reflectance spectroscopy data integration to characterize emerald deposits: The case of the Paraná deposit, Brazil.** J.F. Araújo Neto, S.B. Barreto, T.A. Carrino, I.M.B.A. Souza and G.L. Santos, *Anais da Academia Brasileira de Ciências*, **93**(1), 2021, article e20200236 (23 pp.), https://doi.org/10.1590/0001-3765202120200236.*

**Geology, occurrence and gemmology of Khamti amber from Sagaing Region, Myanmar.** T.T. Nyunt, C. Cho, N.B.B. Kyaw, M. Krishnaswamy, L.H. Ying, T.T. Sun and C. Chanmuang N., *Thai Geoscience Journal*, **2**(2), 2021, 63–73, https://doi.org/10.14456/tgj.2021.6.*

**Identification of different origins of Hetian jade based on statistical methods of multi-element content.** A. Zhou, J. Jiang, C. Sun, X. Xu and X. Lu, *Spectroscopy and Spectral Analysis*, **40**(10), 2020, 3174–3178, www.gpxygpfx.com/EN/Y2020/V40/I10/3174 (in Chinese with English abstract).*

**Interesting mineral finds in the Plast District (South Urals) in 2018–2019.** S.V. Kolisnichenko, *Mineralogical Almanac*, **26**(1), 2021, 58–64.

**The lure of Chief Mountain, Pala pegmatite district, San Diego County, California.** T.P. Moore, *Mineralogical Record*, **52**(1), 2021, 11–46.

**The Medina pegmatite field, Pedra Azul District, Minas Gerais, Brazil.** W. E. Wilson, *Mineralogical Record*, **52**(3), 2021, 225–244.

**Petrogenesis of gem sapphire in a pegmatite-aplite vein from the Alvand batholith, western Iran.** R.S. Gheshlaghi, M. Ghorbani, A.A. Sepahi, R. Deevsalar and R. Shinjo, *Mineralogy and Petrology*, **114**, 2020, 501–513, https://doi.org/10.1007/s00710-020-00716-w.

**Sapat Gali, Mansehra District, Khyber Pakhtunkhwa Province, Pakistan [peridot locality].** W.E. Wilson, *Mineralogical Record*, **51**(6), 2020, 785–801.

**Timan-Ural stone province—Mineral resource base of the gemstones of the Russian Federation.** V. Gadiyatov, P. Kalugin and A. Demidenko, in C. Olegovna, Ed., *Processes in GeoMedia—Volume I*. Springer, Cham, Switzerland, 2020, 193–203, https://doi.org/10.1007/978-3-030-38177-6_21.

**Variety of iron oxide inclusions in sapphire from southern Vietnam: Indication of environmental change during crystallization.** D.T.A. Vu, A. Fanka, A. Salam and C. Sutthirat, *Minerals*, **11**(3), 2021, article 241 (14 pp.), https://doi.org/10.3390/min11030241.*

## INSTRUMENTATION AND TECHNOLOGY

**Characterization of coloured gemstones by X-ray micro computed tomography.** R. Heyn, A. Rozendaal, A. Du Plessis and C. Mouton, *Minerals*, **11**(2), 2021, article 178 (16 pp.), https://doi.org/10.3390/min11020178.*

**The grand color filter comparison.** N. Zolotukhina, *Gemmology Today*, June 2021, 74–80, https://tinyurl.com/96j7dwtt.*

**How to calculate color from spectra of uniaxial gemstones.** C. Shen, A.C. Palke, Z. Sun and M.D. Fairchild, *Gems & Gemology*, **57**(1), 2021, 36–45, https://doi.org/10.5741/gems.57.1.36.*

**Introducing ColourWise.** G. Dominy, *Gemmology Today*, June 2021, 16–22, https://tinyurl.com/8frrvhyc.*

**Non-destructive spectroscopic methods for gem analysis: A short review.** S. Raneri, G. Barone, P. Mazzoleni and D. Bersani, *IMEKO TC-4 International Conference on Metrology for Archaeology and Cultural Heritage*, Trento, Italy, 22–24 October 2020, 501–506.

**Real-time detection of long lived near infrared luminescence from colourless cubic zirconia by time-gated imaging.** P.M.P. Lanigan, C.D. McGuinness, M. Rendle, P.A. Aked, C.G. Bearcroft, D.C. Jones and S.C. Lawson, *Minerals*, **10**(10), 2020, article 891 (9 pp.), https://doi.org/10.3390/min10100891.*

**Smartphone mineral photography.** C. Cramer, *Mineralogical Record*, **51**(6), 2020, 841–847.

## LAPIDARY TOPICS

**Lapidary technology through the ages: Laps and polish.** J. K Prim, *Rivista Italiana di Gemmologia/Italian Gemological Review*, No. 12, 2021, 53–60.

## MISCELLANEOUS

**The birth of "Planeta": New private mineralogical museum in the Urals.** M.V. Tsyganko, *Mineralogical Almanac*, **26**(1), 2021, 42–47.

**Comparative analysis of supervised models for diamond price prediction**. G. Sharma, V. Tripathi, M. Mahajan and A. Kumar Srivastava, *11th International Conference on Cloud Computing, Data Science & Engineering (Confluence 2021)*, 28–29 January 2021, 1019–1022, https://doi.org/10.1109/Confluence51648.2021.9377183.

**Finding beauty in gem photography.** R. Sampson, *Australian Gemmologist*, **27**(5), 2021, 283–286.

**Fluorescent mineral photography: A shot in the dark.** J. Root, *Rocks & Minerals*, **96**(1), 2021, 69–75, https://doi.org/10.1080/00357529.2021.1827913.

**Gem pegmatites: Descriptive summary.** P. Lyckberg, *Rivista Italiana di Gemmologia/Italian Gemological Review*, No. 12, 2021, 30–40.

**Keystone dreams: Trends in retail jewelry markups and their use in the cost approach to value.** S. Gordon, *GemGuide*, **40**(4), 2021, 4–11.

**Overview of the international ruby jewelry auction market and analysis of its price influencing factor.** Q. Zhou, B. Wang, H. Liu, Y. Zhao and Y. Zhou, *Journal of Gems & Gemmology*, **23**(3), 2021, 63–71, https://doi.org/10.15964/j.cnki.027jgg.2021.03.008 (in Chinese with English abstract).

**Ural jasper masterpieces by Russian stone carvers: Collection of the State Hermitage Museum.** E.A. Olkhovaya and N.M. Mavrodina, *Mineralogical Almanac*, **26**(1), 2021, 78–83.

**Women at the dawn of diamond discovery in Siberia or how two women discovered the Siberian diamond province.** E.S. Kiseeva and R.N. Yuzmukhametov, *Geological Society, London, Special Publications*, **506**, 2020, 261–276, https://doi.org/10.1144/sp506-2020-11.

**Zur Ermittlung der Schleifbärte einiger Schmucksteine [Determination of the grinding hardness of some gem materials].** H.A. Hänni, R. Brunk and L. Franz, *Gemmologie: Zeitschrift der Deutschen Gemmologischen Gesellschaft*, **70**(1/2), 2021, 37–54 (in German with English abstract).

## NEWS PRESS

**Military coup clouds control over jade, gems in Myanmar.** E. Fishbein, Nu Nu Lusan and Zau Myet Awng, *Aljazeera*, 22 April 2021, www.aljazeera.com/news/2021/4/22/myanmar-militarys-lucrative-jade-industry.*

**Myanmar sanctions take the shine off Burmese rubies.** R. Taylor, *Financial Times*, 9 April 2021, www.ft.com/content/05ce073b-9fb6-4804-a7df-72d2f31826dd.*

**Semi-precious 'hardstones' make their way into high jewellery.** R. Taylor, *Financial Times*, 8 July 2021, www.ft.com/content/3678a370-199b-4d97-957d-938b60264bdb.*

**Sri Lanka: World's largest star sapphire cluster found in backyard.** A. Ethirajan, BBC News, 27 July 2021, www.bbc.com/news/world-asia-57981046.*

## ORGANIC/BIOGENIC GEMS

**Assignments on Raman peaks of red coral based on experimental Raman spectroscopy and density functional theory calculation.** C. Chen, W. Huang, Q. Gao, L. Fan and A.H. Shen, *Spectroscopy and Spectral Analysis*, **41**(1), 2021, 127–130, www.gpxygpfx.com/EN/Y2021/V41/I01/127 (in Chinese with English abstract).*

**Burmese amber compared using micro-attenuated total reflection infrared spectroscopy and ultraviolet imaging.** M. Musa, T.G. Kaye, W. Bieri and A. Peretti, *Applied Spectroscopy*, **75**(7), 2021, 839–845, https://doi.org/10.1177/0003702820986880.

**Burmese amber fossils, mining, sales and profits.** G. Poinar and S. Ellenberger, *Geoconservation Research*, **3**(1), 2020, 12–16, https://doi.org/10.30486/GCR.2020.1900981.1018.*

**The elephant in the courtroom: An analysis of the United Kingdom's Ivory Act 2018, its path to enactment, and its potential impact on the illegal trade in ivory.** C. Cox, *Journal of International Wildlife Law & Policy*, **24**(2), 2021, 105–130, https://doi.org/10.1080/13880292.2021.1933721.*

**Gemmological and spectral characteristics of *Corallium sp. nov.* from Midway Island.** Q. Yu and L. Li, *Journal of Gems & Gemmology*, **23**(1), 2021, 27–39, https://doi.org/10.15964/j.cnki.027jgg.2021.01.004 (in Chinese with English abstract).

**Identification characteristic of rhinoceros horn and its imitation.** Y. Zhang, L. He, L. Zhang and Z. Xu, *Journal of Gems & Gemmology*, **23**(1), 2021, 48–54, https://doi.org/10.15964/j.cnki.027jgg.2021.01.006 (in Chinese with English abstract).

**Precious coral.** L. Langeslag, *Gemmology Today*, June 2021, 82–86, https://tinyurl.com/dc4mvjh7.*

**Raman spectroscopy allows for the determination of elephant ivory age.** A. Sharikova, L. Peerzada, K. Pisila, T.C. Khoo, A. Cherkinsky and A. Khmaladze, *Applied Spectroscopy*, **74**(8), 2020, 940–947, https://doi.org/10.1177/0003702820930037.

**Structural changes from heating amber and copal as observed by nuclear magnetic resonance spectroscopy.** J.B. Lambert, T.V. Nguyen, A.J. Levy, Y. Wu and J.A. Santiago-Blay, *Magnetic Resonance in Chemistry*, **58**(9), 2020, 812–819, https://doi.org/10.1002/mrc.4992.

**The surface degradation of Baltic amber: The depth-profiling analysis and its application to historical object.** A. Rygula, A. Klisińska-Kopacz, P. Krupska, E. Kuraś and J.M. Hoyo-Meléndez, *Journal of Raman Spectroscopy*, 2020, article 5942 (7 pp.), https://doi.org/10.1002/jrs.5942.

## PEARLS

**How cultured pearls acquire their colour.** Z. Wang, L. Adzigbli, Z. Zheng, C. Yang and Y. Deng, *Aquaculture Research*, **51**(10), 2020, 3925–3934, https://doi.org/10.1111/are.14765.

**Internal structures of known *Pinctada maxima* pearls: Natural pearls from wild marine mollusks.** A. Homkrajae, A. Manustrong, N. Nilpetploy, N. Sturman, K. Lawangwong and P. Kessrapong, *Gems & Gemology*, **57**(1), 2021, 2–21, https://doi.org/10.5741/gems.57.1.2.*

**A pearl spectrometer.** Y. Kwak, S.M. Park, Z. Ku, A. Urbas and Y.L. Kim, *Nano Letters*, **21**(2), 2021, 921–930, https://doi.org/10.1021/acs.nanolett.0c03618.*

**Performance of the winged pearl oyster *Pteria sterna* (GOULD, 1851), implanted for half-pearl (mabé) production in two size groups.** L. Freites, F. Jara, M. Gregori, A. Márquez, P.E. Saucedo and C. Lodeiros, *Aquaculture*, **524**, 2020, article 735267 (7 pp.), https://doi.org/10.1016/j.aquaculture.2020.735267.

**Quahog-Perlen - Natürliche Perlen aus der Venusmuschel *Mercenaria mercenaria* [Quahog pearls – Natural pearls from the venus mussel *Mercenaria mercenaria*].** T. Stephan and S. Müller, *Gemmologie: Zeitschrift der Deutschen Gemmologischen Gesellschaft*, **70**(1/2), 2021, 58–60 (in German with English abstract).

## SIMULANTS

**Aus der Untersuchungspraxis: "Paraiba- und tansanitfarbene" blaue Quarze ['Paraiba- and tanzanite-coloured' blue quartz].** R. Diehl, *Gemmologie: Zeitschrift der Deutschen Gemmologischen Gesellschaft*, **70**(1/2), 2021, 55–57 (in German with English abstract).

**Gemmological characteristic of dyed agate similar to turquoise.** J. Luo, X. Wang, S. Yue, P. Wang, X. Zou and Z. Liu, *Journal of Gems & Gemmology*, **23**(2), 2021, 19–25, https://doi.org/10.15964/j.cnki.027jgg.2021.02.003 (in Chinese with English abstract).

## SYNTHETICS

**$C_3H_6N_6$ doping effect of synthetic diamond under high pressure and high temperature.** J. Wang, S. Li, M. Hu, T. Su, G. Gao, M. Guo, Y. You and Y. Nie, *International Journal of Refractory Metals and Hard Materials*, **87**, 2020, article 105150, https://doi.org/10.1016/j.ijrmhm.2019.105150.

**Coessential-connection by microwave plasma chemical vapor deposition: A common process towards wafer scale single crystal diamond.** G. Shu, B. Dai, A. Bolshakov, W. Wang, Y. Wang, K. Liu, J. Zhao, J. Han *et al.*, *Functional Diamond*, **1**(1), 2021, 47–62, https://doi.org/10.1080/26941112.2020.1869511.*

**Effect of technical process on nucleation and quality of synthetic gem diamond.** J. Liu, S. Xue, T. He, H. Lou and J. Zhang, *Superhard Material Engineering*, **33**(1), 2021, 12–16 (in Chinese with English abstract).

**Research progress on high rate and high quality growth of MPCVD single crystal diamond.** Y. Li, X. Hao, B. Dai, G. Shu, J. Zhao, S. Zhang, X. Liu, W. Wang *et al.*, *Journal of Synthetic Crystals*, **49**(6), 2020, 979–989, http://rgjtxb.jtxb.cn/EN/Y2020/V49/I6/979 (in Chinese with English abstract).*

**Synthesis of diamond crystal with $CH_4N_2S$ additive at HPHT conditions and the study of FT-IR spectra.** Y. Li, J. Liao, Y. Wang, N. Chen and Y. She, *Journal of Synthetic Crystals*, **49**(7), 2020, 1176–1207, http://rgjtxb.jtxb.cn/EN/Y2020/V49/I7/1176 (in Chinese with English abstract).*

## TREATMENTS

**Coloration changes in natural ruby induced by oxygen ion implants correlated with cathodoluminescence data.** T. Tengchaisri, D. Bootkul, S. Intarasiri, U. Tippawan and A.Y. Kuznetsov, *Nuclear Instruments and Methods in Physics Research Section B: Beam Interactions with Materials and Atoms*, **502**, 2021, 29–36, https://doi.org/10.1016/j.nimb.2021.06.002.

**Comparative study of unheated and heated rubies from Myanmar.** Q. Song and A.H. Shen, *Journal of Gems & Gemmology*, **23**(3), 2021, 7–18, https://doi.org/10.15964/j.cnki.027jgg.2021.03.002 (in Chinese with English abstract).

**Heat treatment of dark blue sapphire from Australia.** Y. Xu and J. Di, *Journal of Gems & Gemmology*, **22**(6), 2020, 20–32, http://doi.org/10.15964/j.cnki.027jgg.2020.06.003 (in Chinese with English abstract).

**HPHT annealing of boron and nitrogen Co-doped diamond.** N. Chen, G. Zhang, G. Xu, G. Huang and Z. Zhou, *Journal of Synthetic Crystals*, **49**(10), 2020, 1770–1775 http://rgjtxb.jtxb.cn/EN/Y2020/V49/I10/1770 (in Chinese with English abstract).*

**Identification characteristic of HPHT-treated yellow type Ib CVD synthetic diamond.** W. Zhu, T. Ding, H. Li and Z. Xiaoxia, *Journal of Gems & Gemmology*, **23**(3), 2021, 1–6, https://doi.org/10.15964/j.cnki.027jgg.2021.03.001 (in Chinese with English abstract).

**Stabilité aux hautes températures des inclusions et des absorptions infrarouge dites " lignes Punsiri " observées dans un saphir jaune [High temperature stability of inclusions and infrared absorptions known as 'Punsiri lines' observed in a yellow sapphire].** J.-M. Arlabosse and S. Bensa, *Revue de Gemmologie A.F.G.*, No. 212, 2021, 9–12 (in French).

**Technical evolution and identification of resin-filled turquoise.** L. Liu, M. Yang, Y. Li, J. Di, R. Chen, J. Liu and C. He, *Gems & Gemology*, **57**(1), 2021, 22–35, https://doi.org/10.5741/gems.57.1.22.*

## COMPILATIONS

***G&G* Micro-World.** Thin-film fluid inclusions in aquamarine • Chromite in emerald • Diamond-shaped cloud in diamond • Diamond surface distortion due to radiation staining • Fibrous inclusions in blue opal • Mobile bubble in opal • Iridescent partially healed fissures in sapphire • Phlogopite in topaz. *Gems & Gemology*, **57**(1), 2021, 64–69, www.gia.edu/gg-issue-search?ggissueid=1495326065726&articlesubtype=microworld.*

**Gem News International.** China's gem and jewellery industry reacts to COVID-19 • Market trends in 2021 featuring Constantin Wild, Dudley Blauwet, Eric Braunwart, Gem Shopping Network, Jeff Hapeman, Josh Hyman, Paula Crevoshay, Prida Tiasuwan and Peter Ngumbi • Update on sapphires from Rock Creek, Montana, USA • Somewhere in the Rainbow collection • 'Cookie monster' geode • Hand-drilled hole in antique diamond briolette • Phenakite as a diamond imitation • Imitation of *shi zi hong* agate • Unusual fluorescence in color-enhanced amber bracelet. *Gems & Gemology*, **57**(1), 2021, 70–87, www.gia.edu/gg-issue-search?ggissueid=1495326065726&articlesubtype=gni.*

**Lab Notes.** Asterism in diamond cabochons • Bicolored diamond crystals • Faceted hexagonite • Prominent growth planes in HPHT-processed CVD-grown diamonds • Cat's-eye opal • Green opal displaying aventurescence • Fossil pearls and shell blister from the Florida coast, USA • Lead glass-filled synthetic ruby. *Gems & Gemology*, **57**(1), 2021, 52–62, www.gia.edu/gg-issue-search?ggissueid=1495326065726&articlesubtype=labnotes.*

**Article freely available for downloading or reading online, as of press time*

Gem-A
INSTRUMENTS




OVER **100** PRODUCTS AVAILABLE

# Buy Gem-A Instruments online!


## View the full collection at:
## **shop.gem-a.com**

### GEM-A MEMBERS!

Login to the Gem-A Instruments website and gain instant access to discounted rates.

**Username** is the email address that you have provided to Gem-A Membership.

**Password** is your membership number.

You must log in before adding products to your basket.

We recommend changing your password in the account settings.